NUMERICAL AND EXPERIMENTAL ANALYSIS FOR COMPARISON OF SQUARE, CYLINDRICAL AND PLATE FIN ARRAYS IN EXTERNAL FLOW

A THESIS SUBMITTED TO
THE GRADUATE SCHOOL OF APPLIED AND NATURAL SCIENCES
OF
MIDDLE EAST TECHNICAL UNIVERSITY

BY

AYKUT BARIŞ İNCİ

IN PARTIAL FULFILLMENT OF THE REQUIREMENTS
FOR
THE DEGREE OF MASTER OF SCIENCE
IN
MECHANICAL ENGINEERING

MARCH 2018

Approval of the thesis:

NUMERICAL AND EXPERIMENTAL ANALYSIS FOR COMPARISON OF SQUARE, CYLINDRICAL AND PLATE FIN ARRAYS IN EXTERNAL FLOW

submitted by **AYKUT BARIŞ İNCİ** in partial fulfillment of the requirements for the degree of **Master of Science in Mechanical Engineering Department, Middle East Technical University** by,

Prof. Dr. Halil Kalıpçılar
Dean, Graduate School of **Natural and Applied Sciences** _____

Prof. Dr. M. A. Sahir Arıkan
Head of Department, **Mechanical Engineering** _____

Asst. Prof. Dr. Özgür Bayer
Supervisor, **Mechanical Engineering Dept., METU** _____

Examining Committee Members:

Prof. Dr. İlker Tarı
Mechanical Eng. Dept., METU _____

Asst. Prof. Dr. Özgür Bayer
Mechanical Eng. Dept., METU _____

Assoc. Prof. Dr. Cemil Yamalı
Mechanical Eng. Dept., METU _____

Prof. Dr. Selin Aradağ Çelebioğlu
Mechanical Eng. Dept., TOBB ETÜ _____

Asst. Prof. Dr. Ece Ayli İnce
Mechanical Eng. Dept., ÇANKAYA UNIVERSITY _____

Date: 09.03.2018

I hereby declare that all information in this document has been obtained and presented in accordance with academic rules and ethical conduct. I also declare that, as required by these rules and conduct, I have fully cited and referenced all material and results that are not original to this work.

Name, Last Name: AYKUT BARIŞ İNCİ

Signature:

ABSTRACT

NUMERICAL AND EXPERIMENTAL ANALYSIS FOR COMPARISON OF SQUARE, CYLINDRICAL AND PLATE FIN ARRAYS IN EXTERNAL FLOW

İnci, Aykut Barış
M.S., Department of Mechanical Engineering
Supervisor: Asst. Prof. Dr. Özgür Bayer

March 2018, 105 pages

Geometrical optimization of square, cylindrical and plate fins for heat transfer augmentation is numerically performed in the external flow. Heat transfer performance of fins with different profiles are compared with same Reynolds number. The relation between the thermal characteristic of fins and boundary conditions like free-stream velocity and heat input are investigated.

Experimental studies are performed using manufacturable fins to validate numerical model. Heat transfer correlations are derived in order to find average heat transfer coefficient of square, cylindrical and plate fins at a certain range of Reynolds number and non-dimensional geometric parameters like spanwise and streamwise spacings.

Radiation included numerical analyses for fins having optimum configuration are conducted to increase the accuracy of numerical results. Uncertainty analysis is also performed to define the level of confidence for experimental work.

Superiority of cylindrical fins to ones with square and plate profiles are observed in terms of heat transfer performance.

Keywords: Heat Transfer Augmentation, Optimization, Comparison, Fin, External Flow, Heat Transfer Correlation, CFD.

ÖZ

DIŞ AKIŞTAKİ KARE, SİLİNDİR VE PLAKA KANATÇIK DİZİLERİNİN SAYISAL VE DENEYSEL KARŞILAŞTIRILMASI

İnci, Aykut Barış
Yüksek Lisans, Makina Mühendisliği Bölümü
Tez Yöneticisi: Y. Doç. Dr. Özgür Bayer

Mart 2018, 105 sayfa

Isı transferi artırımı için kare, silindirik ve plaka finlerin geometrik olarak optimizasyonu, dış akış etkisi altında sayısal olarak gerçekleştirilmektedir. Aynı Reynolds Sayısının etkisi altında üç farklı kanatın ısı transfer performansı karşılaştırılmıştır. Finlerin termal karakteristikleri ile serbest akış hızı ve ısı yükü gibi sınır koşulları arasındaki ilişki araştırılmıştır.

Sayısal modeli doğrulamak için üretilebilir finlerle deneysel çalışmalar yapılmıştır. Kare, silindirik ve plaka şeklindeki finlerin belirli bir Reynolds Sayısı ve boyutsuz finler arası boşluk gibi parametreler aralığında ortalama konveksiyonel ısı aktarım katsayısını bulmak için genel korelasyon denklemleri türetilmiştir.

Sayısal sonuçların doğruluğunu artırmak için, optimum konfigürasyona sahip finler için radyasyon dahil edilmiş sayısal analizler yapılmıştır. Deneysel çalışma için güven seviyesini tanımlamak amacıyla belirsizlik analizi yapılmıştır.

Silindirik finlerin ısı transferi performansı açısından diğer finlere göre daha etkili

olduğu gözlemlenmiştir.

Anahtar Kelimeler: Isı Transferi Arttırımı, Optimizasyon, Karşılaştırma, Fin, Harici Akış, Isı Transferi Korelasyonu, Hesaplamalı Akışkanlar Dinamiği.

To my family

ACKNOWLEDGEMENTS

I would like to thank my supervisor Asst. Prof. Dr. Özgür BAYER for his endless support, guidance, patience and contribution during this study.

I am also grateful to Mr.Tahir FİDAN, my manager at ASELSAN, for his great encouragement.

I would like to express my acknowledgement to my best friends; Kadir Eray DOĞANLAR, Burak Alp BİLKAY and Doğuş KÜÇÜKGÖDE, for their endless support during this period.

Family is the most important part of the human being, So, i would like to express my biggest appreciation to my parents; Gülfiraz and Bayram İNCİ, my sister; Neşe and my two nephews; Emir and Ömer.

TABLE OF CONTENTS

APPENDICES

LIST OF TABLES

TABLES

LIST OF FIGURES

FIGURES

LIST OF SYMBOLS

a, b, c, z	Coefficient of correlations
A_{ins}	Heat transfer area of insulation material [m^2]
A_{rad}	Radiative heat transfer area [m^2]
A_T	Total heat transfer area [m^2]
B	Thickness of base plate [mm]
C.V.	Coefficient of variation
C_p	Specific heat [kJ/kgK]
D_h	Characteristic length [mm]
d	Diameter of a cylindrical fin [mm]
e_i	Residual
e	Specific internal energy [kJ/kg]
$F_{(fin)\rightarrow(surr)}$	View factor of fin to surrounding
F_d	Drag force [N]
g_z	Gravity component in z direction [m/s^2]
H	Height of fin [mm]
h	Convective heat transfer coefficient [W/m^2K]
h	Specific enthalpy [kJ/kg]
h_{avg}	Average heat transfer coefficient [W/m^2K]
$h_{avg(l)}$	Lower average heat transfer coefficient [W/m^2K]
$h_{avg(r)}$	Root of average heat transfer coefficient [W/m^2K]
$h_{avg(r)}^{new}$	New root of average heat transfer coefficient [W/m^2K]

$h_{avg(r)}^{old}$	Old root of average heat transfer coefficient [W/m^{2}K]
$h_{avg(u)}$	Upper average heat transfer coefficient [W/m^{2}K]
I	Current [A]
k	Thermal conductivity [W/mK]
k_{air}	Thermal conductivity of air [W/mK]
k_{ins}	Thermal conductivity of insulation material [W/mK]
L	Length of base plate [mm]
n	Number of data
n_{ref}	Refinement level
N	Total number of fins
N_L	Number of fins in streamwise direction
N_T	Number of fins in spanwise direction
Nu	Nusselt number
Nu_{corr}	Correlated Nusselt number
Nu_{exp}	Experimental Nusselt number
Nu_{num}	Numerical Nusselt number
$\overline{Nu_{exp}}$	Mean value of of experimental Nusselt number
p	Pressure [Pa]
Q_{input} or Q	Heat input [W]
Q_{conv}	Convection heat transfer rate [W]
Q_{gen}	Heat generation [W]
Q_{ins}	Heat transfer rate through insulation layer [W]
Q_{rad}	Radiation heat transfer rate [W]
q"	Heat flux [W/m^2]
q_x"	Heat flux in x direction [W/m^2]

R_{sink}	Thermal resistance of heat sink [K/W]
r	Correlation coefficient
r^2	Coefficient of determination
Re	Reynolds number
$\dot{S}_{gen}$	Entropy generation rate [W/K]
s	Edge length of a square fin [mm]
s_{ij}	Strain rate tensor [s^{-1}]
S_L	Inter-fin spacing in streamwise direction [mm]
S_r	Summation of squares of residuals
S_t	Summation of squares of residuals between data points and arithmetic mean
S_T	Inter-fin spacing in spanwise direction [mm]
S_L/L	Non-dimensional streamwise spacing
S_T/W	Non-dimensional spanwise spacing
S_y	Standart deviation
$S_{y/x}$	Standart error of estimate
t	Strip thickness of plate fin [mm]
t	Time [s]
t_{ij}	Viscous stress tensor [N/m^2]
T	Temperature [℃]
T_1	Front side temperature of base plate [℃]
T_2	Back side temperature of base plate [℃]
T_3	Left side temperature of base plate [℃]
T_4	Right side temperature of base plate [℃]
T_5	Bottom temperature of heater [℃]

T_6	Bottom temperature of insulation material [℃]
T_{air_ave}	Average air temperature[℃]
T_{air_i}	Air inlet temperature [℃]
T_{air_o}	Air outlet temperature [℃]
T_{base_ave}	Average temperature of base plate [℃]
T_{ins_ave}	Average insulation temperature[℃]
T_s	Surface temperature [℃]
T_{surr}	Temperature of surrounding [℃]
T_{max}	Maximum temperature on the upper surface of the base plate [℃]
U	Free-stream velocity [m/s]
U_{max}	Maximum velocity in fin [m/s]
u,v,w	Velocity components in x, y and z directions, respectively [m/s]
u_i, u_j	Velocity in tensor notation [m/s]
$\vec{v}$	Velocity vector [m/s]
V	Voltage [V]
y	Predictor variable
W	Width of base plate [mm]
ΔT	Temperature difference between top and bottom layers of insulation material [℃]
η_f	Fin efficiency
η_o	Overall efficiency of fin array
δ	Deviation
δ_{ij}	Kronecker delta
ε	Error between numerical and experimental results
ε_a	Relative error

ε_s	Preset stopping criteria
ρ	Density [kg/m^3]
μ	Dynamic viscosity [kg/ms]
ΔT_{lm}	Logarithmic mean temperature difference [℃]
σ	Stefan Boltzmann constant [5.67 x 10^{-8} W/m^{2}K^4]
ε_{fin}	Emissivity of fin
ε_{surr}	Emissivity of surrounding
ν	Kinematic viscosity of air [m^2/s]
$\emptyset$	Scalar variable
$\widetilde{\emptyset}$	Density weighted time average value of the variable
$\emptyset$"	Fluctuation of the variable.
Γ^{ϕ}	Diffusion coefficient

LIST OF ABBREVIATIONS

CFD	Computational Fluid Dynamics
CPU	Central Processing Unit
Cyl.	Cylindrical
exp	Experimental
EW	Electronic Warfare
FANS	Favre-Averaged Navier-Stokes Equations
FVM	Finite Volume Method
LTE	Local Truncation Error
Nu	Nusselt Number
num	Numerical
num_rad	Radiation Included Numerical
RADAR	Radio Detecting and Ranging
RAM	Random Access Memory
Re	Reynolds Number
REF	Refinement
SIMPLE	Semi Implicit Method for Pressure Linked Equations
TDP	Thermal Design Power

CHAPTER 1

INTRODUCTION

Nearly 50 years ago Moore [1], co-founder of Intel, empirically observed and predicted that the number of components in a chip would double in every two years while dimensions and manufacturing costs would not change. This estimate was justified by recent technological advancements. From this point of view, heat generated by electronic equipments drastically increased and removal of excess heat in more efficient ways became a necessity.

There are various cooling methods in electronic packaging. Çengel [2] classified these techniques as follows:

- Natural convection (gas) and radiation,
- Forced convection (gas),
- Indirect liquid cooling (cold plate),
- Immersion liquid (direct) cooling (natural convection or boiling).

Conduction cooling is inherently an active heat transfer mechanism included in all three methods mentioned above. Basically, heat is transferred from the heating element through the high conductive material by the diffusion mechanism in conduction cooling. Natural convection (gas) and radiation are used for low power applications. Buoyancy effect is the main mechanism of natural convection and there should be no obstacle for the fluid motion. Radiation also plays a role in such a cooling application by virtue of the obstacle-free environment. The difference between air forced convection and natural convection is the existence of a fan or blower. This method is

applied when the cooling with natural convection is insufficient. Radiation is mostly omitted in forced cooling applications due to its low cooling capacity and surroundings created for the airflow around the heating element. Liquid cooling is preferred in high-power applications. However, it is more expansive and difficult to handle than other cooling methods. Liquid cooling is divided into two subgroups called for indirect cooling and direct or immersion cooling. Cold liquid passes inside of a cold plate and heating element is bonded to this cold plate, so there is no direct contact between the cooling liquid and heating element in indirect cooling. Otherwise, it is called as immersion cooling. The heating element is immersed in a tank which is partially filled with dielectric liquid. Depending on the working fluid and operation temperatures, heat can be removed from the object by natural convection or boiling. There are different applications depending on the condensation methods of vapor. Heat pipe and spray cooling are other well-known thermal management methods. Heat removal capacity of different cooling methods with respect to the temperature difference between heating object and the cooling medium is illustrated in Figure 1.1 [2].

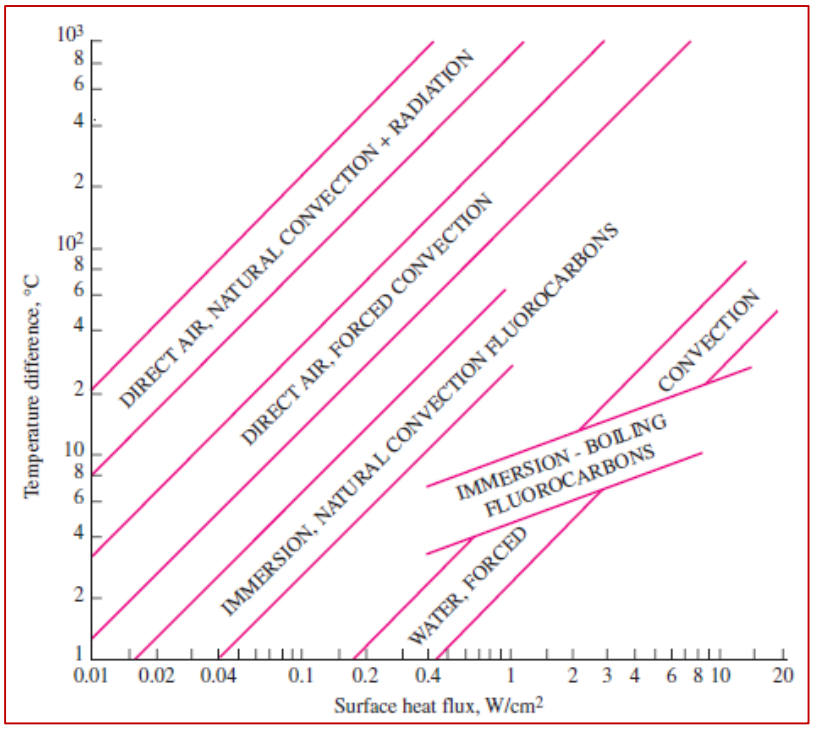

Figure 1.1 Cooling performance of different methods [2]

Extended surfaces as shown in Figure 1.2 increasing heat transfer area are called as heat sink or fin. Fins are widely used in electronic cooling applications. There are various types of fins with different dimensions, profiles and orientations.

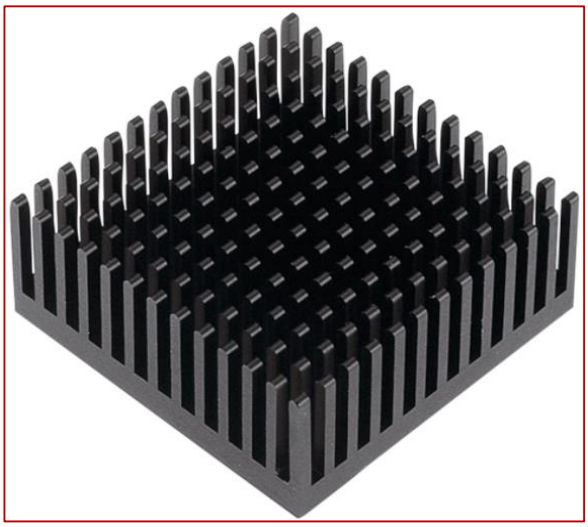

Figure 1.2 General view of a heat sink [3]

Fins are classified into four groups with respect to the cooling method in the study of Lee [4]. Passive fins are the components operating in natural convection applications. Semi-active fins are used at the existence of a fan, whereas active fins have their own fans. Moreover, liquid cooled cold plates including machined or brazed passages in where cooling liquid circulate are assumed as a fin.

Fins can also be classified according to manufacturing method [4]. Stampings are widely used in mass production and suitable for copper and aluminum materials. Extrusions are preferred for high wattage applications. Complex two-dimensional shapes can be produced by the extrusion method. Fractions of fin thickness to height, fin height to inter-fin spacing determine extrusion limits. In bonding method, extruded plates are bonded to a base plate with an epoxy-based adhesive, but adhesive material creates a thermal resistance for the fin. This method is more expensive than other

manufacturing techniques. Folded sheet metal is attached to the base plate in the folding method. This operation is done by brazing or soldering. Bended parts of the sheet metal become straight during brazing operation and perfectly attach to the base plate. So, there will not be any contact resistance problem. Folding method like bonding offer design flexibility for usage of different materials. Another manufacturing method is forging. The raw material is punched into a molding die. Additional treatment like etching or polishing may be required due to choking. Durable fins with low tolerances can be produced by this method. Forging, skiving and machining are other known production methods.

1.1 Present Study

High performance requirements in military radar and electronic warfare systems result in demanding high amount of energy and exposing excess heat. Maintaining an electronic component's temperature at its operating range in an efficient and a reliable way is vital for performance and durability of the component. The present study aims to perform geometrical optimization and comparison of heat transfer performance of fins with different profiles in forced external flow both numerically and experimentally.

Navier-Stokes equations and fundamental formulas related to the conduction, convection and radiation heat transfers are presented in CHAPTER 3. Moreover, parametrization of geometrical and boundary condition variables of square, cylindrical and plate fins are done in this chapter.

The numerical domain is introduced in CHAPTER 4. Finite Volume Method, which is the discretization technique of FLoEFD CFD software, is briefly explained. Then, boundary conditions and numerical setup are explained in details. Meshing and mesh independency procedure are represented, too in this chapter.

The experimental work is performed to validate numerical results. Experimental setup is constructed at ASELSAN Gölbaşı Campus. Experimental setup and components

used in the experiments are presented in CHAPTER 5.

Numerical and experimental results are presented in CHAPTER 6. Comparison between the numerical and experimentel results are done. Average heat transfer coefficient for the tested fins are calculated. Then, heat transfer correlations are derived at a certain range of Reynolds number and non-dimensional geometrical parameters. Then, uncertainty analysis is done to define deviations at average heat transfer coefficient and Nusselt number.

A brief summary is presented, discussion related to the numerical and experimental results are done in CHAPTER 7. Radiation included numerical analyses for optimized fin configurations are conducted to increase the accuracy of numerical results. Recommendations about possible future work are presented in this chapter, too.

1.2 Motivation

Majority of the electronic failures in military applications are due to temperature related problems, as presented in Figure 1.3 [5]. Customer's need and demand about the capacity of Radar (Radio Detection and Ranging) and EW (Electronic Warfare) systems increase day by day. This situation increases not only power consumption of systems but also the amount of heat generated.

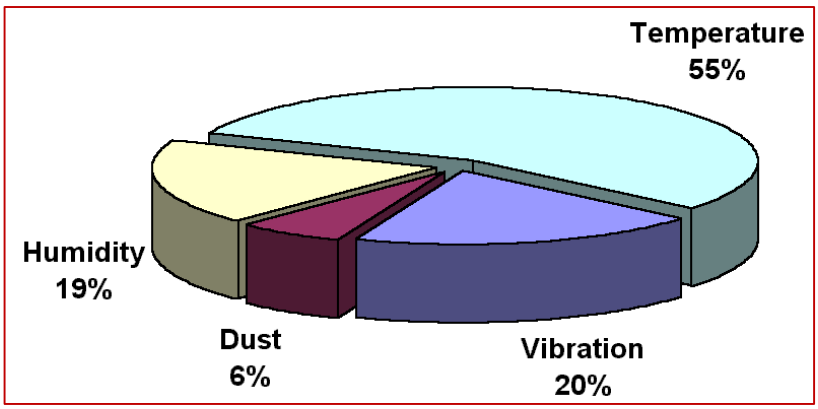

Figure 1.3 Failure mechanisms in military applications [5]

Capacities of different cooling techniques are already shown in Figure 1.1. Liquid cooling's capacity is much higher than the capacity of natural convection and forced convection with air, but there are some difficulties related to this application. it is much more expensive than air cooling. it requires regular maintenance like changing particle filter. there are some operational risks like leakage at the fittings, failures caused by overpressure. It is really difficult to compensate high pressure drop of cooling liquid especially at the naval platforms due to elevation difference between the pump and antenna chassis mounted on the top of foremast or aftmast., there is a corrosion problem inside of the piping. The rust may pass to the cooling fluid and this rust may clog the fluid channels. Therefore capacity of air cooling should be improved and air cooling can be used in possible cases. Fins are the key elements of air cooling applications. There are lots of studies in the literature about the heat transfer performance of fins. Researches in literature can be summarized as:

- Geometrical optimization of fins having monotype cross-section (cylindrical, square, etc.) for heat transfer augmentation is studied,
- Heat transfer performance comparison of fins with different profiles is investigated,
- Fins are mostly in internal (confined flow or flow with zero bypass) and rarely in external (unconfined or flow with bypass) flow.

The present study, conducted both numerically and experimentally, aims to investigate the geometrical optimization of the square, cylindrical and plate fins for heat transfer augmentation in the transition regime external flow at steady state conditions. As a continuation, comparison of heat transfer characteristics of optimized geometries is performed. Furthermore, heat transfer correlations including thermal, hydraulic and geometrical parameters are derived for tested fins with different profiles.

Results of this study can be used for thermal management of a military electronic equipment placed at the outside of military vehicles like combat ships, trucks, helicopters or aircrafts and being exposed to unconfined flow due to the wind.

CHAPTER 2

LITERATURE REVIEW

There are numerous studies in the literature which investigate and aim to increase heat transfer performance of fins. Relations between parameters like inter-fin spacing, base plate dimensions, number of fins, height of fin, hydraulic diameter of fin, fin geometry, fin material, thermal resistance, heat flux, base plate temperature, fin alignment as inline or staggered, free-stream velocity, pumping power, flow type as external or internal, Reynolds number, heat transfer coefficient, Nusselt number, pressure loss, friction factor, blockage area are studied in [4], [6]-[26]. Some of these parameters in literature are changed to get optimum design points for heat transfer augmentation, to compare the thermal or hydrodynamic performance of fins with different profiles with respect to each other and to create correlations between these parameters.

Researchers numerically compared the heat transfer performance of fins with different profiles in internal flow [6]–[8].

Sahiti et al. [6] classified fins according to two geometric comparison criteria groups. One of them consists of equal hydraulic diameter, coverage ratio and fin length, the other one consists of equal blockage area, distance between fins and fin length. Free-stream velocity is changed from 1.5 m/s to 4 m/s. The ratio of fin length to the diameter is taken as 10. Reynolds number was kept below 1000 and the flow was assumed laminar according to the study of Zukauskas [7].

Sahiti et al. [6] observed that fins with cylindrical profiles have better heat transfer performance than ones with NACA, drop form, lancet, elliptic and square profiles

when the first group of comparison criteria is applied for in-line arrangement, whereas the thermal performance of elliptic fins is better than others for the second comparison group with in-line arrangement. Moreover, elliptic fins are superior to the others according to both comparison criteria groups with a staggered arrangement.

Behnia et al. [8] compared circular, square, elliptic and plate in terms of their thermal and hydrodynamic performance, too. Ratios of cross-sectional area to base area and wetted surface area to base area and flow passage area are kept constant to make a fair comparison. Free-stream velocity is changed from 0.5 m/s to 5 m/s. It is figured out that pressure drop observed at plate fin is much lower than fins with other profiles. Circular fins in staggered arrangement have the highest heat transfer coefficient.

Numerical studies including Taguchi method or minimization of entropy generation were employed to optimize thermal or hydrodynamic performance of fins by researchers, too [9]–[11].

Yang et al. [9] studied about the heat transfer enhancement of square fins in air jet flow. Taguchi Method with three levels is implemented to rank four design parameters (a, b, c and H in Figure 2.1) according to order of importance on thermal resistance. $k-\epsilon$ turbulence model is used. Heat input of 20 W is applied. Simplec algorithm is used to solve Navier-Stokes Equations. Design parameters are ranked as $a > H > c > b$ with decreasing importance on overall thermal resistance. Increasing inter-fin spacing "a" leads to decrease thermal performance, however increasing inter-fin spacing "c" enhances thermal performance. Because there is pressure drop problem near the fins around edges, but flow reaching the centre is much enough to overcome pressure losses. Inter-fin spacing "b" has an optimum value around 4.2 mm. A value lower or higher than this worsens the thermal performance.

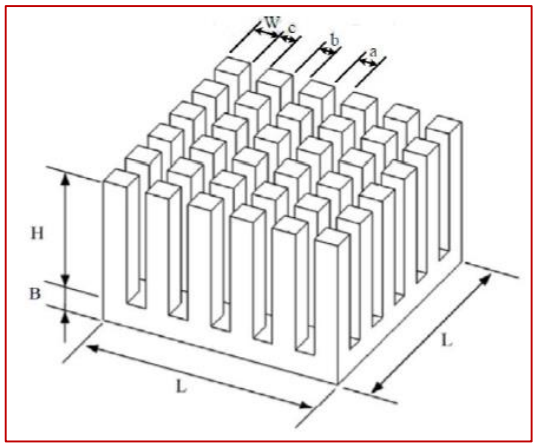

Figure 2.1 Geometrical parameters used in Taguchi Method [9]

Khan [10] determines all independent variables affecting fin thermal performance at the beginning of study. Some of these parameters like length and width of the base plate, heat input or base plate temperature and ambient temperature are restricted by designer or manufacturer. Therefore, fin height, density, diameter and free-stream velocity are left as design parameters affecting optimization criteria like minimum base plate temperature, pressure drop, fin weight. Variable parameters and design criteria are connected to each other by a mathematical relation. Similarly, geometrical and flow parameters, heat input and material properties are optimized to determine the minimum base temperature at plate fin in the study of Culham and Muzychka [11]. First and second laws of thermodynamics are combined to derive a mathematical relation. The heat input (Q), fin thermal resistance (R_{sink}), drag force (F_d), free-stream velocity (U) and ambient temperature (T_{surr}) are connected to entropy generation rate ($\dot{S}_{gen}$) with this formula:

$$\dot{S}_{gen} = \frac{Q^2 R_{sink}}{T_{surr}^2} + \frac{F_d U}{T_{surr}} \tag{2.1}$$

After setting derivative of entropy generation rate with respect to variables to zero and doing iterative solutions, optimized values of fin numbers, free-stream velocity and height of the fin are found to be 19.07, 1.21 m/s and 122 mm, respectively.

Besides numerical works, researchers also experimentally studied about the heat transfer performance comparison, geometrical or hydrodynamic optimization of fins in internal (confined or no bypass) flow [12]–[15].

Deshmukh [12] analytically and experimentally optimized and compared the performance of circular and elliptical fins placed in the direction of gravity and in mixed convection. Mixed convection flow is defined as the forced convection assisted by natural convection. Fraction of Grashof and Reynolds numbers must be between 1 and 100 for a mixed convection flow. Void fraction, which is the ratio of the area between fins to the total fin cross-sectional area, free-stream velocity and arrangement as in-line or staggered are changed to observe fin's thermal resistance. Minimum thermal resistance is observed when the value of void fraction is 0.702. Beyond this point, thermal resistance tends to increase in all cases. Elliptical fin in the staggered arrangement is much more effective than the fin combinations including cylindrical fins or in-line arrangement.

Diani et al. [13] experimentally and numerically investigated the performance of plate and cylindrical fins. The numerical model is created for a sample plate fin. Then, an experimental study is performed for this sample fin and the numerical model is validated. Validated analysis settings are kept constant for whole analysis. Only one channel of fins is analyzed due to symmetry. Decreasing pitch distance and increasing fin thickness lead heat transfer coefficient to increase. However, fin height does not have any effect on it. Dimensionless streamwise spacing has a poor effect on the heat transfer coefficient, however dimensionless spanwise spacing has a major effect on it.

Babus' Haq et al. [14] aimed to find optimum streamwise and spanwise spacings of cylindrical fins and compare heat transfer performance of different materials. Different steady state heat fluxes are applied and base temperature of fin is kept constant at 40°C for each experiment. Effect of different free-stream velocities, arrangements as in-line or staggered and fin materials on optimum spanwise and streamwise spacings were studied. Decreasing fin to fin spacing increases heat transfer area, but it increases pressure drop for a fin structure whose base area is fixed. Optimum streamwise and

spanwise spacings are shown in Figure 2.2 for different free-stream velocities and fin materials.

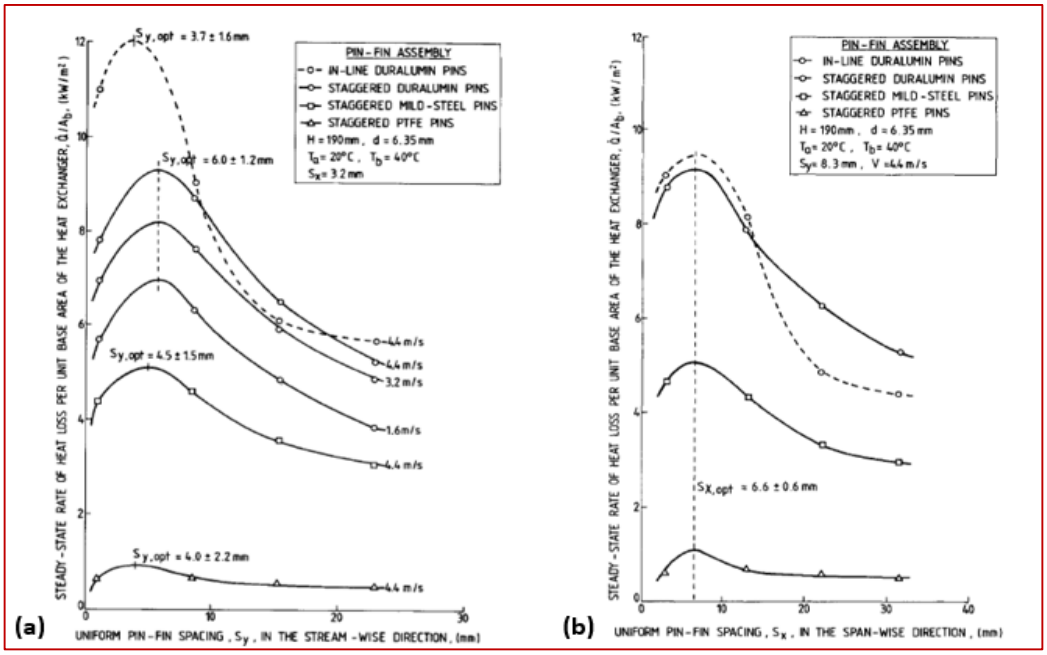

Figure 2.2 Optimum (a) streamwise, (b) spanwise spacing [14]

A geometrical correlation between streamwise spacing, fin material and fin diameter is created:

$$S_{L\_opt} / d = 0.59 + 6.67 \times 10^{-2} e^{0.01k} \tag{2.2}$$

Furthermore, pressure drop increased with the increasing free-stream velocities and decreasing the streamwise spacing between fins.

Tahat et al. [15] researched the heat transfer performance of cylindrical fins in staggered and in-line arrangements. Optimum spanwise and streamwise spacing values leading heat transfer augmentation were found. Heat transfer correlations are derived:

$$Nu = 9.02x10^{-3} Re^{1.011} (S_T / W)^{0.285} (S_L / L)^{0.212} \text{ (inline)} \quad (2.3)$$

$$Nu = 7.04x10^{-3} Re^{0.953} (S_T / W)^{0.091} (S_L / L)^{0.053} \text{ (staggered)} \quad (2.4)$$

Unlike above researches, following experimental studies are about thermal and hydrodynamic performance of fins in external (unconfined, bypass) flow [16]–[21].

Matos et al. [16] numerically and experimentally investigated on the optimization and comparison of cylindrical and elliptical fins' thermal performance in the external flow. Cylindrical and elliptic fins in the fixed volume are placed in the staggered arrangement. Ellipse eccentricity values are changed from 0.4 to 1 (cylindrical fin). Non-dimensional inter-fin spacing value is set to maximum 1.5. This value is reduced to find an optimum design point. Equivalent pressure drop across the cylindrical and elliptic fins is the constraint for a fair comparison. Reynolds number based on swept length of fins varies from 852 to 8520. Non-dimensional inter-fin spacing value resulting in maximum heat transfer performance for 0.5 eccentricity is observed around 0.3. Increasing eccentricity pushes optimum inter-fin spacing up to 0.7 with %20 decrease thermal performance. Higher Reynolds number enhances the heat transfer performance as expected but does not change optimum design point.

Heat transfer performance comparison of fins with elliptic, square, cylindrical and plate profiles in staggered or in-line arrangements was studied in terms of fin numbers in the study of Yang et al. [17]. Fin density can be defined as the number of pins per base area. Major dimension, which is the diameter of a cylindrical fin, the edge length of a square fin, the minor diameter of an elliptic fin are taken as 2 mm. Free-stream velocity varies between 1 m/s and 5 m/s. Cylindrical fins with in-line arrangement have higher heat transfer coefficient than other fins. Superiority of cylindrical fins is explained by Coanda effect. Ishigai and Nishikawa [18] define Coanda effect as attachment of flow field to the bodies with curvature. Increasing number of fins for in-line arrangement leads to increase heat transfer coefficient of circular and elliptic fins. However, any significant increase is not observed for square fins as shown in

Figure 2.3. In staggered arangement, higher fin density increases the heat transfer coefficient for fins with four different profiles as presented in Figure 2.3.

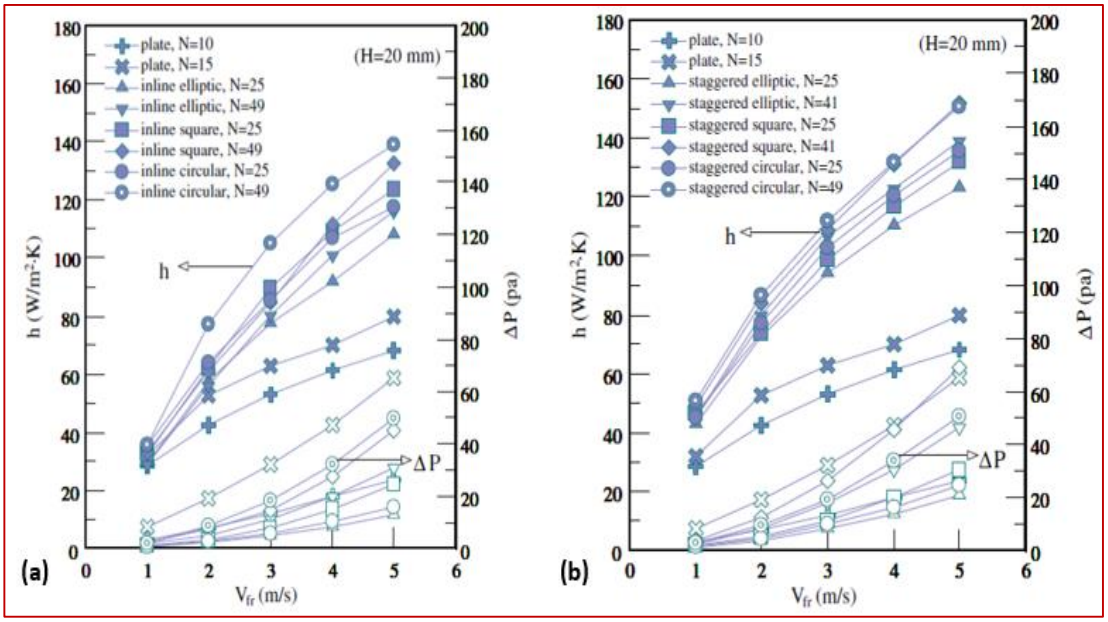

Figure 2.3 Heat transfer coefficient and pressure drop relation with changing free-stream velocity (a) in-line arrangement, (b) staggered arrangement [17]

Fowler et al. [19] numerically and experimentally investigated optimum geometrical configuration of parallel plates in forced convection flow. Plates in the staggered arrangement were placed in a tunnel. Flow is classified as external because the plates are not bounded. Geometrical parameters like spanwise spacing, number of plates in one row, swept length along streamwise direction are variable. The non-dimensional term like Reynolds number based on swept length changes from 1000 to 6000. Non-dimensional optimum spanwise spacing term is observed around 0.09 in the specified Reynolds number range.

Azar and Mandrone [20] aimed to find hydrodynamic and geometrical optimum design points for cylindrical fins to increase heat transfer performance. The base plate temperature of fins is kept constant. Fin density and free-stream velocity are changed

to seek optimum design points. Both natural convection and forced convection exist as flow type. Increasing free-stream velocity leads the thermal resistance to decrease, but decrease of the thermal resistance is getting slower after a certain velocity. Increasing fin density after a certain point worsens the thermal performance of pin fins.

Jonsson and Moshfegh [21] compared thermal and hydrodynamic performance of cylindrical, square and strip fins in both staggered and in-line arrangements. Moreover, plate fins are studied. Fin's height and clearance ratio of the duct are changed to investigate flow bypass around fins while the height of the duct and width of the base plate are kept constant. Free-stream areas of fins with different profiles at the same number of fins are also kept constant to make a fair comparison with respect to same Reynolds number. Reynolds number varies between 2000 and 16500. In narrowest duct condition, high Reynolds number causes pin fins to experience more pressure drop and less thermal resistance decrease rather than plate and strip fins in both staggered and in-line arrangements. Therefore, pin fins are not suggested to be used at high Reynolds number. Plate and strip fins which longer than pin fins in flow direction perform lower pressure drops because there is only one contraction and expansion area along the fin, whereas other fins which have multiple discontinuities have lots of contraction and expansion area. Similarly, in-line arrangement and circular fin have lower pressure drop than staggered arrangement and square fin. Thermal resistance values of all fin types except plate fin decrease and converge with increasing Reynolds number. Decreasing free flow area in the duct by changing fin height or/and width of the plate increases pressure drop.

In literature, there are some other experimental studies searching for heat transfer performance of fins in both internal and external flows [4], [22]–[24]. Effects of changing flow condition on the thermal and hydrodynamic performance of fins were researched.

Optimization and characterization of a plate fin were analytically done with respect to different design parameters in the study of Lee [4]. The analytical method was experimentally validated with a sample case. The number of fins are changed and their

effects on heat transfer performance are investigated in unconfined flow. Heat transfer performance enhances up to some point with the increasing number of fins, but if the number of fins continues to increase, pressure drop phenomenon becomes dominant. The thermal resistance reaches its minimum value when the number of fins at spanwise direction is around 11 as shown in Figure 2.4. Then flow regime is changed to confined. Heat transfer performance significantly increases according to the case with bypass flow. Increasing number of fins decreases thermal resistance and any optimum design point is not observed as shown in Figure 2.4, but the pressure drop increases so much that the pumping power is needed to be increased to keep free-stream velocity constant.

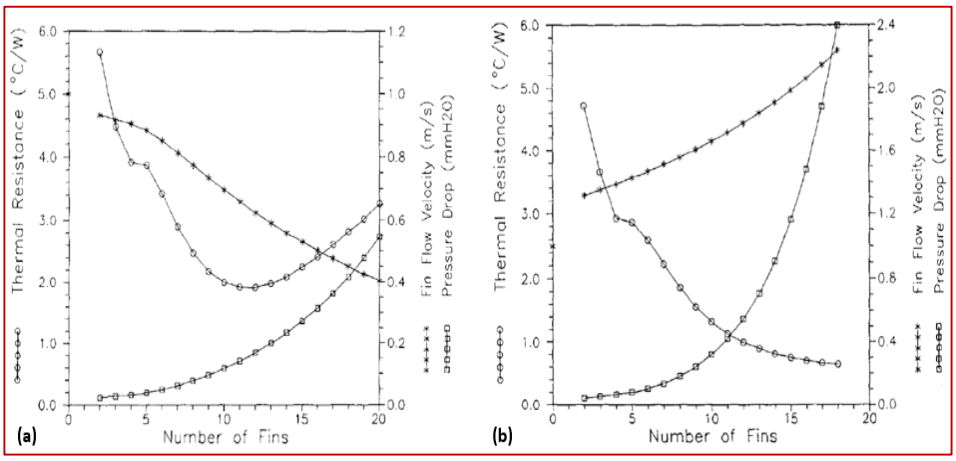

Figure 2.4 Thermal and hydrodynamic performance relation with changing fin numbers (a) unconfined flow, (b) confined flow [4]

Jubran et al. [22] investigated the effect of inter-fin spacing on cylindrical fins and focused on finding optimum spanwise and streamwise spacing with different shroud clearance above fins in staggered and in-line arrangements. Cylindrical fins have an optimum fin to fin spacing values in both directions and arrangements at 2.5d. Increasing shroud clearance causes to decrease heat transfer performance of cylindrical fins. The correlation between Nusselt and Reynolds number was derived for the shroud clearance ratio value of "0" :

$$Nu = 0.45Re^{0.71}(S_T / W)^{0.40}(S_L / L)^{0.51} \text{(inline)} \quad (2.5)$$

$$Nu = 0.30Re^{0.98}(S_T / W)^{0.35}(S_L / L)^{0.24} \text{ (staggered)} \quad (2.6)$$

The correlation for the shroud clearance ratio value of "1" :

$$Nu = 0.58Re^{0.51}(S_T / W)^{0.18}(S_L / L)^{0.21} \text{ (inline)} \quad (2.7)$$

$$Nu = 0.31Re^{0.92}(S_T / W)^{0.20}(S_L / L)^{0.21} \text{ (staggered)} \quad (2.8)$$

Chapman et al. [23] numerically and experimentally compared thermal performance of rectangular, elliptical and plate fins in both confined and unconfined flow. In unconfined flow, elliptical fins reach highest bypass values, whereas minimum bypass occurs at plate fins. In parallel with these results, the thermal resistance of plate fins has the minimum value. Rectangular and elliptic fins have surprisingly similar thermal resistance characteristic. This result shows that, elliptical fins have higher heat transfer coefficient than rectangular fins. Switching flow type from bypass to no bypass condition most significantly improves the thermal performance of elliptical fins, because elliptical fins are most affected by bypass phenomenon. Similarly, lowest refinement happens at plate fins due to low bypass effect.

Samarth and Sawankar [24] studied the heat transfer and hydrodynamic performance of perforated and solid cylindrical fins. Clearance ratio and non-dimensional streamwise spacing change from 0 to 1 and 1.208 to 3.417, respectively. Reynolds number varies from 13500 to 42000. Heat transfer and pressure drop comparison of perforated and solid fins within each other and with respect to nonfinned base plate are done. Perforated cylindrical fins perform better than solid ones in both manners.
Some of these parameters like base plate dimensions, fin height, base plate temperature or heat flux and Reynolds number should be fixed in order to be able to make a fair heat transfer comparison based on the fin shape.

Definition of Reynolds number plays an important role affecting parametrization of fins. There are different Reynolds number definitions related with fin studies in literature [6], [7], [10], [16], [19], [21], [25], [26]. Free-stream velocity and diameter of a cylindrical fin are selected as the main parameters in Reynolds number definition in the study of Kobus and Oshio [25]. Free-stream velocity and length of the base plate are taken into consideration in the studies of Matos et al. [16] and Fowler et al. [19]. Moreover, Matos et al. [16] used inter-fin spacing as a characteristic length to define an another Reynolds number. It was kept below 6000 in these researches [16], [19]. Maximum flow velocity based on minimum flow area in the tunnel is used instead of free-stream velocity in the research of Jonsson and Moshfegh [21]. Hydraulic diameter of wind tunnel is taken as a characteristic length instead of a dimension related to fin and Reynolds number can reach up to 10000 in this study [21]. Li et al. [26] used maximum flow velocity and circumference diameter of an elliptic fin to determine Reynolds number between 1000 and 10000.

Defining flow type as laminar or turbulent according to Reynolds number in fin problems is not easy like in flat plate or pipe problems due to the geometry of fins. In literature, researchers [6], [10] making studies about fin problems benefit from the study of Zukauskas [7] in order to classify flow type. Zukauskas [7] conducted an analytical and experimental study about hydrodynamic and thermal characteristics of single tube and tube banks in crossflow. Reynolds number is defined in terms of maximum flow velocity based on minimum flow area and diameter of the cylinder in this study. According to Reynolds number, flow type is classified:

- flow is predominantly laminar if $Re < 10^3$,
- flow is in transition regime if $5\ x\ 10^2 < Re < 2\ x\ 10^5$,
- flow is dominantly turbulent if $Re > 2\ x\ 10^5$.

In the study of Sahiti et al. [6], heat transfer performance of fins with different profiles was compared. Refering to Zukauskas [7], flow was laminar with Reynolds number value below 1000. Moreover, Khan [10] addresses this study [7] in terms of hydrodynamic matters. On the contrary, Khan [10] mentions that creating an analogy

between fin studies and Zukauskas's tube bank study [7] is not appropriate in terms of thermal issues due to two reasons. Fluid passes inside of the tubes and tube wall temperature is kept uniform. However, temperature gradient occurs at the fin surface. Moreover, tubes are relatively longer than fins and end wall effects are neglected near the base plate, but end wall effects are an important phenomenon in fin problems.

CHAPTER 3

METHODOLOGY

3.1 Governing Equations

Conducted numerical analyses are based on Favre-Averaged Navier-Stokes (FANS) Equations [27], [28]. In Favre-Averaging, a variable can be decomposed into following form:

$$\phi = \tilde{\phi} + \phi'' \tag{3.1}$$

where;

ϕ : variable,

$\tilde{\phi}$: density weighted time average value of the variable,

ϕ'' : fluctuation of the variable.

FANS Equations can be expressed as:

Continuity:

$$\frac{\partial \rho}{\partial t} + \frac{\partial (\rho u_i)}{\partial x_i} = 0 \tag{3.2}$$

Momentum:

$$\frac{\partial}{\partial t}(\rho u_i) + \frac{\partial}{\partial x_j}(\rho u_i u_j) = -\frac{\partial \rho}{\partial x_i} + \frac{\partial t_{ij}}{\partial x_j} \tag{3.3}$$

Energy:

$$\frac{\partial}{\partial t}\left[\rho(e+\frac{1}{2}u_i u_i)\right]+\frac{\partial}{\partial x_j}\left[\rho u_j(h+\frac{1}{2}u_i u_i)\right]=\frac{\partial}{\partial x_j}\left(u_j t_{ij}\right)-\frac{\partial q_j}{\partial x_j} \tag{3.4}$$

Viscous stress tensor (t_{ij}) can be expressed as:

$$t_{ij}=2\mu(s_{ij}-\frac{1}{3}\frac{\partial u_k}{\partial x_k}\delta_{ij}) \tag{3.5}$$

Strain-rate tensor (s_{ij}) can be stated as:

$$s_{ij}=\frac{1}{2}\left(\frac{\partial u_i}{\partial x_j}+\frac{\partial u_i}{\partial x_i}\right) \tag{3.6}$$

where;

ρ : density,

t : time,

u_i, u_j : velocity in tensor notation,

h : specific enthalpy,

e : specific internal energy,

μ : dynamic viscosity,

δ_{ij} : Kronecker delta.

Beside Favre-Averaged Navier-Stokes Equations, conduction, convection and radiation equations are used [29]:

1-D Conduction :

$$q_x^{"}=-k\frac{dT}{dx} \tag{3.7}$$

where;

k : thermal conductivity,

T : temperature,

q''_x : heat flux in x direction,

Convection:

$$q'' = h\left(T_{base\_ave} - T_{surr}\right) \tag{3.8}$$

where;

q" : heat flux

h : convection heat transfer coefficient,

T_{base_ave} : average temperature of base plate,

T_{surr} : temperature of surrounding.

Alternatively, convection heat transfer rate can be written as [17]:

$$Q_{conv} = h_{avg} A_T \eta_o \Delta T_{lm} \tag{3.9}$$

where;

h_{avg} : average heat transfer coefficient,

A_T : total heat transfer area,

η_o : overall efficiency of fin array,

ΔT_{lm} : logarithmic mean temperature difference.

Radiation :

$$Q_{rad} = \frac{\sigma\left(T_{base\_ave}^4 - T_{surr}^4\right)}{\frac{1-\varepsilon_{fin}}{\varepsilon_{fin} A_{rad}} + \frac{1}{A_{rad} F_{(fin)(surr)}} + \frac{1-\varepsilon_{sur}}{\varepsilon_{surr} A_{surr}}} \tag{3.10}$$

where;

σ : Stefan Boltzmann constant (5.67 x 10^{-8} W/m^2K^4),

ε_{fin}, ε_{surr} : emissivity of fin and surrounding, respectively,

A_{rad}, A_{surr} : radiation heat transfer area of fin and surrounding, respectively,

$F_{(fin)\rightarrow(surr)}$: view factor of fin to surrounding.

Following equation can be written on the basis of energy conservation [30]:

$$Q_{input} = Q_{conv} + Q_{rad} + Q_{ins} \tag{3.11}$$

where;

Q_{input} : heat input,

Q_{conv} : convection heat transfer rate,

Q_{rad} : radiation heat transfer rate,

Q_{ins} : heat transfer rate through insulation layer.

3.2 Parametrization

Square, cylindrical and plate fins as illustrated in Figure 3.1 are used in the present study. The geometrical optimization procedure is applied for heat transfer augmentation, then heat transfer performance comparison is done between geometrically optimized fins with three different profiles. Dimensions of the base plate and height of the fins are constant in this study.

Fin height is an important parameter due to the manufacturing and heat transfer efficiency concerns. According to infinite fin approach [2], higher fin height increases heat transfer rate of a single fin upto some point, heat transfer performance will not significantly improve beyond this point as temperature value of the fin tip converges to the ambient temperature. According to Çengel [2], fin height values, which transfer 76.2 percentage of the maximum heat transfer rate that infinitely long fin perform, are found as 41 mm, 35 mm and 70 mm for a single square, cylindrical and plate fin,

respectively after the numerical and experimental studies. However, increasing fin height results in higher pressure drop for a fin array. So, thermal performance of the fin array worsens. In manufacturing concerns, The ratio between the fin height and inter-fin spacing value can be at a maximum value of 10 for aluminum alloys to get desired inter-fin spacings in milling which is most common, fast and cheap production technique for a fin array. Moreover, higher fin length will increase the weight and cost. Furthermore, researchers [17], [21], [26] used fins whose height varies from 10 mm to 20 mm in their experimental studies. Fin height (H) is taken as 20 mm, when the factors mentioned above are considered together. Overall surface efficiency is found around 0.97 for all three fin arrays. Base plate whose edge length (L and W) is 100 mm has a square cross-section and its thickness (B) is taken as 10 mm.

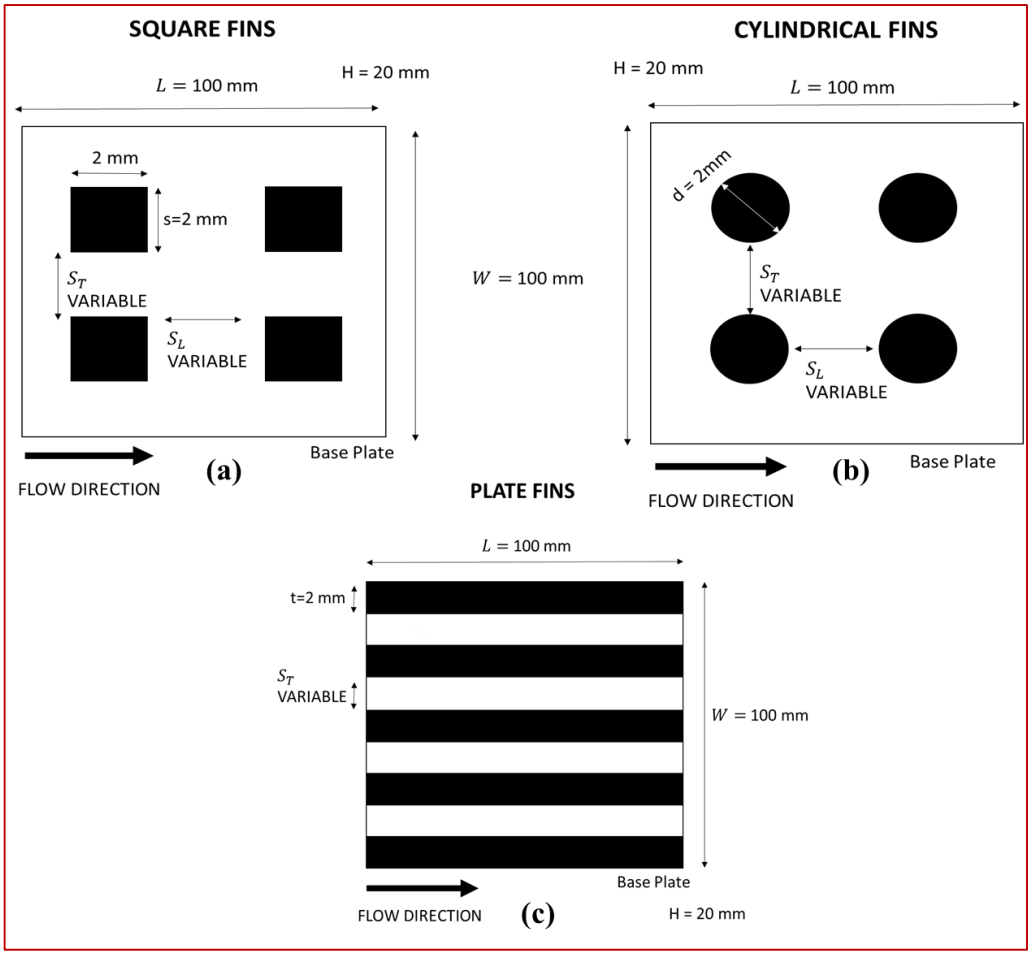

Figure 3.1 Geometric parameters for (a) square, (b) cylindrical, (c) plate fins

Non-dimensional spanwise (S_T/W) and streamwise (S_L/L) spacings have 5 different values. 25 different geometries presented in Table 3.1 and Table 3.2 are obtained for square and cylindrical fins. Plate fins have only 5 different geometries as tabulated in Table 3.3. Parametrization results in 55 different geometries.

Table 3.1 Non-dimensional spanwise and streamwise spacing values for square fins

Non-dimensional Parameters		**S_L/L**				
		0.0500	**0.0316**	**0.0208**	**0.0138**	**0.0088**
S_T/W	**0.0500**	Geom. 1	Geom. 2	Geom. 3	Geom. 4	Geom. 5
	0.0316	Geom. 6	Geom. 7	Geom. 8	Geom. 9	Geom. 10
	0.0208	Geom.11	Geom. 12	Geom. 13	Geom. 14	Geom. 15
	0.0138	Geom. 16	Geom. 17	Geom. 18	Geom. 19	Geom. 20
	0.0088	Geom. 21	Geom. 22	Geom. 23	Geom. 24	Geom. 25

Table 3.2 Non-dimensional spanwise and streamwise spacing values for cyl. fins

Non-dimensional Parameters		**S_L/L**				
		0.0500	**0.0316**	**0.0208**	**0.0138**	**0.0088**
S_T/W	**0.0500**	Geom. 26	Geom. 27	Geom. 28	Geom. 29	Geom. 30
	0.0316	Geom. 31	Geom. 32	Geom. 33	Geom. 34	Geom. 35
	0.0208	Geom.36	Geom. 37	Geom. 38	Geom. 39	Geom. 40
	0.0138	Geom. 41	Geom. 42	Geom. 43	Geom. 44	Geom. 45
	0.0088	Geom. 46	Geom. 47	Geom. 48	Geom. 49	Geom. 50

Table 3.3 Non-dimensional spanwise and streamwise spacing values for plate fins

Non-dimensional Parameters		**S_L/L**
		-
S_T/W	**0.0500**	Geom. 51
	0.0316	Geom. 52
	0.0208	Geom. 53
	0.0138	Geom. 54
	0.0088	Geom. 55

Diameter of a cylindrical fin (d), strip thickness of a plate fin (t) and edge length of a square fin (s) are assumed as characteristic length (D_h) and taken as 2 mm. Equalizing thickness or diameter of fins result in same free-stream area. Reynolds number is calculated based on maximum flow velocity and characteristic length of a single fin as in literature [7], [10]. So, Reynolds number is kept constant for fins with different profiles and same spanwise spacing as illustrated in Figure 3.2 for a fair comparison. Free-stream velocities of 3 m/s, 5 m/s and 7 m/s are selected to observe the effect of Reynolds number on the optimum design points.

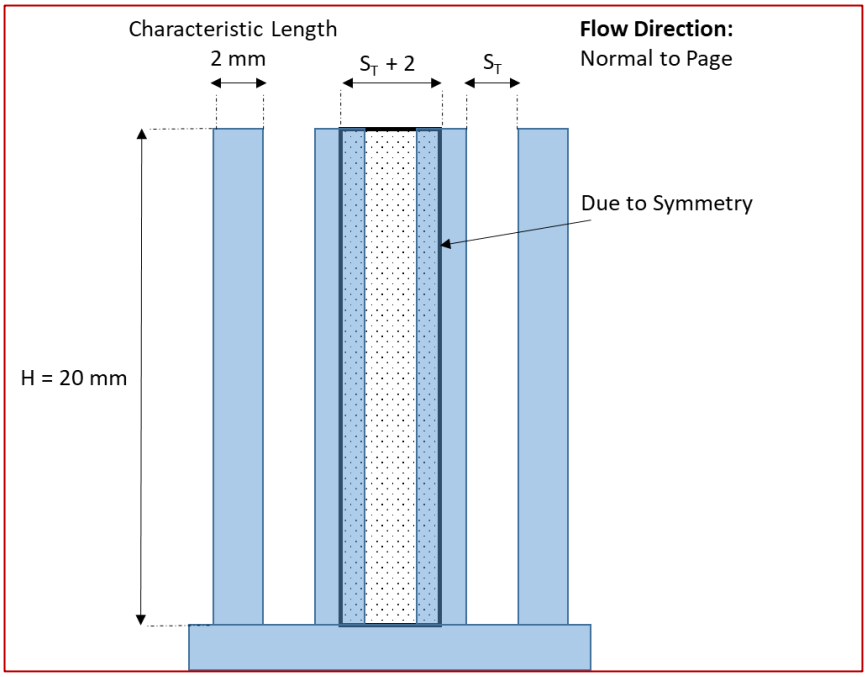

Figure 3.2 Fin orientation normal to flow direction

Equations used during Reynolds number calculation can be written as:

$$Re = \frac{U_{max} D_h}{\nu} \tag{3.12}$$

$$U_{max} = U \frac{S_T + 2}{S_T} \tag{3.13}$$

where;

U : free-stream velocity (3 m/s, 5 m/s and 7 m/s),

U_{max} : maximum velocity,

D_h : characteristic length (2 mm),

S_T : spanwise spacing (5 mm, 3.16 mm, 2.08 mm, 1.38 mm and 0.88 mm),

ν : kinematic viscosity of air (15.89×10^{-6} m^2/s @ 300 K) [29].

Reynolds number varies between 528.6, for S_T = 5 mm and U = 3 m/s case, and 2883 for S_T = 0.88 mm and U = 7 m/s case. Therefore, the flow in present study can be defined in transition regime according to Zukauskas [7] .

Products' data sheets of Intel world biggest CPU supplier are considered in order to define a heat input boundary condition which is close to current technological trends and limits as an order of magnitude. Thermal design power (tdp) defined as heat dissipation amount of a processor when all cores are active under high-complexity load is taken as reference for heat boundary condition [31]. Intel Xeon Platinum 8164 processor with 26 cores introduced in the 3rd quarter of 2017 and used in high-performance workstations has 150 W thermal design power [31].

The dependency of non-dimensional spanwise spacing values which result in minimum T_{max} at the base plate on heat input rate is researched. In order to define higher heat inputs than 150 W, technological limits are investigated and it is observed that Intel Xeon Phi 7290F processor [32] with 72 cores introduced in 2016 dissipates 260 W which is the maximum thermal design power (tdp) among the other processors [33] commercially available by Intel. Therefore, heat input values of 200 W and 250 W with free-stream velocities of 3 m/s, 5 m/s, and 7 m/s are applied to geometries optimized in streamwise direction for each fin with different profiles. T_{max} of fins are compared with each other for different boundary conditions.

Geometrical, hydraulic and thermal parameters used in numerical and experimental studies are presented for square, cylindrical and plate fins in Table 3.4, Table 3.5 and Table 3.6, respectively.

Table 3.4 Numerical and experimental study matrix for square fins

Square		Numerical									Experimental		
		Q (W)									Q (W)		
		150			200			250			150		
		U (m/s)			U (m/s)			U (m/s)			U (m/s)		
S_L/L	S_T/W	3	5	7	3	5	7	3	5	7	3	5	7
0.0500	0.0500	✔[a]	✔	✔	O[b]	O	O	O	O	O	✔	✔	✔
	0.0316	✔	✔	✔	O	O	O	O	O	O	✔	✔	✔
	0.0208	✔	✔	✔	O	O	O	O	O	O	✔	✔	✔
	0.0138	✔	✔	✔	O	O	O	O	O	O	X[c]	X	X
	0.0088	✔	✔	✔	O	O	O	O	O	O	X	X	X
0.0316	0.0500	✔	✔	✔	O	O	O	O	O	O	✔	✔	✔
	0.0316	✔	✔	✔	O	O	O	O	O	O	✔	✔	✔
	0.0208	✔	✔	✔	O	O	O	O	O	O	✔	✔	✔
	0.0138	✔	✔	✔	O	O	O	O	O	O	X	X	X
	0.0088	✔	✔	✔	O	O	O	O	O	O	X	X	X
0.0208	0.0500	✔	✔	✔	O	O	O	O	O	O	✔	✔	✔
	0.0316	✔	✔	✔	O	O	O	O	O	O	✔	✔	✔
	0.0208	✔	✔	✔	O	O	O	O	O	O	✔	✔	✔
	0.0138	✔	✔	✔	O	O	O	O	O	O	X	X	X
	0.0088	✔	✔	✔	O	O	O	O	O	O	X	X	X
0.0138	0.0500	✔	✔	✔	✔	✔	✔	✔	✔	✔	X	X	X
	0.0316	✔	✔	✔	✔	✔	✔	✔	✔	✔	X	X	X
	0.0208	✔	✔	✔	✔	✔	✔	✔	✔	✔	X	X	X
	0.0138	✔	✔	✔	✔	✔	✔	✔	✔	✔	X	X	X
	0.0088	✔	✔	✔	✔	✔	✔	✔	✔	✔	X	X	X
0.0088	0.0500	✔	✔	✔	O	O	O	O	O	O	X	X	X
	0.0316	✔	✔	✔	O	O	O	O	O	O	X	X	X
	0.0208	✔	✔	✔	O	O	O	O	O	O	X	X	X
	0.0138	✔	✔	✔	O	O	O	O	O	O	X	X	X
	0.0088	✔	✔	✔	O	O	O	O	O	O	X	X	X

[a] : performed or manufactured
[b] : not necessary to be performed
[c] : not manufacturable

Table 3.5 Numerical and experimental study matrix for cylindrical fins

Cylindrical		Numerical									Experimental		
		Q (W)									Q (W)		
		150			200			250			150		
		U (m/s)			U (m/s)			U (m/s)			U (m/s)		
S_L/L	S_T/W	3	5	7	3	5	7	3	5	7	3	5	7
0.0500	0.0500	✔	✔	✔	0	0	0	0	0	0	✔	✔	✔
	0.0316	✔	✔	✔	0	0	0	0	0	0	✔	✔	✔
	0.0208	✔	✔	✔	0	0	0	0	0	0	✔	✔	✔
	0.0138	✔	✔	✔	0	0	0	0	0	0	X	X	X
	0.0088	✔	✔	✔	0	0	0	0	0	0	X	X	X
0.0316	0.0500	✔	✔	✔	0	0	0	0	0	0	✔	✔	✔
	0.0316	✔	✔	✔	0	0	0	0	0	0	✔	✔	✔
	0.0208	✔	✔	✔	0	0	0	0	0	0	✔	✔	✔
	0.0138	✔	✔	✔	0	0	0	0	0	0	X	X	X
	0.0088	✔	✔	✔	0	0	0	0	0	0	X	X	X
0.0208	0.0500	✔	✔	✔	0	0	0	0	0	0	✔	✔	✔
	0.0316	✔	✔	✔	0	0	0	0	0	0	✔	✔	✔
	0.0208	✔	✔	✔	0	0	0	0	0	0	✔	✔	✔
	0.0138	✔	✔	✔	0	0	0	0	0	0	X	X	X
	0.0088	✔	✔	✔	0	0	0	0	0	0	X	X	X
0.0138	0.0500	✔	✔	✔	0	0	0	0	0	0	X	X	X
	0.0316	✔	✔	✔	0	0	0	0	0	0	X	X	X
	0.0208	✔	✔	✔	0	0	0	0	0	0	X	X	X
	0.0138	✔	✔	✔	0	0	0	0	0	0	X	X	X
	0.0088	✔	✔	✔	0	0	0	0	0	0	X	X	X
0.0088	0.0500	✔	✔	✔	✔	✔	✔	✔	✔	✔	X	X	X
	0.0316	✔	✔	✔	✔	✔	✔	✔	✔	✔	X	X	X
	0.0208	✔	✔	✔	✔	✔	✔	✔	✔	✔	X	X	X
	0.0138	✔	✔	✔	✔	✔	✔	✔	✔	✔	X	X	X
	0.0088	✔	✔	✔	✔	✔	✔	✔	✔	✔	X	X	X

Table 3.6 Numerical and experimental study matrix for plate fins

Plate		Numerical									Experimental		
		Q (W)									Q (W)		
		150			200			250			150		
		U (m/s)			U (m/s)			U (m/s)			U (m/s)		
S_L/L	S_T/W	3	5	7	3	5	7	3	5	7	3	5	7
-	0.0500	✔	✔	✔	✔	✔	✔	✔	✔	✔	✔	✔	✔
	0.0316	✔	✔	✔	✔	✔	✔	✔	✔	✔	✔	✔	✔
	0.0208	✔	✔	✔	✔	✔	✔	✔	✔	✔	✔	✔	✔
	0.0138	✔	✔	✔	✔	✔	✔	✔	✔	✔	X	X	X
	0.0088	✔	✔	✔	✔	✔	✔	✔	✔	✔	X	X	X

CHAPTER 4

NUMERICAL STUDY

4.1 Numerical Domain

A channel whose dimensions are 400 mm (height) x 600 mm (width) x 500 mm (length) is placed in a numerical domain whose dimensions are 750 mm (height) x 800 mm (width) x 750 mm (length) as shown in Figure 4.1. An insulation layer which has same width and length with channel and 150 mm height is placed below the channel. Fin, gap pad and heater are placed to the 250 mm in front of the inlet of the channel.

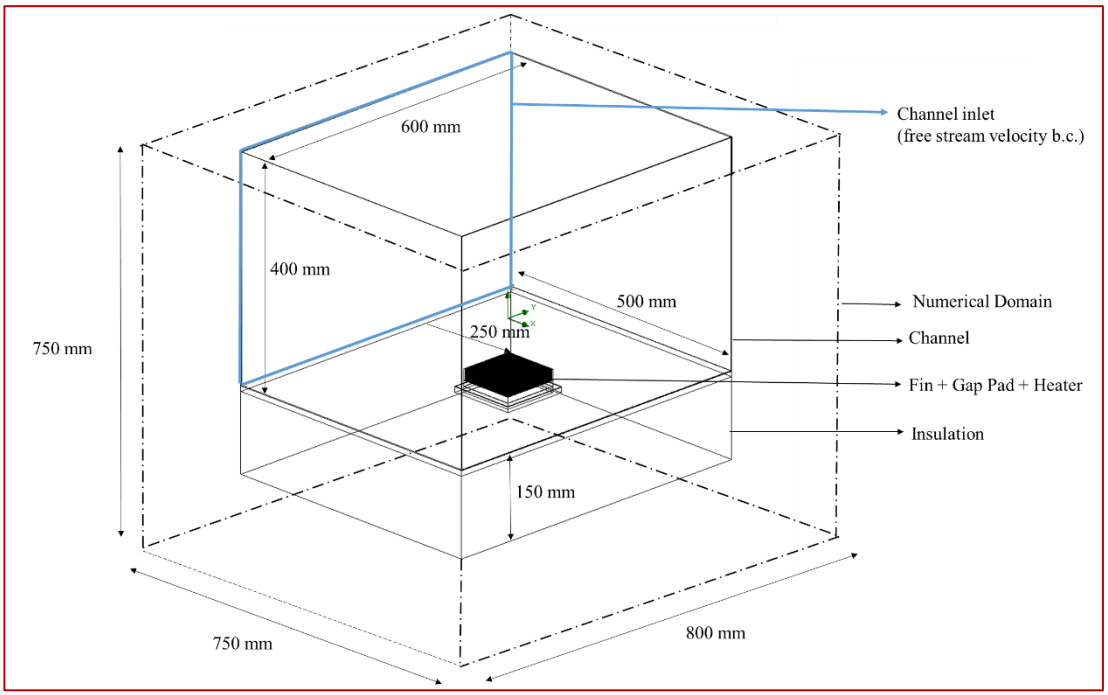

Figure 4.1 General view of the numerical domain

Preliminary analyses are conducted to see the effect of the channel on the free-stream air velocity. Channel's width and height that do not accelerate flow in contracting areas around fin are assumed as channel's cross-section dimensions normal to the flow. Free-stream velocity of 7 m/s, which is maximum velocity in present study, is applied to a square fin having 0.0088 non-dimensional spacing in both stream and spanwise directions and velocity distribution are presented in Figure 4.2. Channel's height and width value of 600 mm and 400 mm, respectively are assumed to be sufficient for external flow condition in the channel.

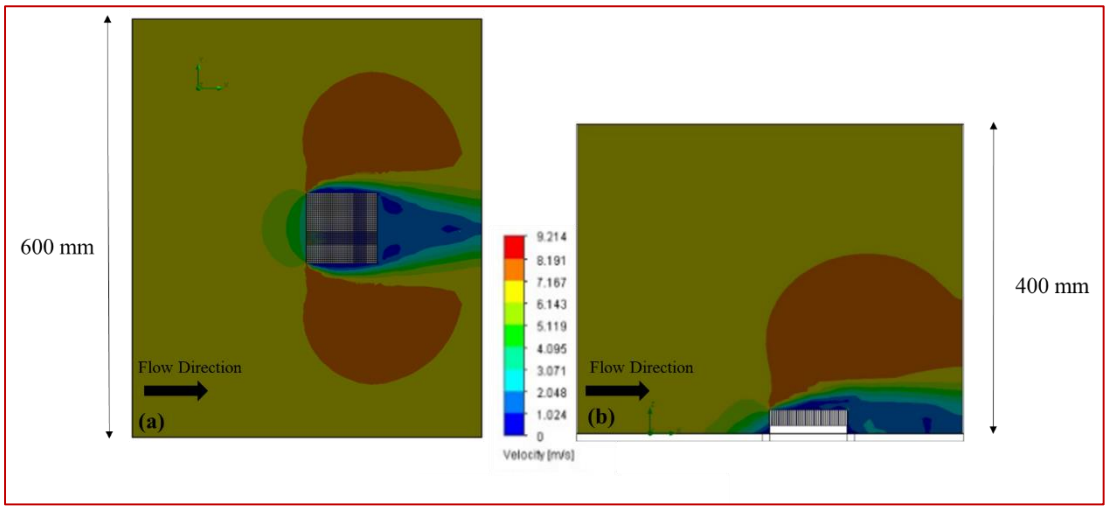

Figure 4.2 Flow pattern around fin (a) top view of channel, (b) side view of channel

4.2 Numerical Approach

FLoEFD 14 is used as a commercial CFD software to conduct analyses. FLoEFD solves the Navier-Stokes equations based on Finite Volume Method (FVM) [27]. FLoEFD store all variables at the mass center of the cells. This method is known as cell-centered Finite Volume Method [34] .

In FVM, the domain is discritized into control volumes, and governing equations specified in section 3.1 are integrated over these control volumes.

General conservation equation for a variable (ϕ) can be denoted as [34]:

$$\frac{\partial(\rho\phi)}{\partial t} + \nabla.\left(\rho\vec{v}\phi\right) = \nabla.\left(\Gamma^{\phi}\nabla\phi\right) + Q^{\phi} \tag{4.1}$$

where;

Q^{Φ} : source term,

$\vec{v}$: velocity vector,

Γ^{Φ} : diffusion coefficient,

t : time,

ρ : density.

First and second term on the left-hand side in equation (4.1) are transient and convective terms respectively, while first and second term on the right-hand side are diffusion and source terms. In present study, transient term is neglected and equation (4.1) turns into following form [34]:

$$\nabla.\left(\rho\vec{v}\phi\right) = \nabla.\left(\Gamma^{\phi}\nabla\phi\right) + Q^{\phi} \tag{4.2}$$

Equation (4.2) is integrated over the control volume C seen in Figure 4.3 and this operation can be stated as [34]:

$$\int_{V_c}\nabla.\left(\rho\vec{v}\phi\right)\mathrm{dV} = \int_{V_c}\nabla.\left(\Gamma^{\phi}\nabla\phi\right)\mathrm{dV} + \int_{V_c}Q^{\phi}\mathrm{dV} \tag{4.3}$$

where;

$\int_{V_c}$: volume integral over the volume V_c.

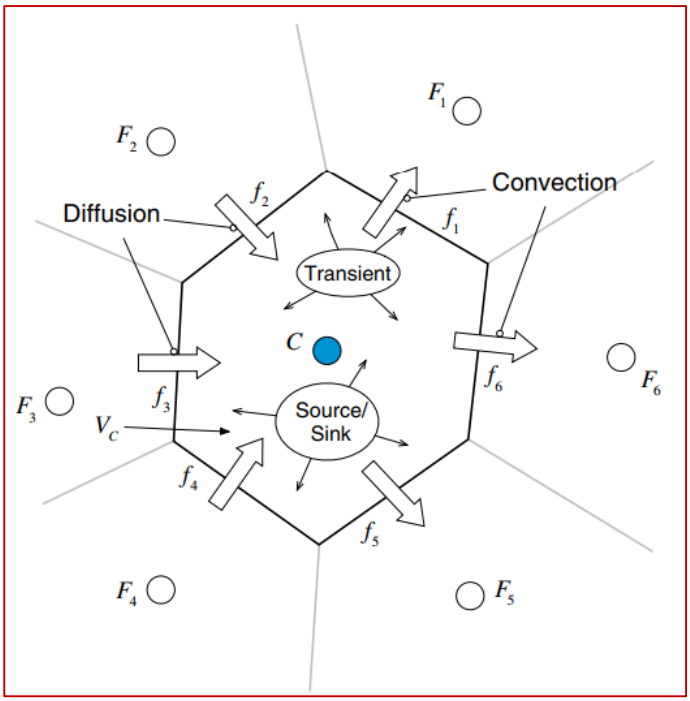

Figure 4.3 Control volume [34]

By applying Gauss's Divergence Theorem, equation (4.3) turns into following form [34]:

$$\oint_{\partial V_c} \left(\rho \vec{v} \phi\right).\mathrm{dS} = \oint_{\partial V_c} \left(\Gamma^{\phi} \nabla \phi\right).\mathrm{dS} + \oint_{V_c} Q^{\phi} \mathrm{dV} \tag{4.4}$$

where;

$\oint_{\partial V_c}$: surface integral over the volume V_c.

Discretization of convective terms are done by second order upwind scheme. In second order upwind scheme, a linear profile for the value of ϕ is constructed between the node U and C as shown in Figure 4.4. Then, value at face (f) is extrapolated. Arrow ($\overset{V_f}{\rightarrow}$) indicates the direction of flow [34].

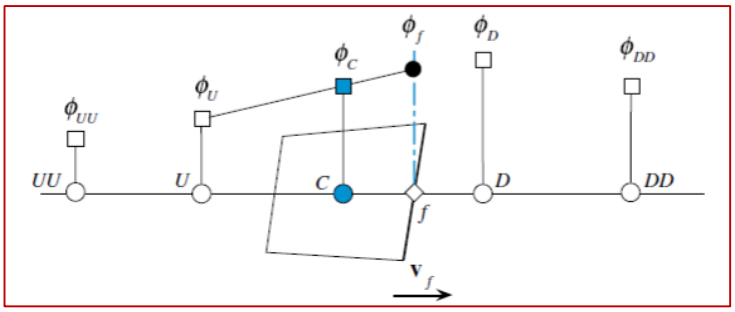

Figure 4.4 Upwind scheme [34]

Central difference scheme is used for discretization of diffusive terms. Value of ϕ at face e is estimated by an interpolation between node C and E as seen in Figure 4.5.

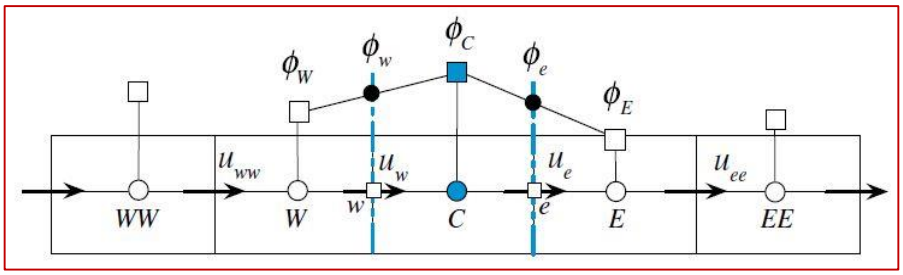

Figure 4.5 Central difference scheme [34]

After discretization procedure, Semi-Implicit Method for Pressure-Linked Equations (SIMPLE) is used for solving linear algebraic systems obtained from Finite Volume Method [27].

4.3 Numerical Analyses

Analyses are conducted at steady state conditions. Radiation is neglected. Ambient temperature and pressure are set to 25 ℃ and 1 atm, respectively. Free-stream velocities are set to 3 m/s, 5 m/s and 7 m/s at the inlet of the channel. 1 atm pressure is defined at the outlet of the channel.

The heater and gap pad is placed below the fin as illustrated in Figure 4.6. Dimensions of heater are 100 mm (width) x 100 mm (length) x 10 mm (height). Heater is defined as a volumetric heat source with power values of 150 W, 200 W and 250 W. Gap pad material is placed between the heater and fin. Gap pad material, whose thickness is 0.5 mm, has thermal conductivity and specific heat values of 5 W/mK and 1 kJ/kgK, respectively [35]. Fins are placed above the gap pad. Fin material is selected as 6063-T6 series aluminum alloy having thermal conductivity and specific heat values of 200 W/mK and 0.9 kJ/kgK, respectively [36]. Sides and bottom of the heater are covered with an insulation material having thermal conductivity and specific heat values of 0.048 W/mK and 0.84 kJ/kgK, respectively [37].

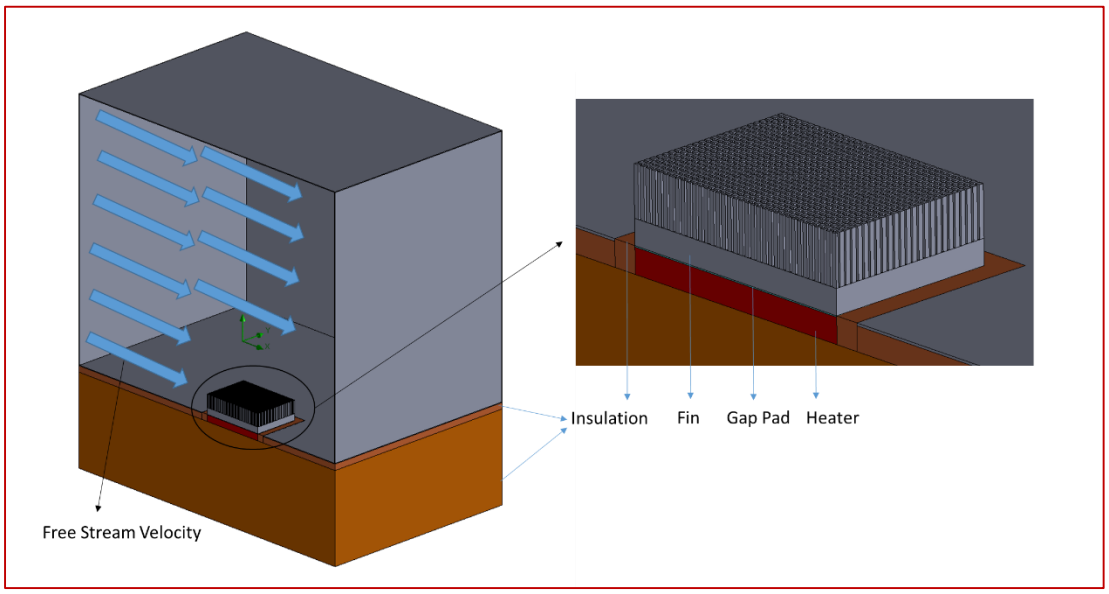

Figure 4.6 Section view of the channel

FLoEFD uses Favre-Averaged Navier-Stokes equations to model turbulent flow [27]. $k-\varepsilon$ turbulence model is used in software. Dong et al. [38] and Yuan et al. [39] mention the agreement of $k-\varepsilon$ turbulence with the experimental results in their studies related to heat transfer investigation about fins.

Goal is a hydraulic or thermal parameter which is monitored during the iterations and used for finishing calculations. The convergence criteria for a goal is automatically calculated by FLoEFD and goal is assumed as converged, when the dispersion between last iterations is below the convergence criteria [40]. Maximum temperature on the upper surface of the base plate is considered as the goal in the present study. Mesh refinement is applied after the convergence of goal as presented in Figure 4.7. After the second refinement, solution is ended by software when goal converges. Mesh refinement procedure in more details is discussed in section 4.4.

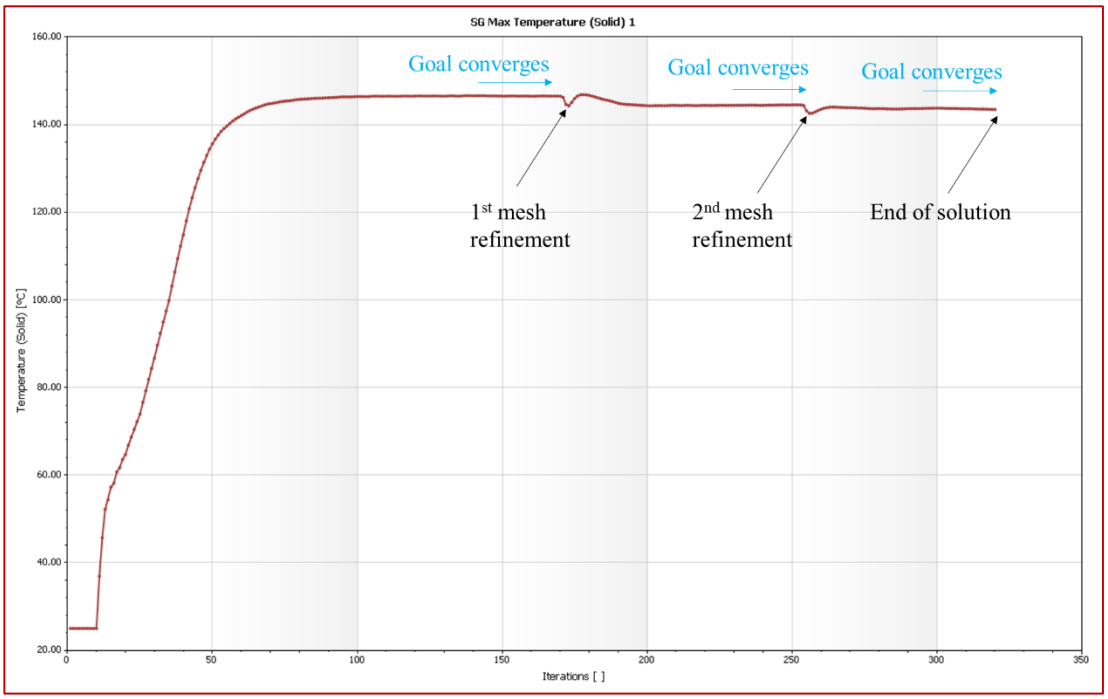

Figure 4.7 Convergence of a goal

4.4 Meshing and Mesh Independency Procedure

FLoEFD uses cartesian rectangular cells [40]. There are 3 types of cells called as solid cells, fluid cells and partial cells. Solid and fluid cells are constructed in solid and fluid mediums, respectively. Partial cells occur near the solid/fluid boundaries and have

region both in the solid and fluid mediums. Denser mesh is used near the fin region as shown in Figure 4.8 as important part of the problem is solved here.

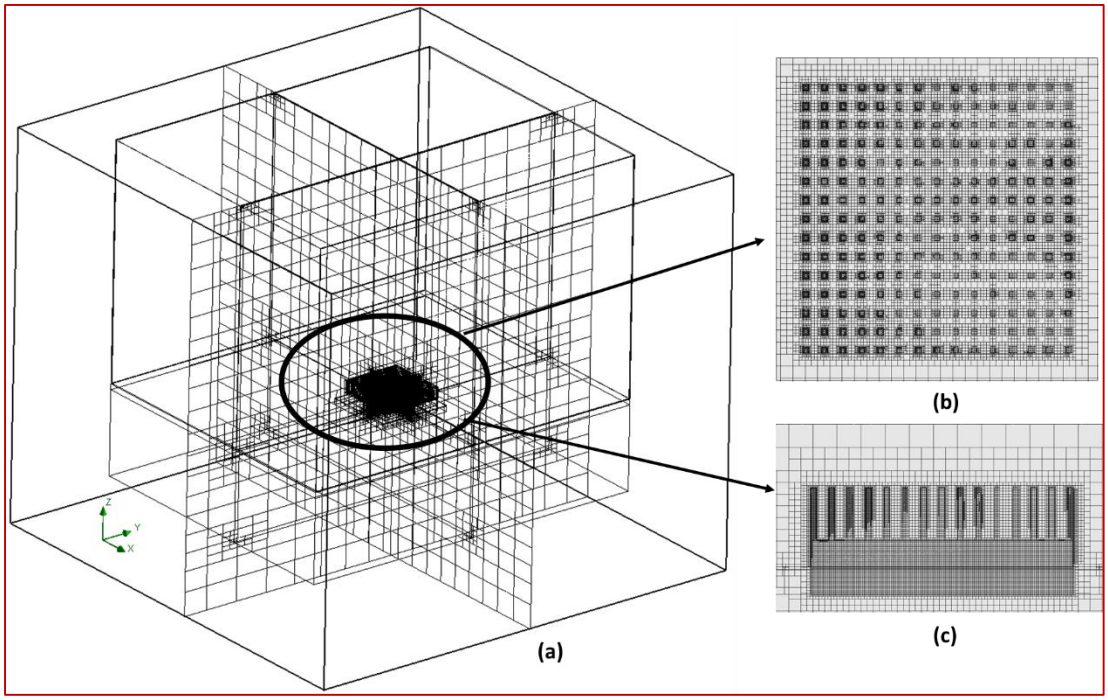

Figure 4.8 View of the mesh (a) for numerical domain, (b) from top of fin, (c) from side of fin

FLoEFD software has a solution adaptive meshing technique which can be used to get mesh independent solutions [40]. Mesh is constructed over the whole domain before the solution and mesh near the fin region is locally refined during the solution in present study. Local truncation error between neighbour cells (LTE) is calculated by software at refinement stage. If this error is large enough, the cells are divided into maximum $8^{n_{ref}}$ subcells [40]. If LTE is small, cells are merged.

where;

n_{ref} is the refinement level.

Refinement level is taken as 2 in present study and refinement is done twice during the solutions. Mesh and T_{max} details for the most intense geometries of square (S_T/W & S_L/L =0.0088), cylindrical (S_T/W & S_L/L =0.0088) and plate (S_T/W = 0.0088) fins with free-stream velocity of 3 m/s and heat input value of 150 W are presented in Table 4.1.

Table 4.1 Mesh refinement results

Fin Geometry	**Mesh Type**	**Initial**	**T_{max} (°C)**	**1st ref.**	**T_{max} (°C)**	**2nd ref.**	**T_{max} (°C)**
Square	Total	2503361	**180.60**	3721011	**172.15**	3999450	**172.02**
	Solid	1416539		1627279		1642591	
	Fluid	282349		809899		984649	
	Partial	804473		1283833		1372210	
Cylindrical	Total	1797222	**152.33**	2789654	**159.04**	5995017	**159.37**
	Solid	1119078		1319465		2233301	
	Fluid	300856		689213		1826019	
	Partial	377288		780976		1935697	
Plate	Total	2339246	**212.67**	3871462	**217.81**	5899530	**217.95**
	Solid	1562472		2049330		2739495	
	Fluid	213534		595798		1223680	
	Partial	563240		1226334		1936355	

CHAPTER 5

EXPERIMENTAL WORK

5.1 Experimental Setup

Experimental setup presented in Figure 5.1 and Figure 5.2 is constructed in Heat Transfer Laboratory at Aselsan Gölbaşı Campus. Width of the tunnel is 600 mm, height of the tunnel is 400 mm and length of it is 1500 mm. Base plate of the wind tunnel is constructed with 3 mm sheet aluminum, whereas other sides of the wind tunnel are made width 5 mm thick plexiglass for possible future studies like application of flow visualization techniques to investigate the hydrodynamic behaviour of airflow around the fin. Plexiglass panel is also used to be casing for fans at the inlet of the tunnel. Outlet of the tunnel is open to atmosphere.

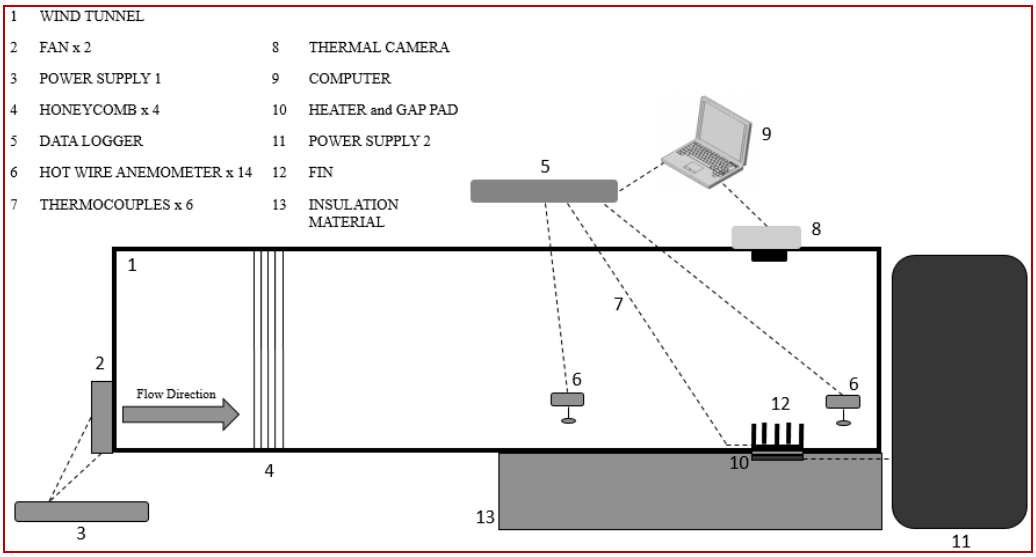

Figure 5.1 Experimental setup schematic

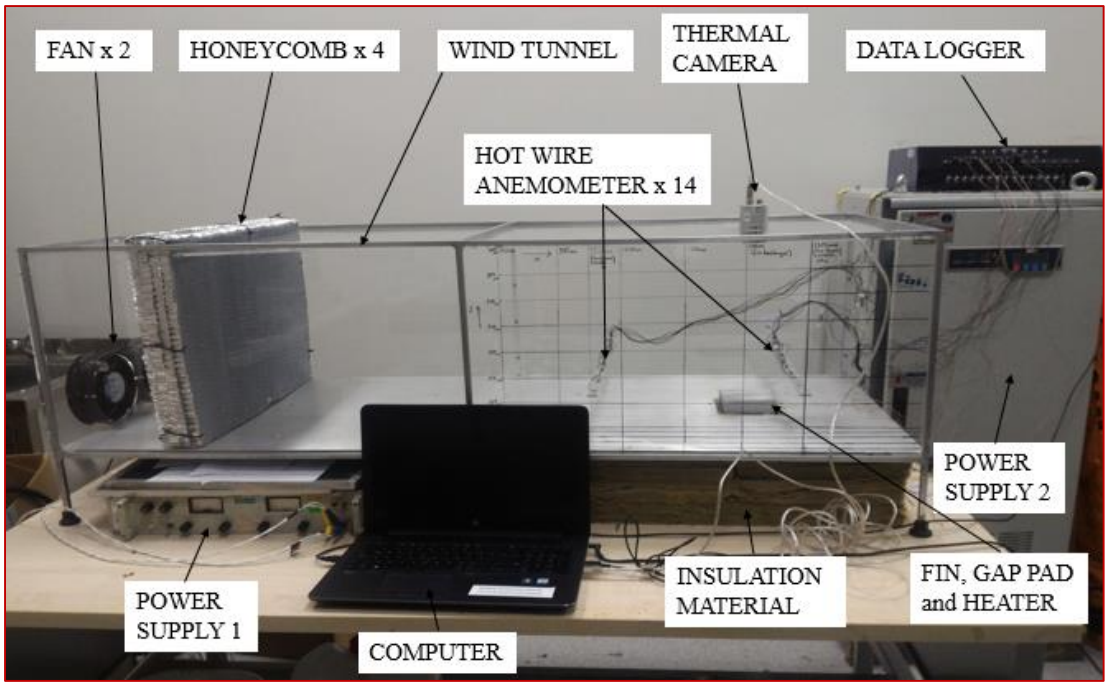

Figure 5.2 Experimental setup

Pumping power is supplied by two identical axial fans located at the inlet of the tunnel as shown in Figure 5.3. Fan maximum speed and airflow capacities are 7000 rpm and 710 m^3/h, respectively [41].

Figure 5.3 Fans

Fan’s nominal voltage value is 24 VDC and it can operate in a voltage range between 16 VDC and 36 VDC [41]. The fans are connected in parallel to Power Supply 1. Power Supply 1 seen in Figure 5.4 has voltage capacity up to 40 VDC and current capacity up to 5A.

Figure 5.4 Power supply 1

Flow straighteners are used to get uniform velocity profile along the tunnel. In the present study, aluminum honeycomb panels with 18 mm thickness and 6 mm cell size are used. The number of aluminum honeycomb panels is determined as 4 after iterations and measurements. End of honeycombs is placed at x = 255 mm as illustrated in Figure 5.5. Velocity profile of the channel is measured by hot wire anemometers placed at x = 950 mm. Fin is placed at x = 1200 mm.

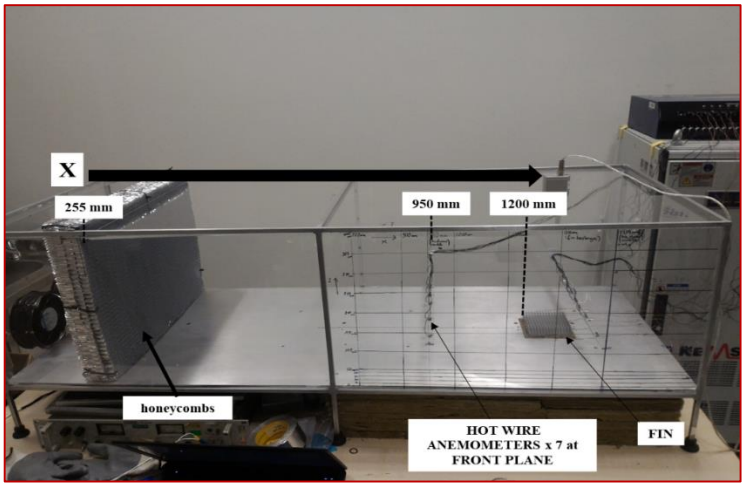

Figure 5.5 Honeycomb and velocity measurement positions

Seven different hot wire anemometers are placed at y = 50 mm, 150 mm, 250 mm, 300 mm, 350 mm, 450 mm and 550 mm positions as shown in Figure 5.6. Position of the bar holding anemometers are shifted from z = 10 mm to z = 50 mm with 10 mm increments and from z = 50 mm to 400 mm with 50 mm increments.

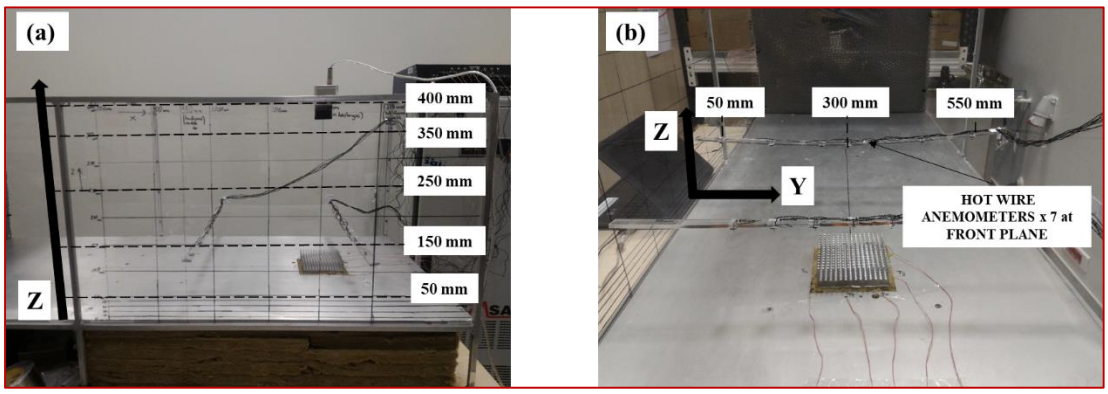

Figure 5.6 Hot wire anemometer locations (a) side view, (b) back view

It is aimed to establish 3 m/s free-stream velocity profile around the fin region. Velocity values are measured for each point and their averages are tabulated in Table 5.1. The region shown in red refers the effective velocity area for 3 m/s free-stream velocity. The free-stream velocity tends to decrease at the outside of this region through the walls of the channel. It is clearly seen from Table 5.1 that fin that has 30 mm height and 100 mm width remains inside the effective velocity area. Same measurements are done for other free-stream velocities of 5 m/s and 7 m/s, too.

Table 5.1 Velocity measurements for the honeycomb integration

VELOCITY (m/s)		Y (mm)						
		50	150	250	300	350	450	550
Z (mm)	400	0.5	0.4	0.4	0,5	0.5	0.6	0.5
	350	0.5	0.4	0.4	0,5	0.6	0.6	0.6
	300	0.6	0.4	0.4	0,5	0.6	0.7	0.6
	250	0.6	0.5	0.4	0,5	0.6	0.6	0.6
	200	0.6	1.0	0.9	0,8	0.8	0.7	0.6
	150	0.9	2.1	2.4	1,9	2.3	1.5	0.6
	100	0.8	3.4	3.0	3.5	3.1	3.0	0.8
	50	0.9	3.3	3.2	3.5	3.0	3.3	0.9
	40	0.9	3.2	3.1	3.4	2.9	3.6	1.1
	30	0.9	2.9	3.2	3.4	2.9	3.6	1.2
	20	0.9	2.5	3.0	3.3	3.0	3.5	1.1
	10	0.9	2.3	2.8	3.2	2.7	3.0	1.2

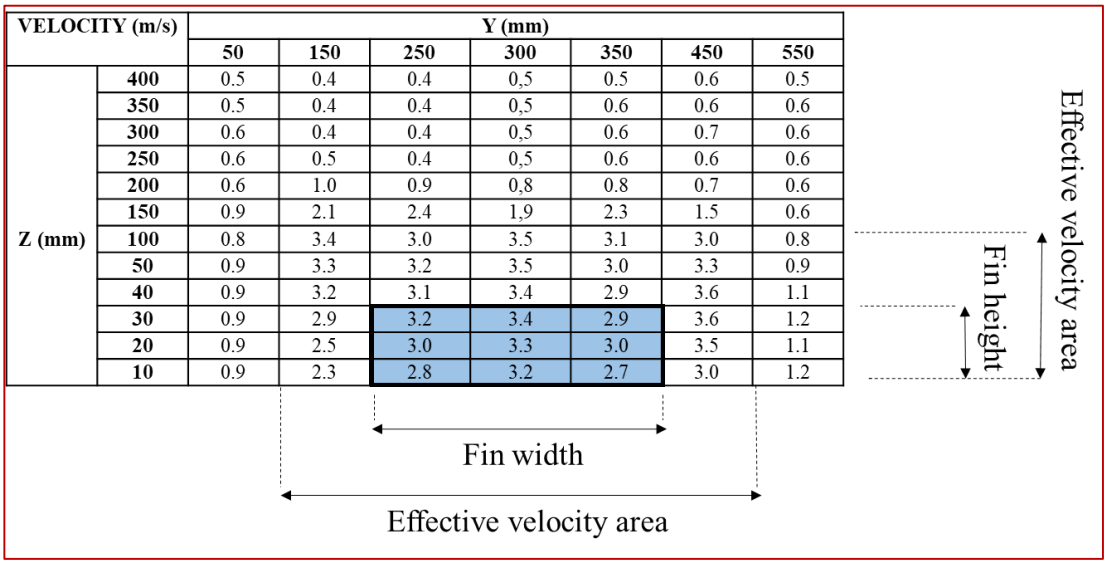

Plate heater that can operate up to 300 W is produced by casting aluminum over resistance. The heater has 100 mm x 100 mm cross-section and 10 mm height. The heater is connected to Power Supply 2 presented in Figure 5.7. Power Supply 2 can provide maximum 75 A at 115 VAC. Voltage and current are measured with multimeter and clamp meter, respectively [42], [43].

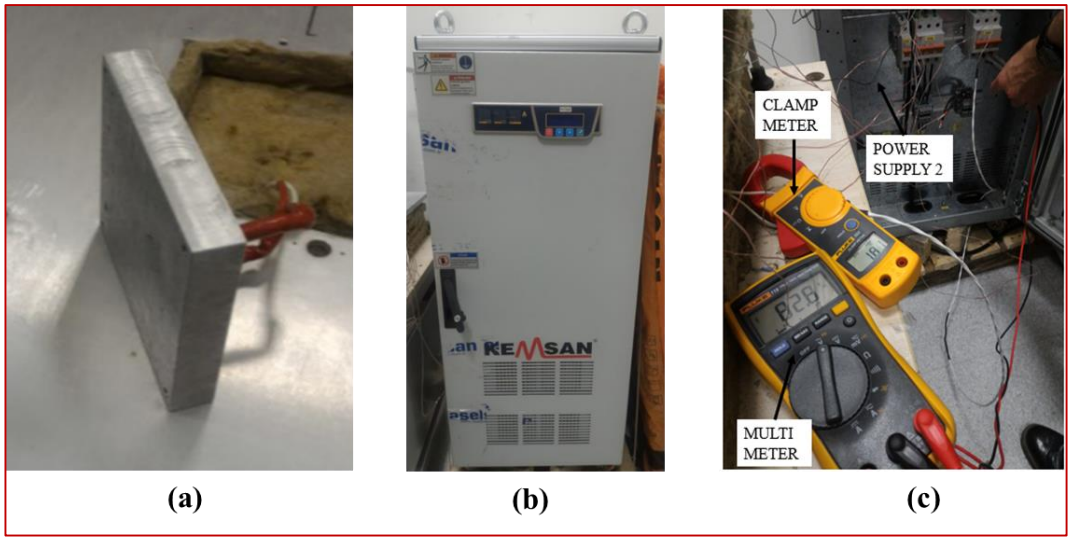

Figure 5.7 (a) Heater, (b) Power supply 2, (c) multimeter and clamp meter

Gap pad shown in Figure 5.8 is made of fiberglass-reinforced filler and polymer. It is placed between fin and heater to compensate surface irregularities and improve thermal conductivity from heater to fin. It has a thickness value of 0.5 mm, a thermal conductivity value of 5 W/mK and a specific heat value of 1 kJ/kgK [35].

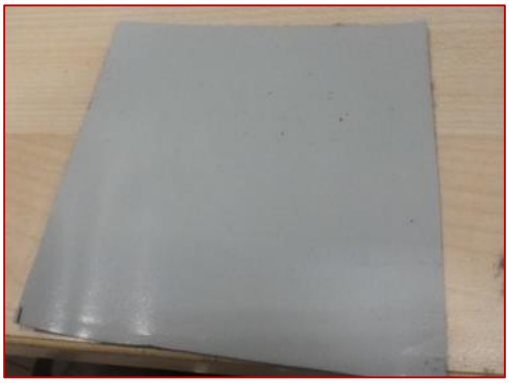

Figure 5.8 Gap pad

Stone wool which has 150 mm thickness, 750 mm length and 600 mm width is placed under and near the heater for insulation. Insulation material can operate up to 600°C and has a thermal conductivity value of 0.048 W/mK, a specific heat value of 0.84 kJ/kgK [37]. Velocity and temperature measurements are stored a data logger shown in Figure 5.9 [44]. The data logger can be managed from its own software installed on a computer. J type thermocouples are used for temperature measurements at fin, heater and insulation material. J type thermocouples perform better at low-temperature applications and nonoxidizing atmosphere [45]. Hot wire anemometers are used for air velocity and air temperature measurements.

Figure 5.9 Data logger

The thermal camera shown in Figure 5.10 is used to monitor temperature distribution over the upper surface of the base plate and determine maximum temperature. It has 640 x 480 resolution and can be managed from a computer installed its own software [46].

Figure 5.10 Thermal camera

Six J type thermocouples are used. T_1, T_2, T_3 and T_4 are used to measure temperature of the base plate, at the front side, back side, right side and left side, respectively as presented in Figure 5.11. T_5 is placed the bottom of the heater. T_6 is used to measure bottom temperature of the insulation material.

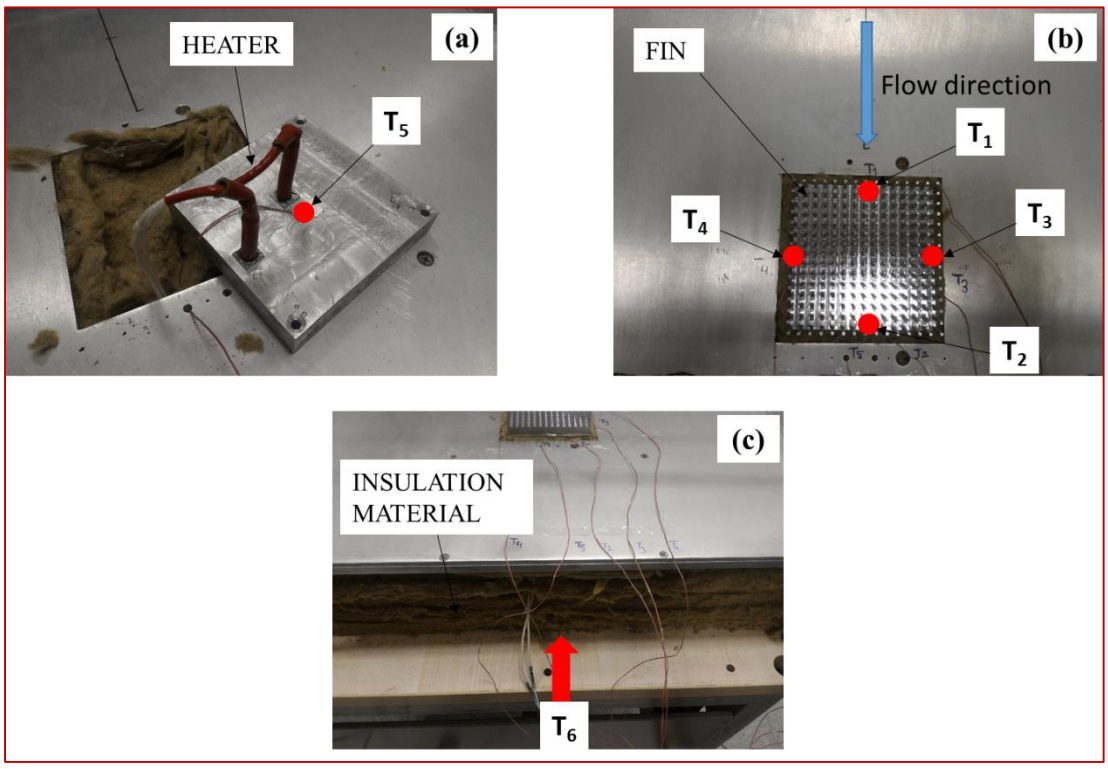

Figure 5.11 Thermocouples position (a) fin, (b) heater, (c) insulation material

15 different fins (6 square, 6 cylindrical, 3 plate) are manufactured from 6063-T6 aluminum as shown in Figure 5.12. Tape whose emissivity is known as 0.95 is stuck to the base plate of the fins. So, more accurate results are taken from the thermal camera. Some of the fins can be used by changing their streamwise and spanwise axis. More details related to the geometrical parameters of fins are presented in Table 5.2.

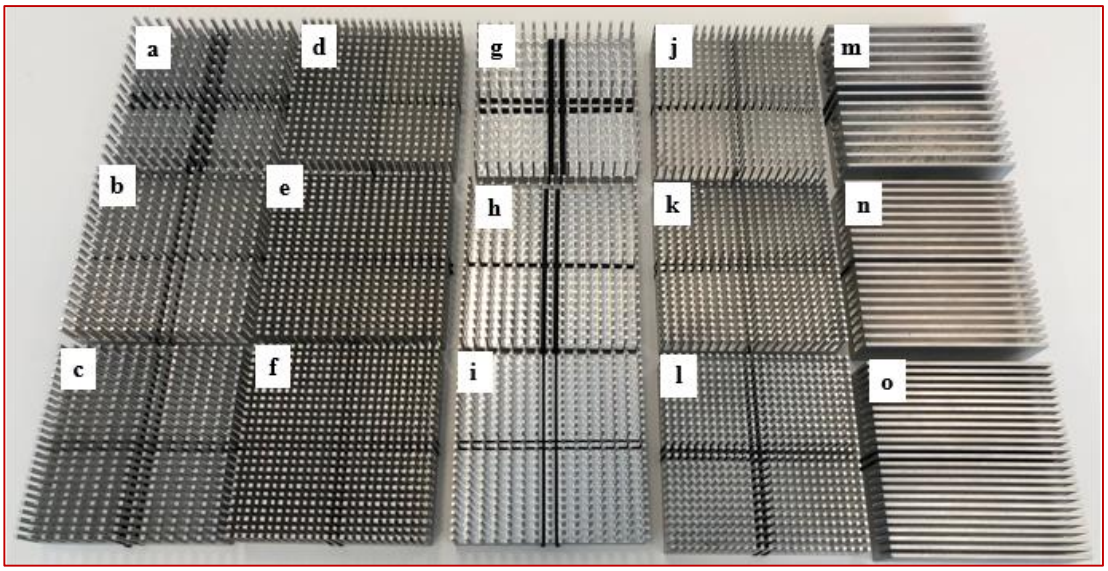

Figure 5.12 General view of manufactured fins

Table 5.2 Geometrical properties of fins

Fin Shape	N_L	N_T	S_L (mm)	S_T (mm)	Index
Square	15	15	5.00	5.00	a
	15	20	5.00	3.16	b
	15	25	5.00	2.08	c
	20	15	3.16	5.00	b
	20	20	3.16	3.16	d
	20	25	3.16	2.08	e
	25	15	2.08	5.00	c
	25	20	2.08	3.16	e
	25	25	2.08	2.08	f
Cylindrical	15	15	5.00	5.00	g
	15	20	5.00	3.16	h
	15	25	5.00	2.08	i
	20	15	3.16	5.00	h
	20	20	3.16	3.16	j
	20	25	3.16	2.08	k
	25	15	2.08	5.00	i
	25	20	2.08	3.16	k
	25	25	2.08	2.08	l
Plate	-	15	-	5.00	m
	-	20	-	3.16	n
	-	25	-	2.08	o

CHAPTER 6

NUMERICAL AND EXPERIMENTAL RESULTS

Numerical analyses are conducted for square, cylindrical and plate fins with 150 W heat input value of 150 W and free-stream velocities of 3 m/s, 5 m/s and 7 m/s. Then, non-dimensional streamwise spacing values resulting in minimum T_{max} at the base plate for all fins with three different profiles are chosen for further numerical analyses with higher heat input values (200 W and 250 W) and heat transfer performance comparison. Geometries which have non-dimensional stream and spanwise spacing values higher than 0.02 are manufactured. These geometries are experimentally studied with heat input value of 150 W and free-stream velocities of 3 m/s, 5 m/s and 7 m/s to validate numerical model.

6.1 Numerical Results

Analyses are done on a HP Z 820 workstation which has 32 cores and 64 gb RAM [47]. Calculations were conducted in around three months.

6.1.1 Square Fins with 150 W and 3 m/s, 5 m/s and 7 m/s Boundary Conditions

Numerical analyses are done for square fins with non-dimensional streamwise and spanwise spacing values varying between 0.0088 and 0.0500 for heat input value of 150 W. T_{max} relation with geometrical parameters are plotted in Figure 6.1, Figure 6.2 and Figure 6.3 for free-stream velocities of 3 m/s, 5 m/s and 7 m/s, respectively. Square fins, whose non-dimensional streamwise spacing value is 0.0138, satisfy minimum T_{max} at the upper surface of the base plate among other square fins.

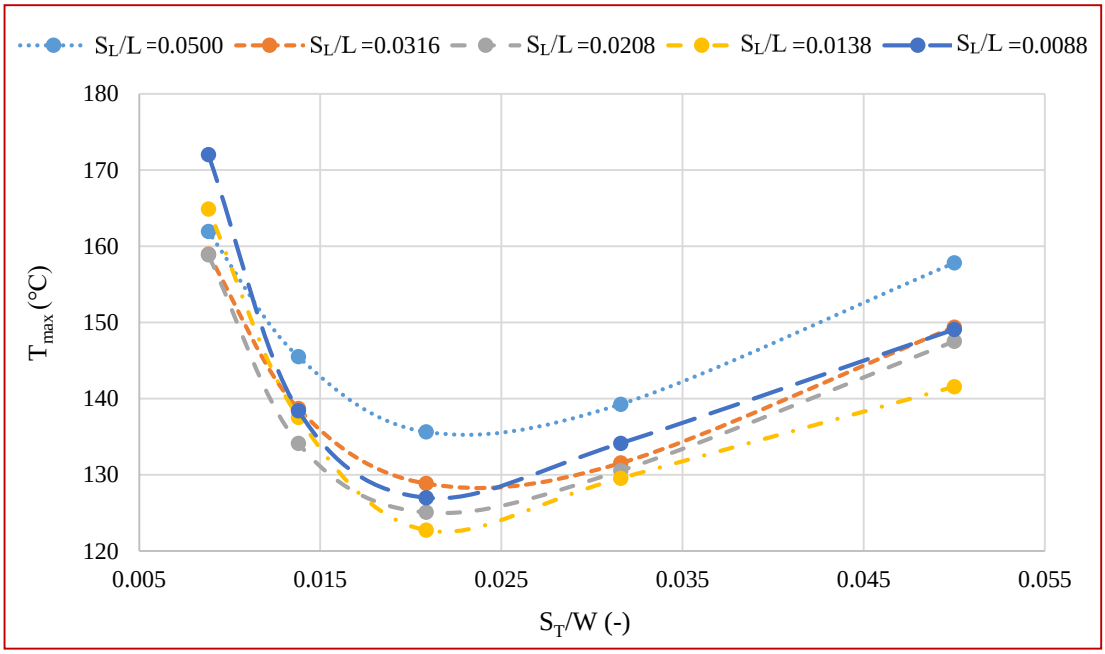

Figure 6.1 Square fins with U = 3 m/s and Q = 150 W

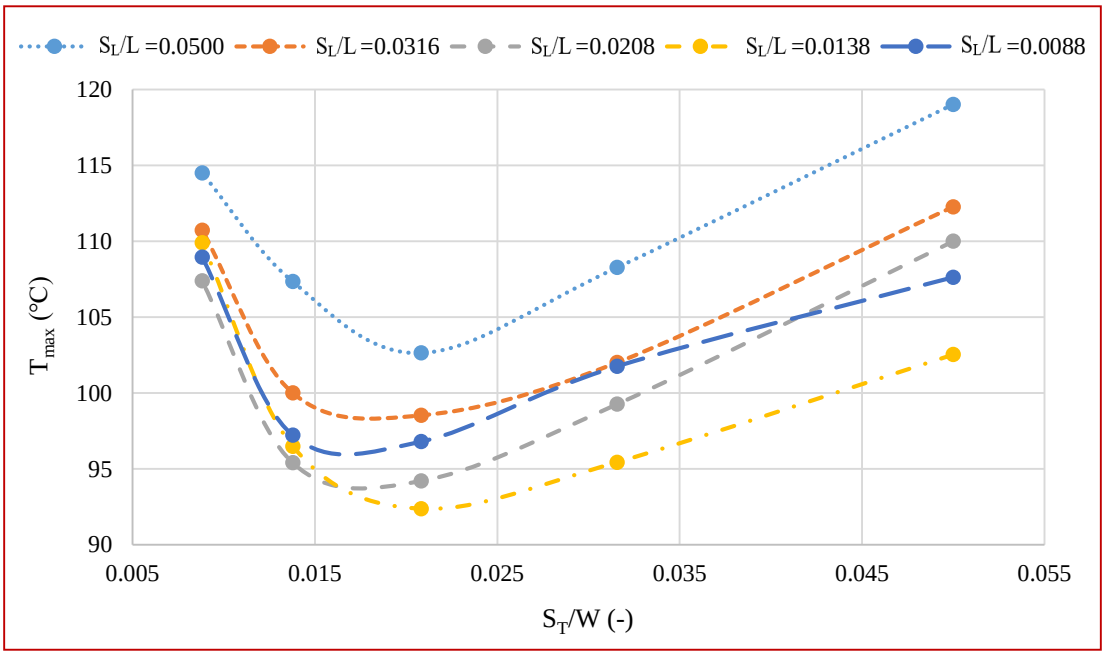

Figure 6.2 Square fins with U = 5 m/s and Q = 150 W

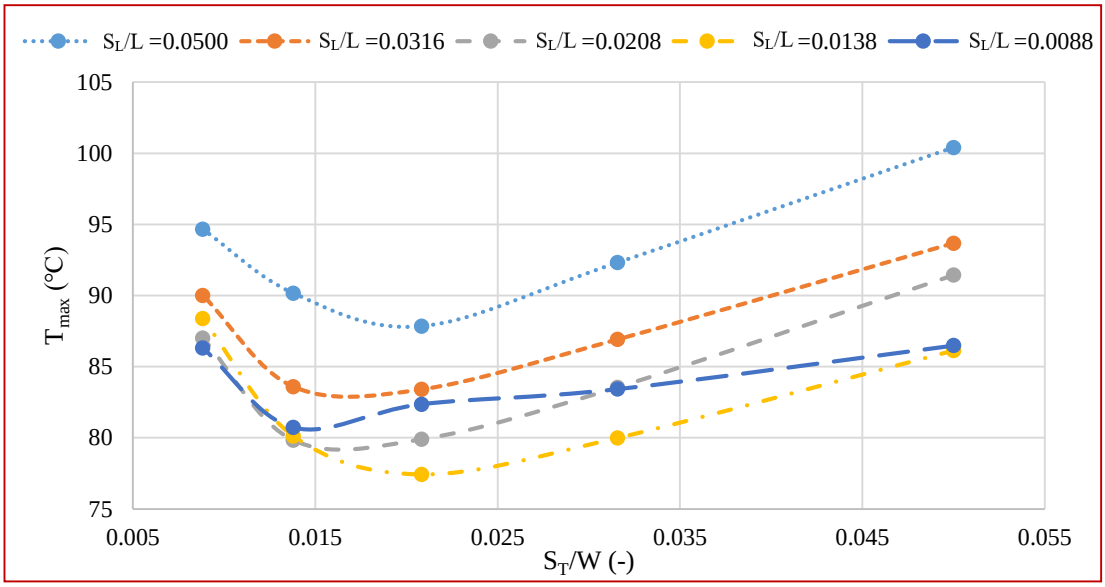

Figure 6.3 Square fins with U = 7 m/s and Q = 150 W

Temperature and velocity profiles of the square fin (S_L/L=0.0138, S_T/W=0.0208) at 7 m/s free-stream velocity are illustrated in Figure 6.4.

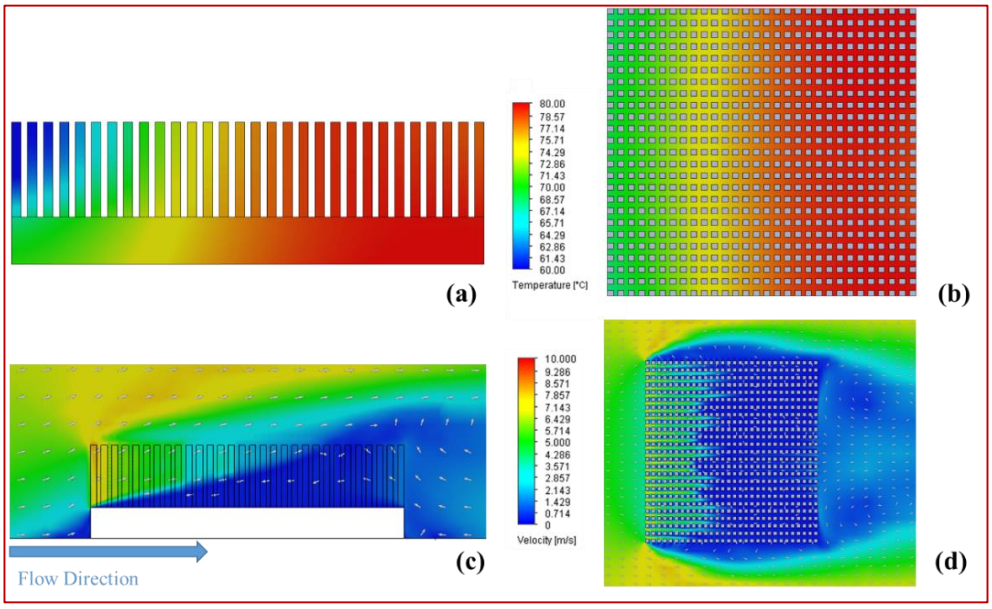

Figure 6.4 Square fin (S_L/L = 0.0138, S_T/W = 0.0208) temperature profile from (a) side, (b) top view and velocity profile from (c) side, (d) top view

6.1.2 Optimum Square Fin Configuration (S_L/L = 0.0138) in Streamwise Direction with U = 3 m/s, 5 m/s, 7 m/s and Q = 150 W, 200 W, 250 W Boundary Conditions

Numerical analyses are already done for square fins with changing non-dimensional streamwise and spanwise spacing values from 0.0088 to 0.0500 with heat input value of 150 W. Square fins whose non-dimensional streamwise spacing value satisfying minimum T_{max} among others are chosen for further analyses. The behaviour of these fins are studied in this section with heat input values of 200 W and 250 W. T_{max} relation with non-dimensional spanwise spacing value and different free-stream velocities are plotted in Figure 6.5, Figure 6.6 and Figure 6.7 for heat input values of 150 W, 200W and 250W, respectively.

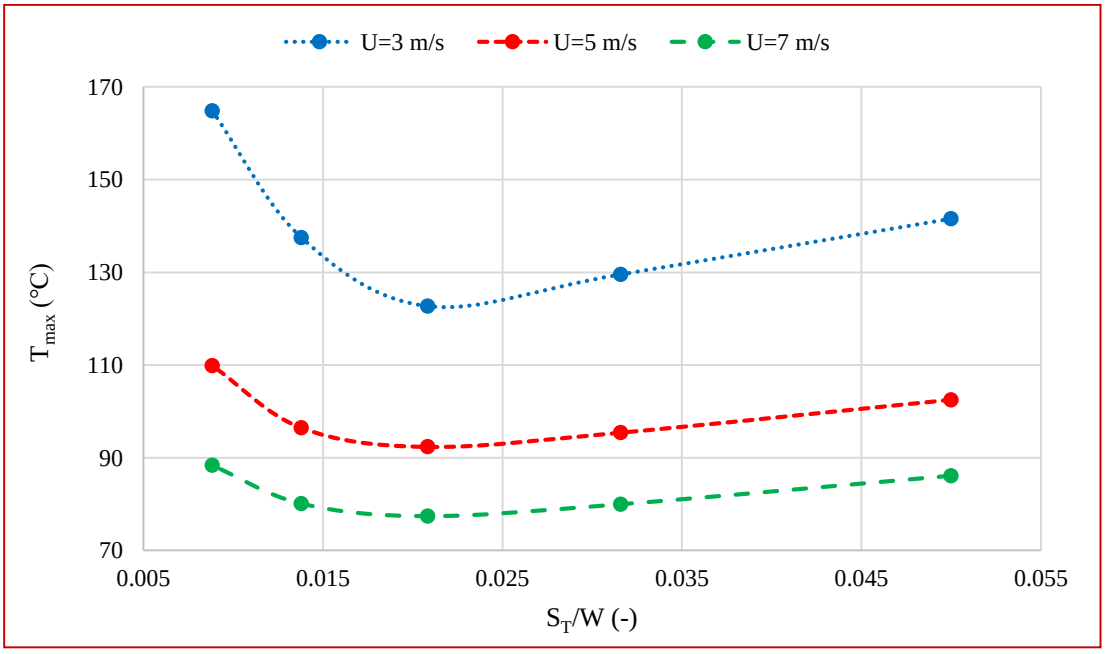

Figure 6.5 Square fins (S_L/L = 0.0138) with U = 3 m/s, 5 m/s, 7 m/s and Q = 150 W

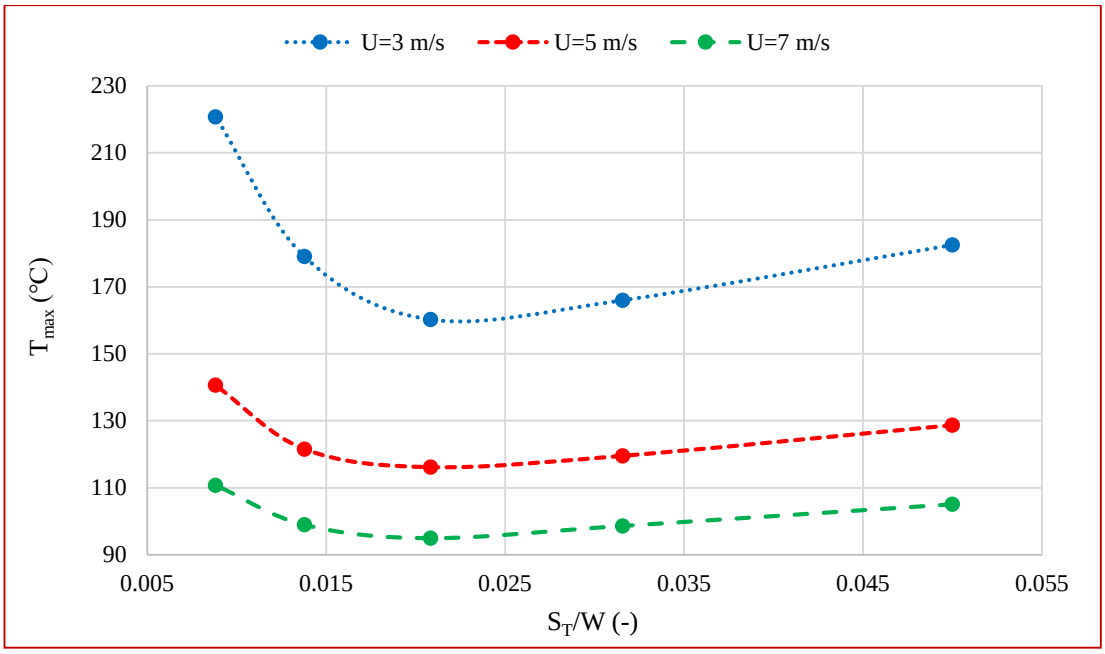

Figure 6.6 Square fins (S_L/L = 0.0138) with U = 3 m/s, 5 m/s, 7 m/s and Q = 200 W

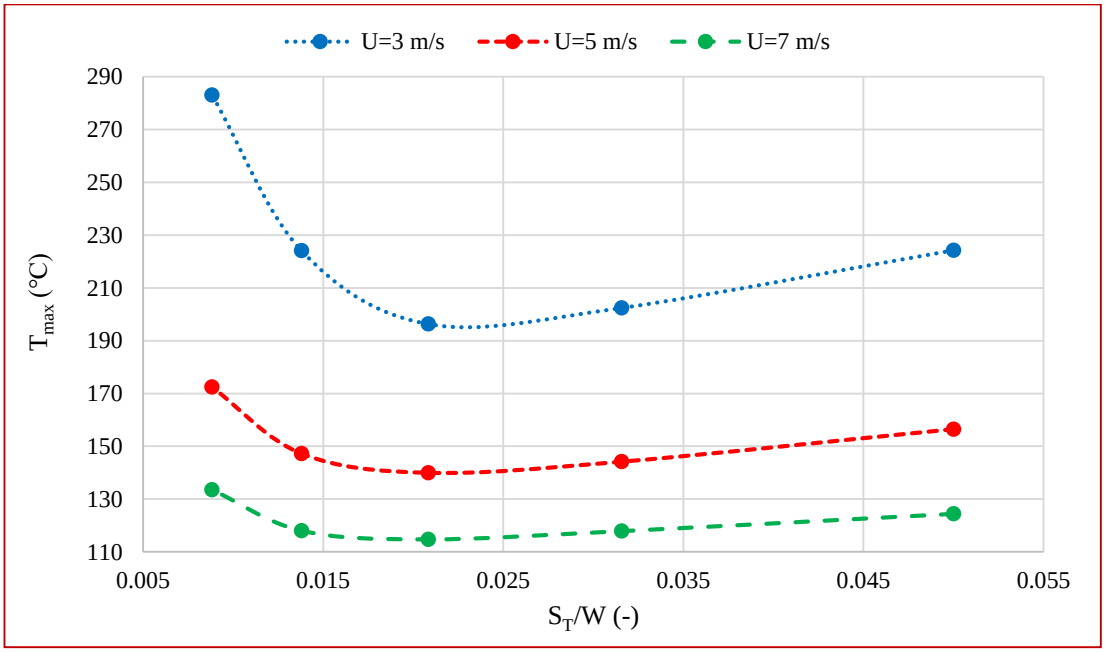

Figure 6.7 Square fins (S_L/L = 0.0138) with U = 3 m/s, 5 m/s, 7 m/s and Q = 250 W

6.1.3 Cylindrical Fins with 150 W and 3 m/s, 5 m/s and 7 m/s Boundary Conditions

Numerical analyses are done for cylindrical fins with non-dimensional streamwise and spanwise spacing values varying between 0.0088 and 0.0500 for heat input value of 150 W. T_{max} relation with geometrical parameters are illustrated in Figure 6.8, Figure 6.9 and Figure 6.10 for free-stream velocities of 3 m/s, 5 m/s and 7 m/s, respectively. Cylindrical fins, whose non-dimensional streamwise spacing value is 0.0088, satisfy minimum T_{max} at the base plate among other cylindrical fins. So, these fins have been used for further analyses with heat input values of 200 W and 250 W.

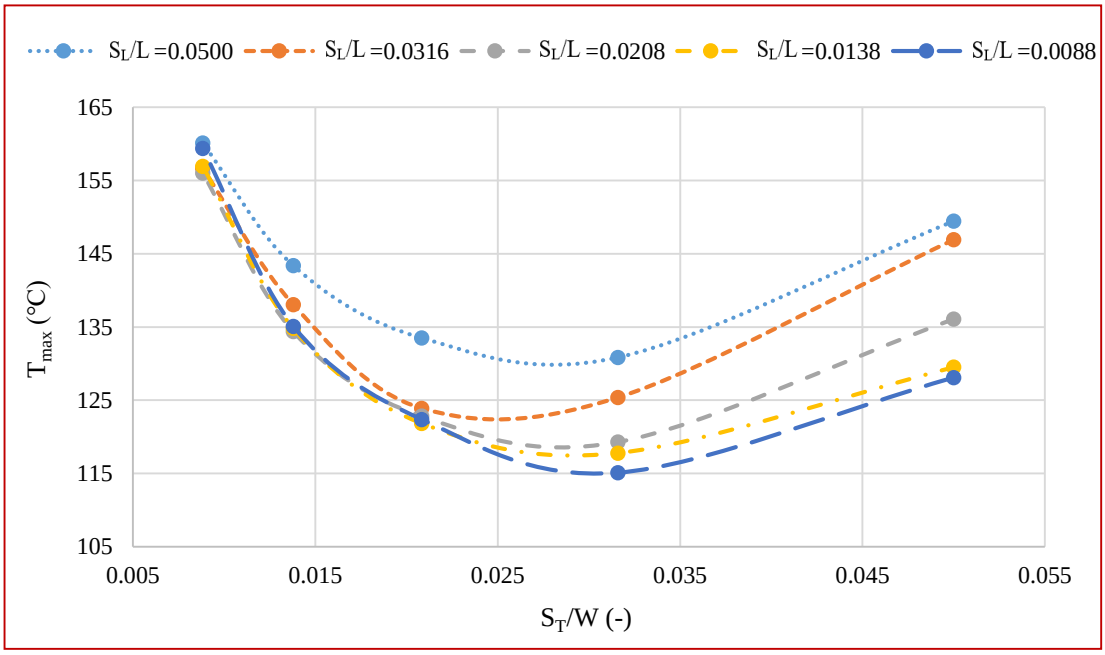

Figure 6.8 Cylindrical fins with U = 3 m/s and Q = 150 W

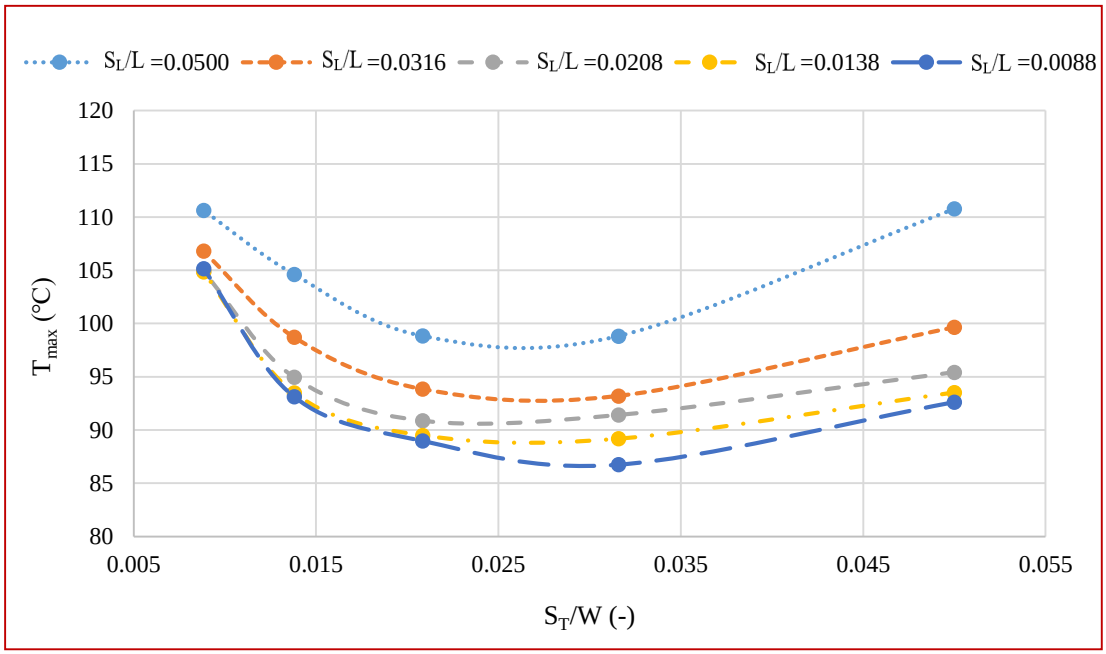

Figure 6.9 Cylindrical fins with U = 5 m/s and Q = 150 W

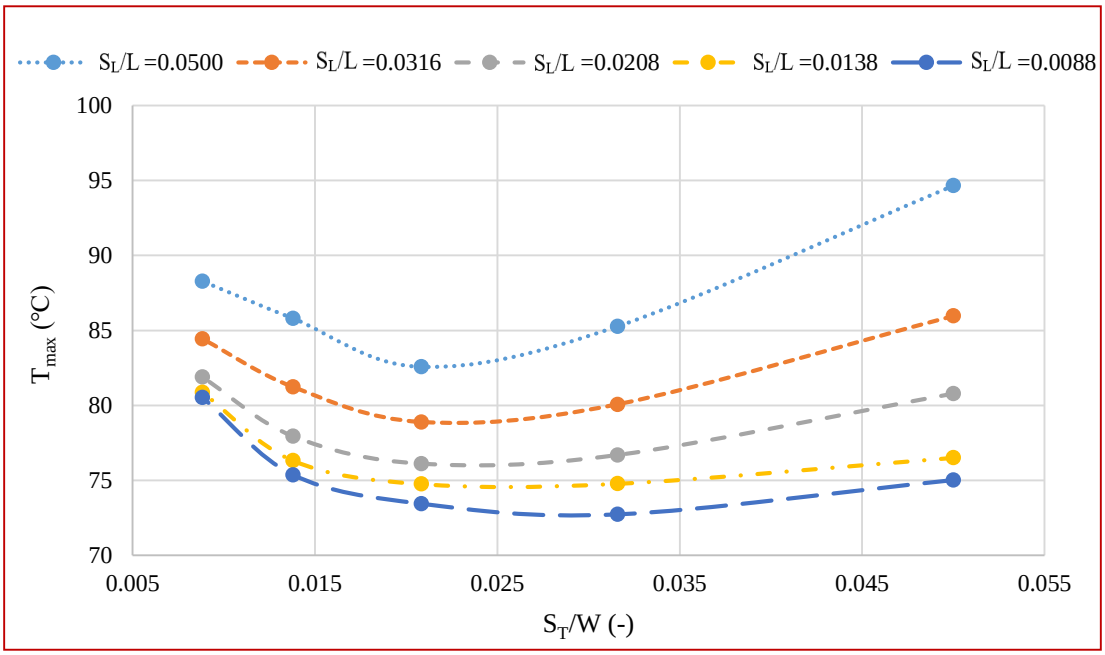

Figure 6.10 Cylindrical fins with U = 7 m/s and Q = 150 W

Temperature and velocity profiles of the cylindrical fin (S_L/L=0.0088, S_T/W=0.0316) at 7 m/s free-stream velocity are illustrated in Figure 6.11.

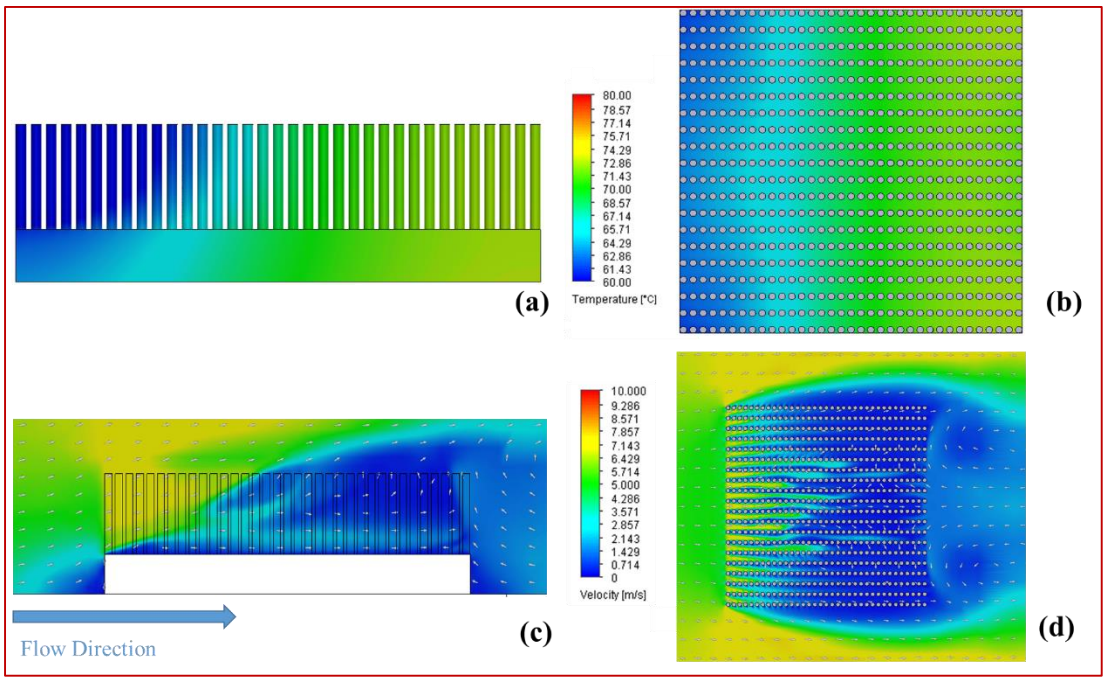

Figure 6.11 Cylindrical fin (S_L/L = 0.0088, S_T/W = 0.0316) temperature profile from (a) side, (b) top view and velocity profile from (c) side, (d) top view

6.1.4 Optimum Cylindrical Fin Configuration (S_L/L = 0.0088) in Streamwise Direction with U = 3 m/s, 5 m/s, 7 m/s and Q = 150 W, 200 W, 250 W Boundary Conditions

Cylindrical fins whose non-dimensional streamwise spacing value satisfy minimum T_{max} among others are chosen for further analyses. Behaviour of these fins are studied in this section with heat input values of 200 W and 250 W. T_{max} relation with non-dimensional spanwise spacing value and free-stream velocities are illustrated in Figure 6.12, Figure 6.13 and Figure 6.14 for heat input values of 150 W, 200 W and 250 W, respectively.

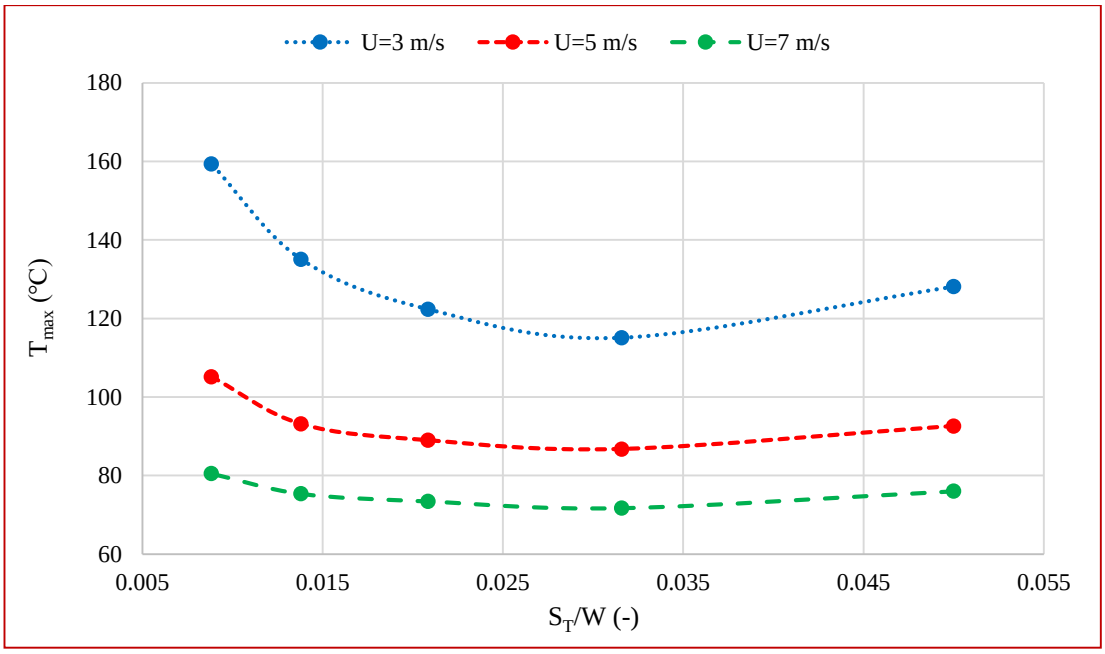

Figure 6.12 Cyl. fins (S_L/L = 0.0088) with U = 3 m/s, 5 m/s, 7 m/s and Q = 150 W

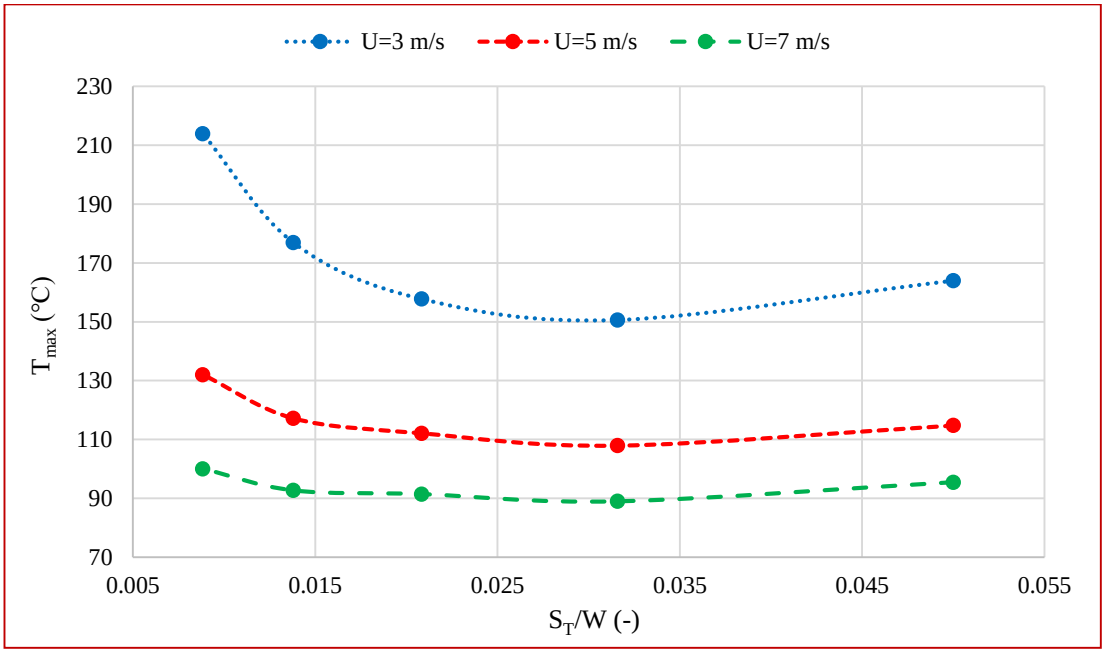

Figure 6.13 Cyl. fins (S_L/L = 0.0088) with U = 3 m/s, 5 m/s, 7 m/s and Q = 200 W

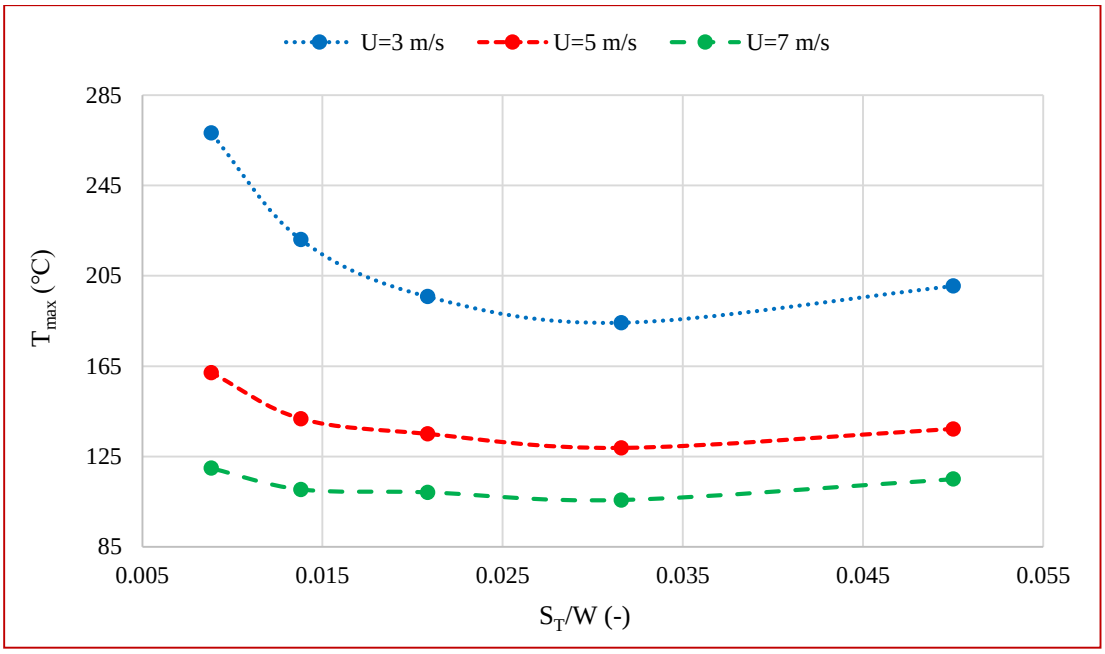

Figure 6.14 Cyl. fins (S_L/L = 0.0088) with U = 3 m/s, 5 m/s, 7 m/s and Q = 250 W

6.1.5 Plate Fins with 150 W and 3 m/s, 5 m/s and 7 m/s Boundary Conditions

Numerical analyses are performed for plate fins with non-dimensional streamwise and spanwise spacing values varying from 0.0088 to 0.0500 with heat input value of 150 W. T_{max} relation with non-dimensional spanwise spacing and free-stream velocities are figured out in Figure 6.15. Temperature and velocity profiles of the plate fin at 7 m/s free velocity are illustrated in Figure 6.16.

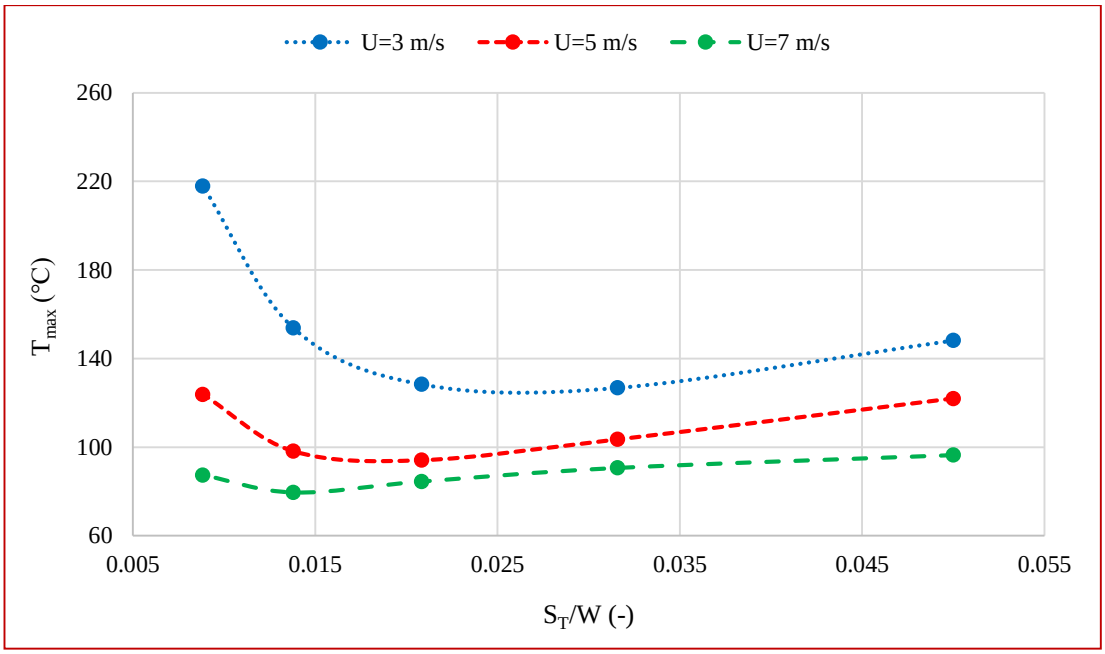

Figure 6.15 Plate fins with U = 3 m/s, 5 m/s, 7 m/s and Q = 150 W

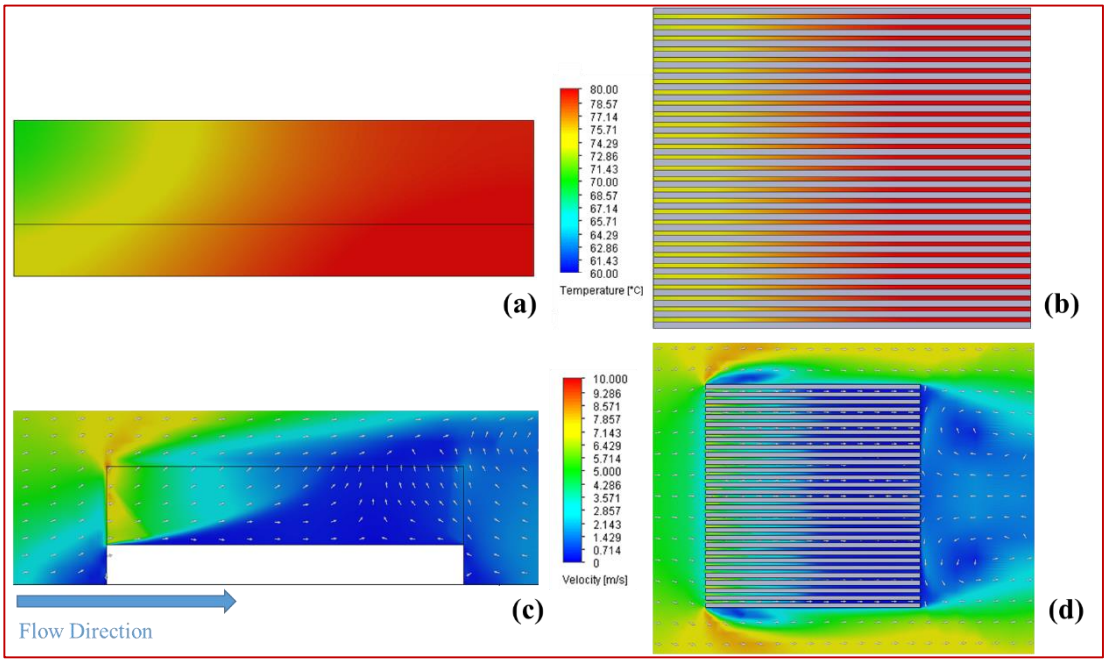

Figure 6.16 Plate fin (S_T/W = 0.0138) temperature profile from (a) side, (b) top view and velocity profile from (c) side, (d) top view

6.1.6 Plate Fins with U = 3 m/s, 5 m/s, 7 m/s and Q = 150 W, 200 W, 250 W Boundary Conditions

Heat transfer characteristic of plate fins are studied in this section with higher heat input values (200 W and 250 W). T_{max} relation with non-dimensional spanwise spacing value and free-stream velocities are presented in Figure 6.17, Figure 6.18 and Figure 6.19 for 150 W, 200W and 250W heat inputs, respectively.

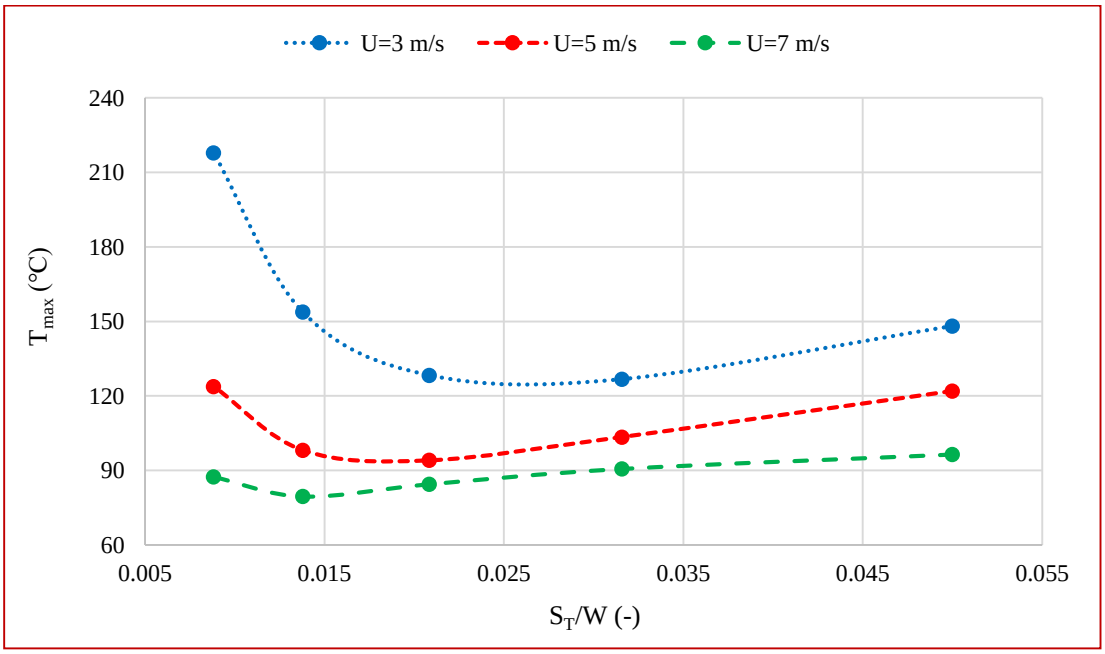

Figure 6.17 Plate fins with U = 3 m/s, 5 m/s, 7 m/s and Q = 150 W

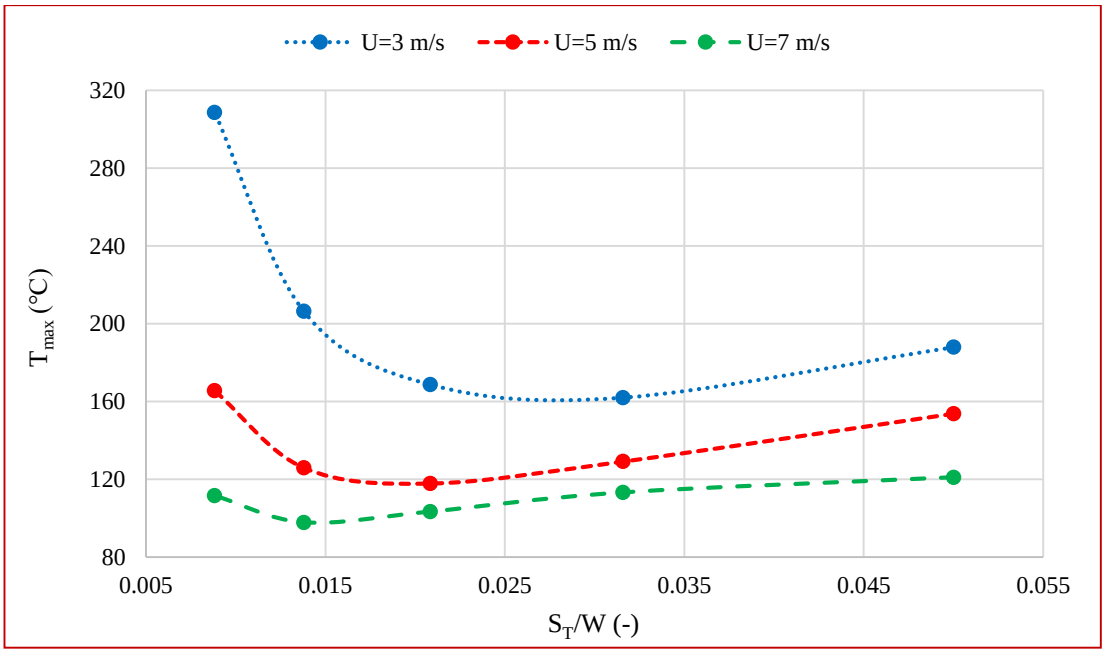

Figure 6.18 Plate fins with U = 3 m/s, 5 m/s, 7 m/s and Q = 200 W

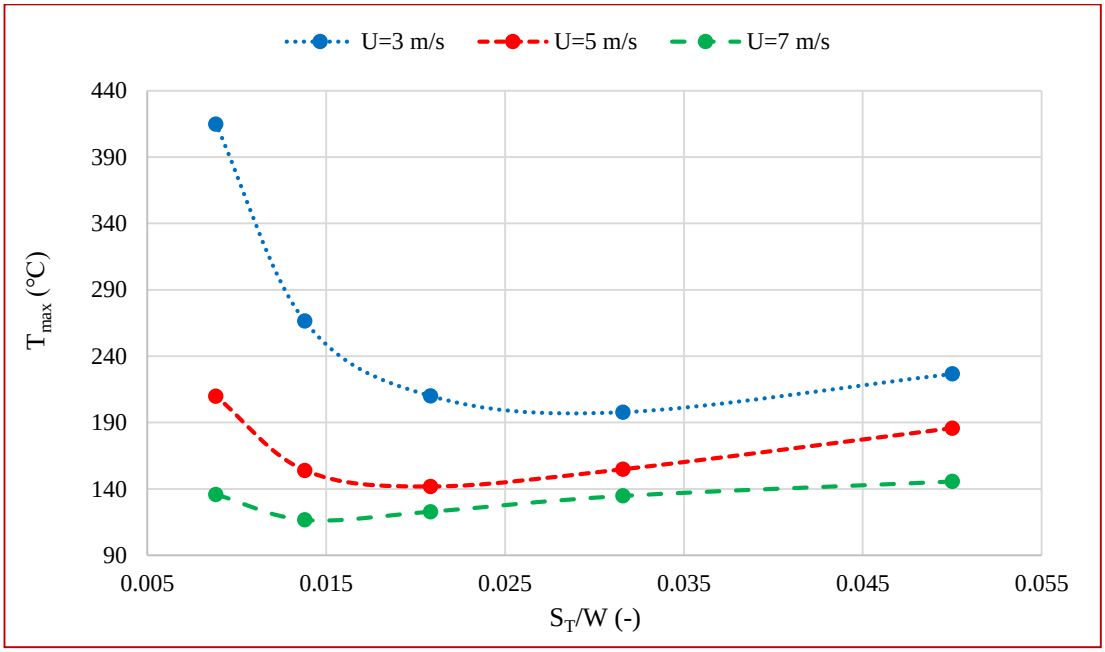

Figure 6.19 Plate fins with U = 3 m/s, 5 m/s, 7 m/s and Q = 250 W

6.1.7 Heat Transfer Performance Comparison of Square, Cylindrical and Plate Fins

Since square and cylindrical fins with non-dimensional streamwise spacing values of 0.0138 and 0.0088 respectively have shown a better heat transfer performance among others, these set of samples and plate fins are compared with each other when free-stream velocity, heat input and Reynolds number values are kept constant.

T_{max} for all three fin profiles with heat input value of 150 W are illustrated in Figure 6.20, Figure 6.21 and Figure 6.22 for free-stream velocities of 3 m/s, 5 m/s and 7 m/s, respectively.

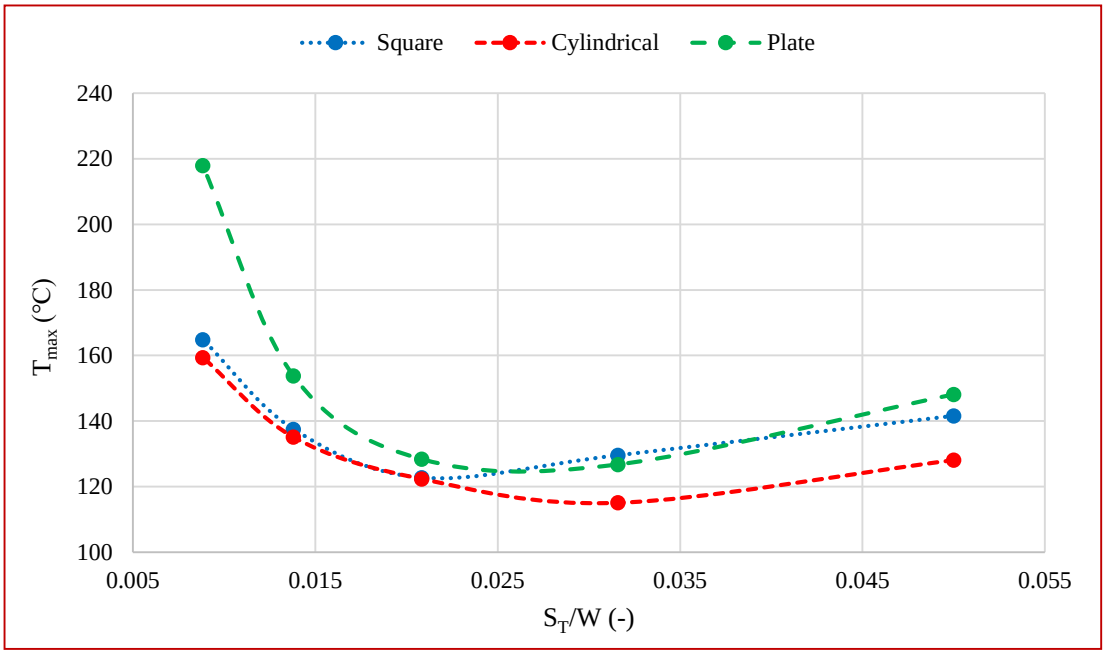

Figure 6.20 Comparison of square (S_L/L = 0.0138), cylindrical (S_L/L = 0.0088) and plate fins with U = 3 m/s and Q = 150 W

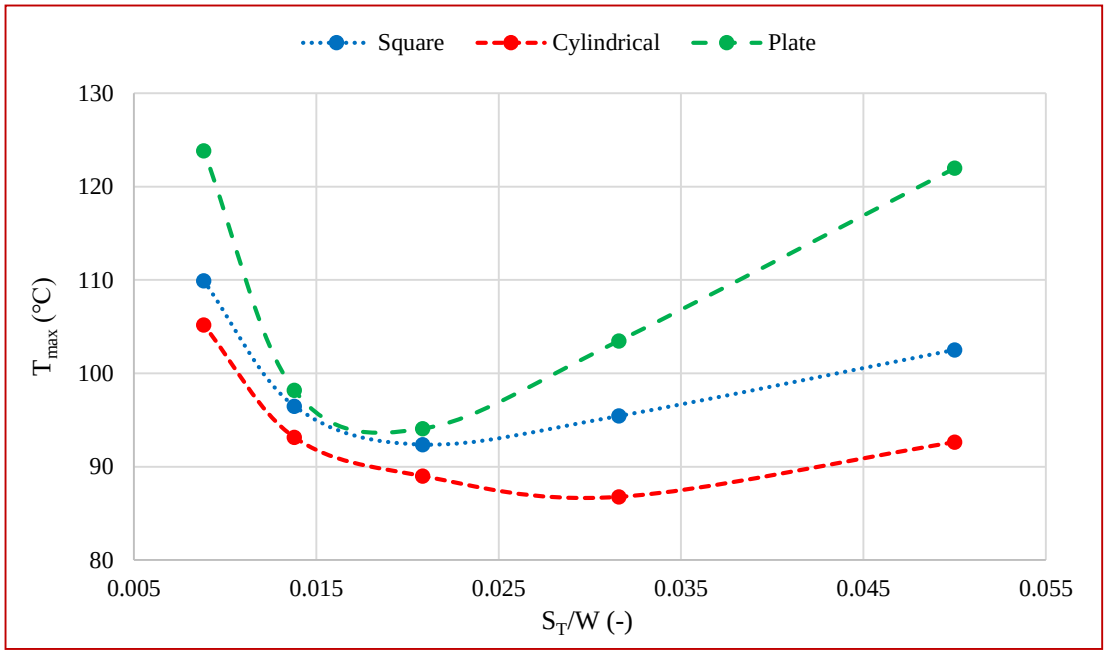

Figure 6.21 Comparison of square (S_L/L = 0.0138), cylindrical (S_L/L = 0.0088) and plate fins with U = 5 m/s and Q = 150 W

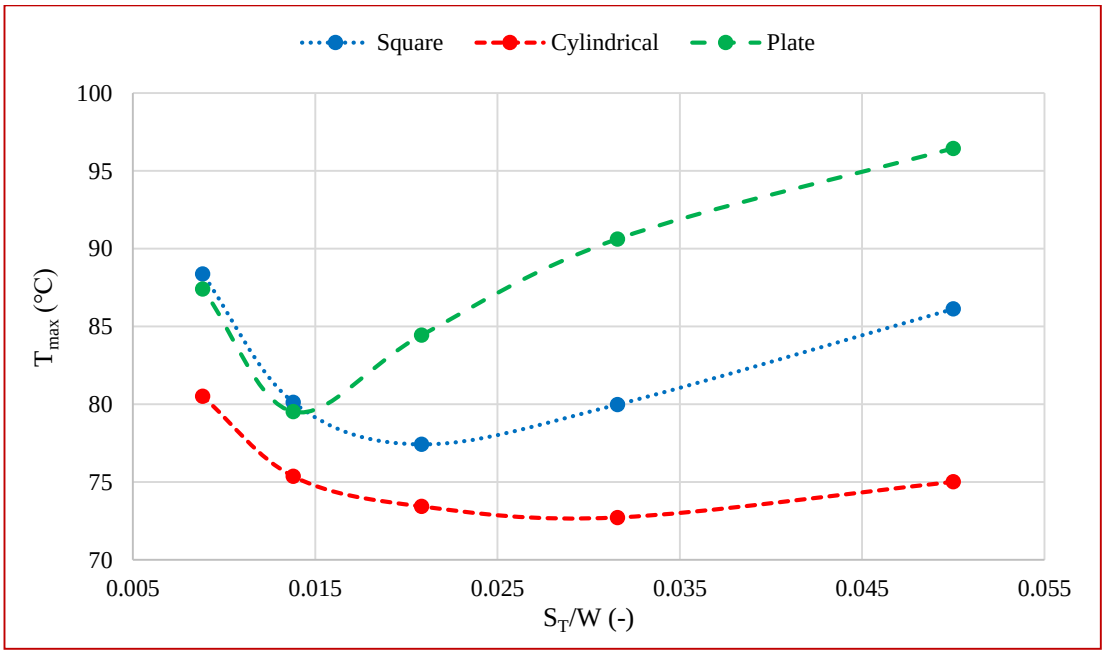

Figure 6.22 Comparison of square (S_L/L = 0.0138), cylindrical (S_L/L = 0.0088) and plate fins with U = 7 m/s and Q = 150 W

Higher heat input value (200 W) is applied and T_{max} of fins with three different profiles are figured out in Figure 6.23, Figure 6.24 and Figure 6.25 for free-stream velocities of 3 m/s, 5 m/s and 7 m/s, respectively.

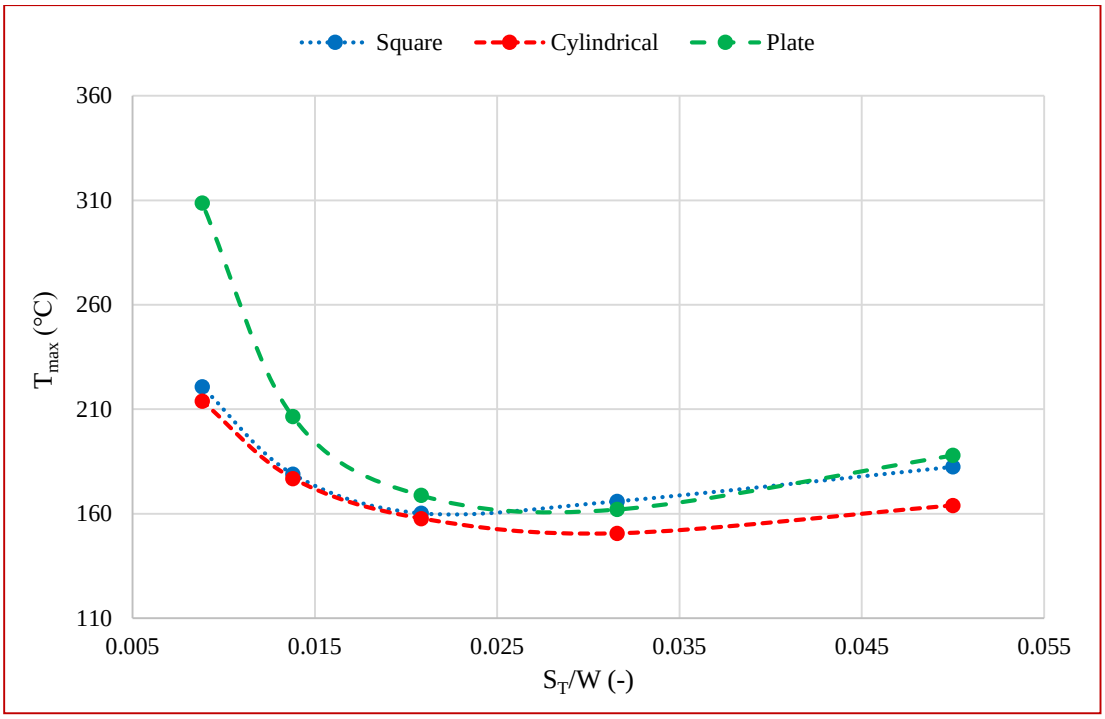

Figure 6.23 Comparison of square (S_L/L = 0.0138), cylindrical (S_L/L = 0.0088) and plate fins with U = 3 m/s and Q = 200 W

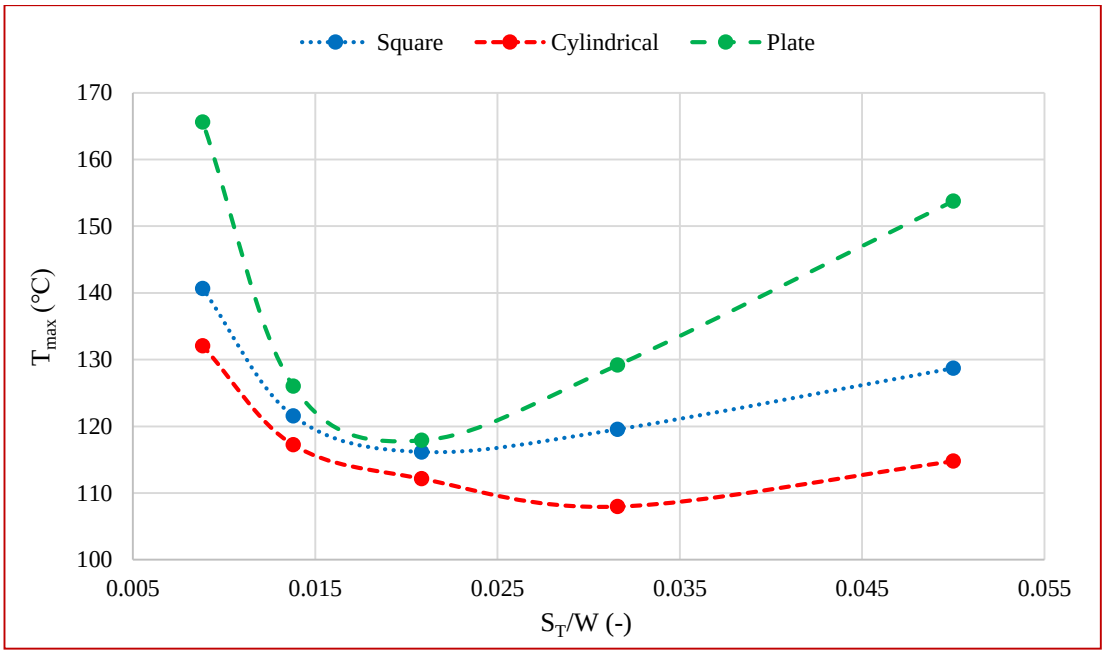

Figure 6.24 Comparison of square (S_L/L = 0.0138), cylindrical (S_L/L = 0.0088) and plate fins with U = 5 m/s and Q = 200 W

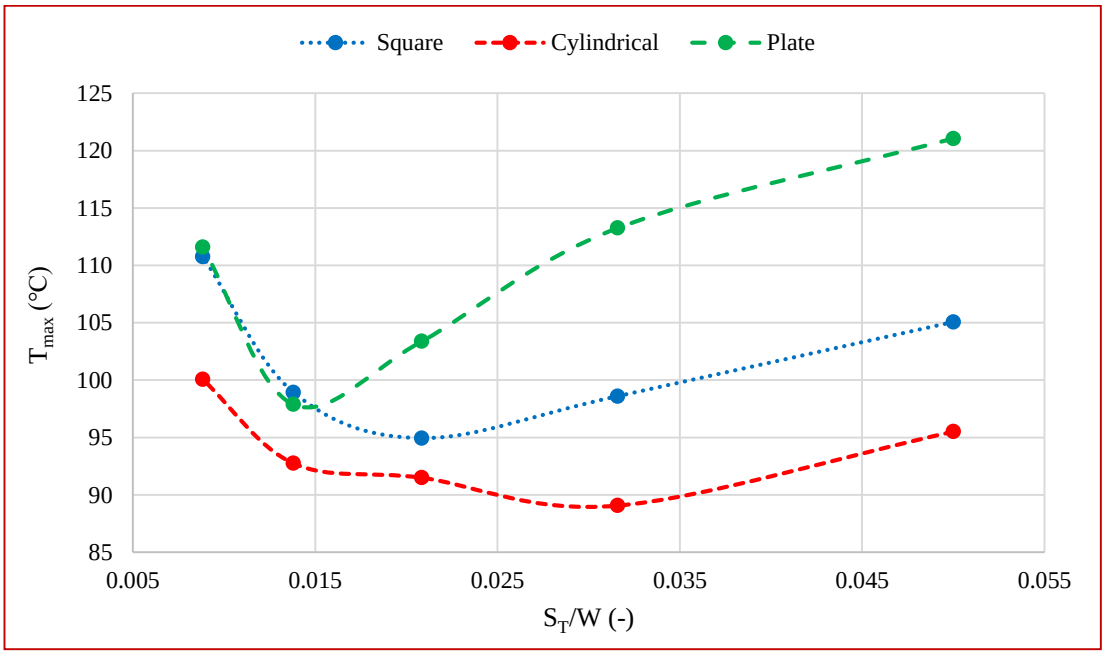

Figure 6.25 Comparison of square (S_L/L = 0.0138), cylindrical (S_L/L = 0.0088) and plate fins with U = 7 m/s and Q = 200 W

T_{max} for all three fin types with 250 W heat input are plotted in Figure 6.26, Figure 6.27 and Figure 6.28 for 3 m/s, 5 m/s and 7 m/s free-stream velocities, respectively.

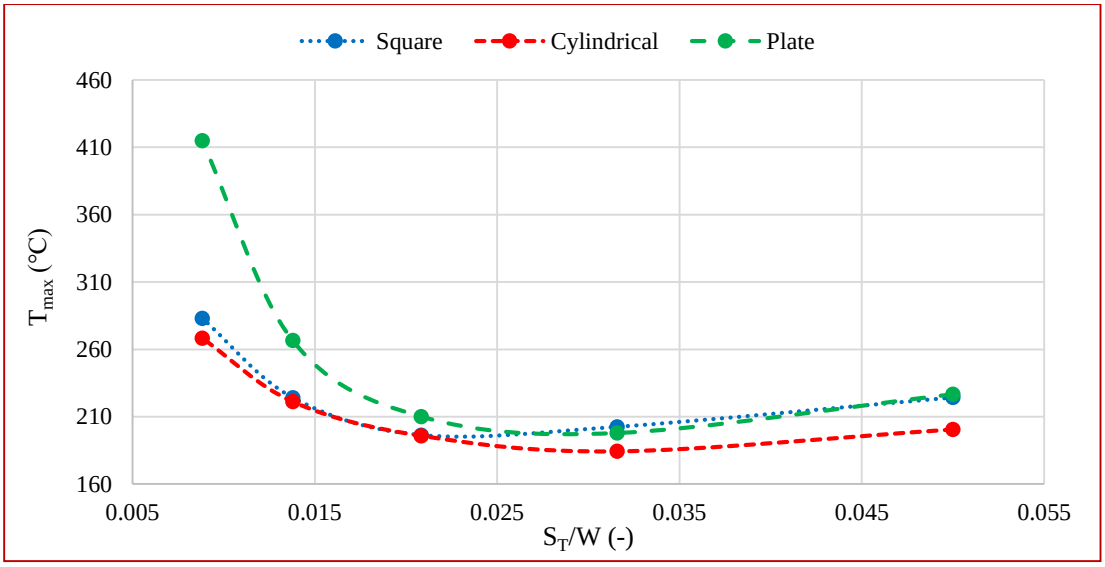

Figure 6.26 Comparison of square (S_L/L = 0.0138), cylindrical (S_L/L = 0.0088) and plate fins with U = 3 m/s and Q = 250 W

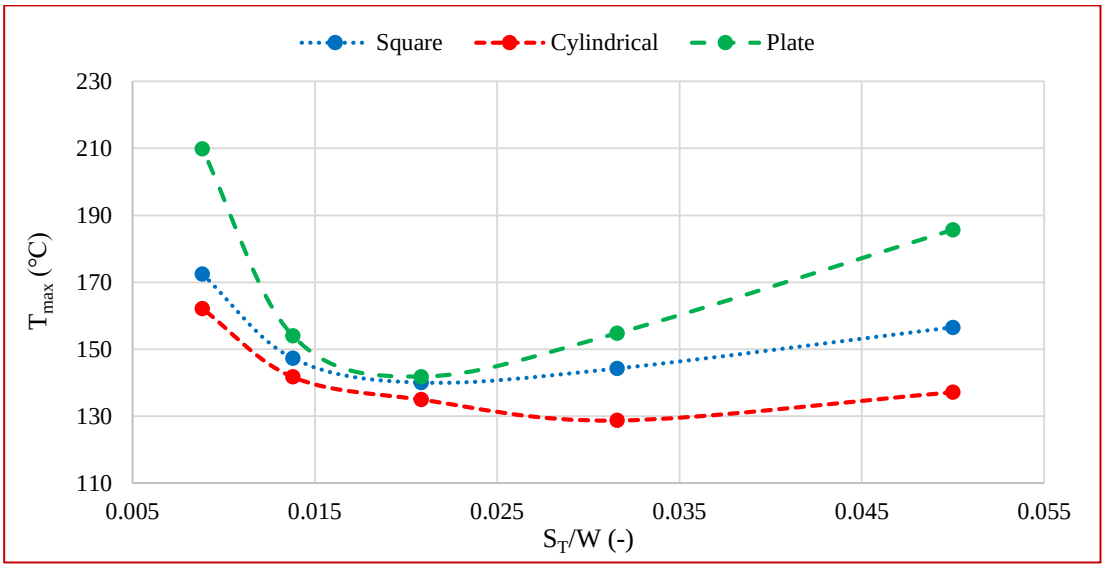

Figure 6.27 Comparison of square (S_L/L = 0.0138), cylindrical (S_L/L = 0.0088) and plate fins with U = 5 m/s and Q = 250 W

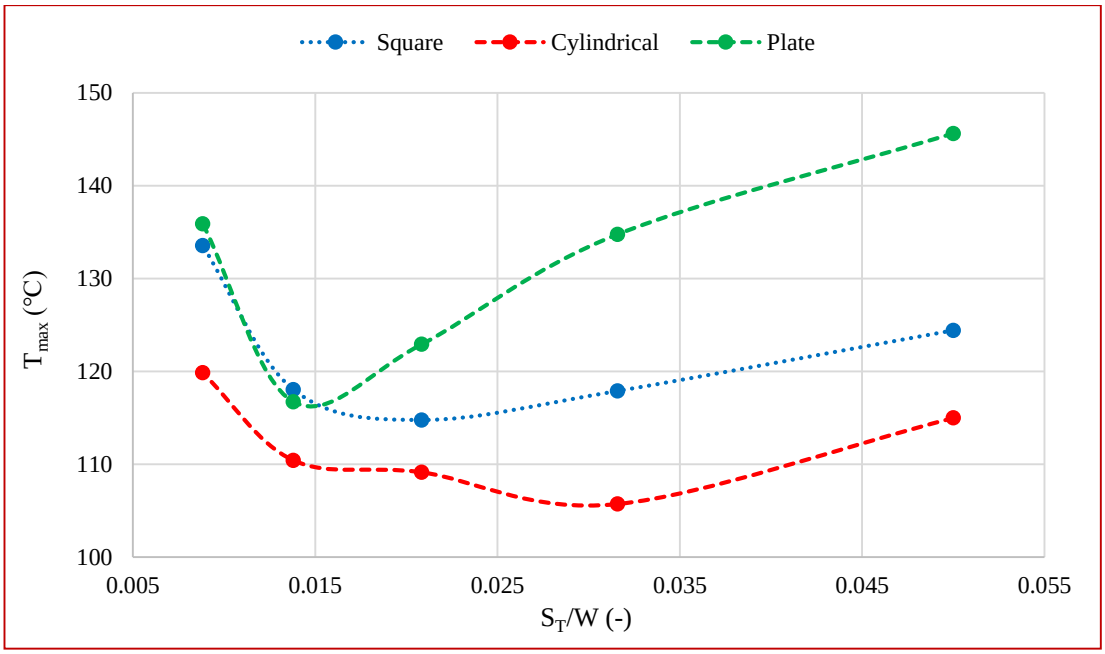

Figure 6.28 Comparison of square (S_L/L = 0.0138), cylindrical (S_L/L = 0.0088) and plate fins with U = 7 m/s and Q = 250 W

6.2 Experimental Results

Experiments are conducted to validate numerical results. Geometries defined in Table 3.4, Table 3.5 and Table 3.6 are tested. Experiments are conducted with heat input value of 150 W at steady state conditions and ambient temperature is kept 25℃.

Maximum temperatures on the upper surface of the base plates (T_{max}) are monitored with a thermal camera and it is read on the tape at the middle section of the fins. T_{max} of the square fin (S_L/L = 0.0208, S_T/W = 0.0208), cylindircal fin (S_L/L = 0.0208, S_T/W = 0.0316) and plate fin (S_T/W = 0.0208) at 7 m/s free-stream velocity boundary condition are illustrated in Figure 6.29, Figure 6.30 and Figure 6.31, respectively.

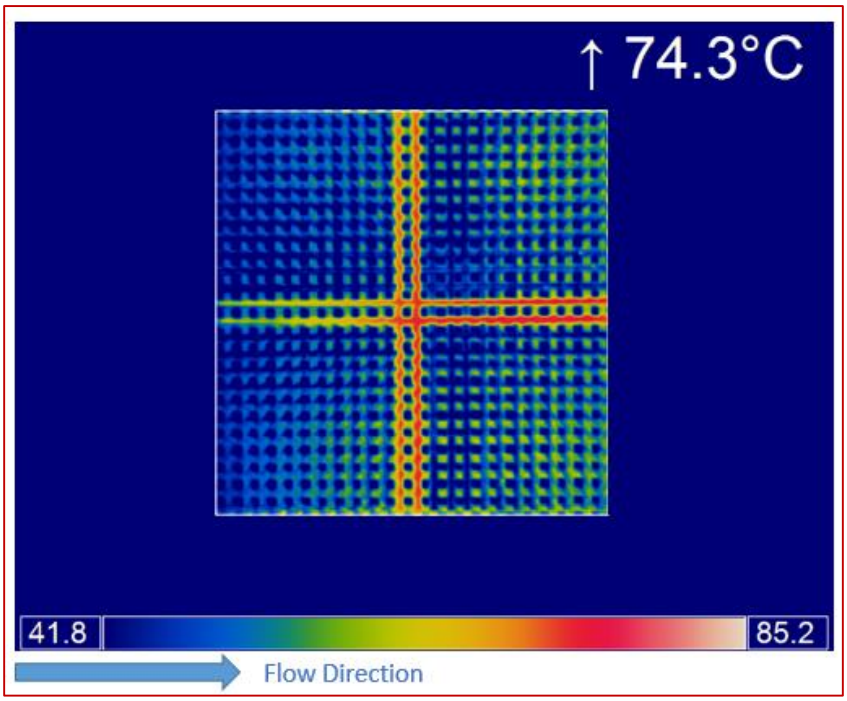

Figure 6.29 T_{max} for the square fin (S_L/L = 0.0208, S_T/W = 0.0208) with U = 7 m/s

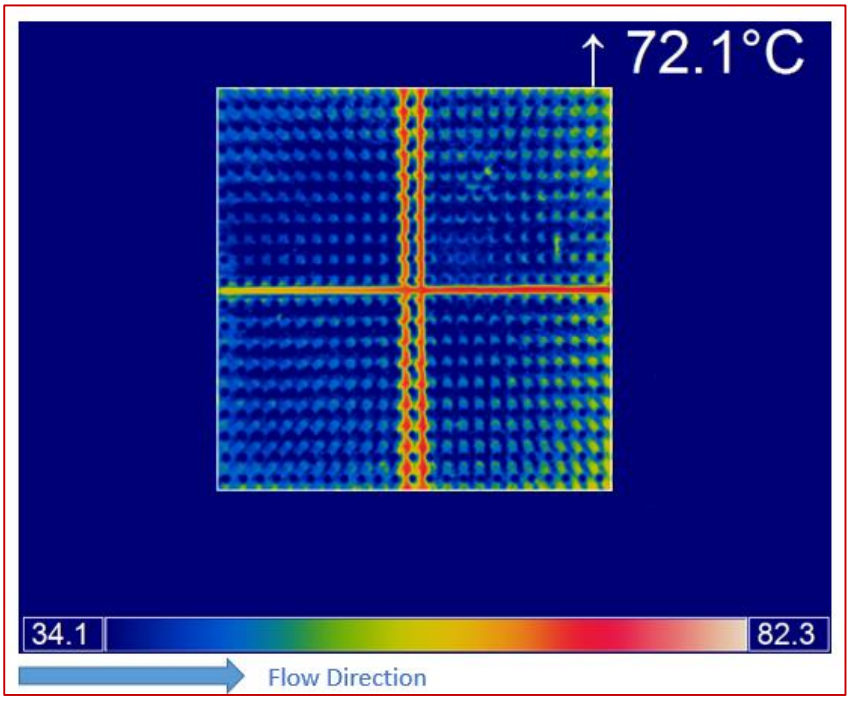

Figure 6.30 T_{max} for the cyl. fin (S_L/L = 0.0208, S_T/W = 0.0316) with U = 7 m/s

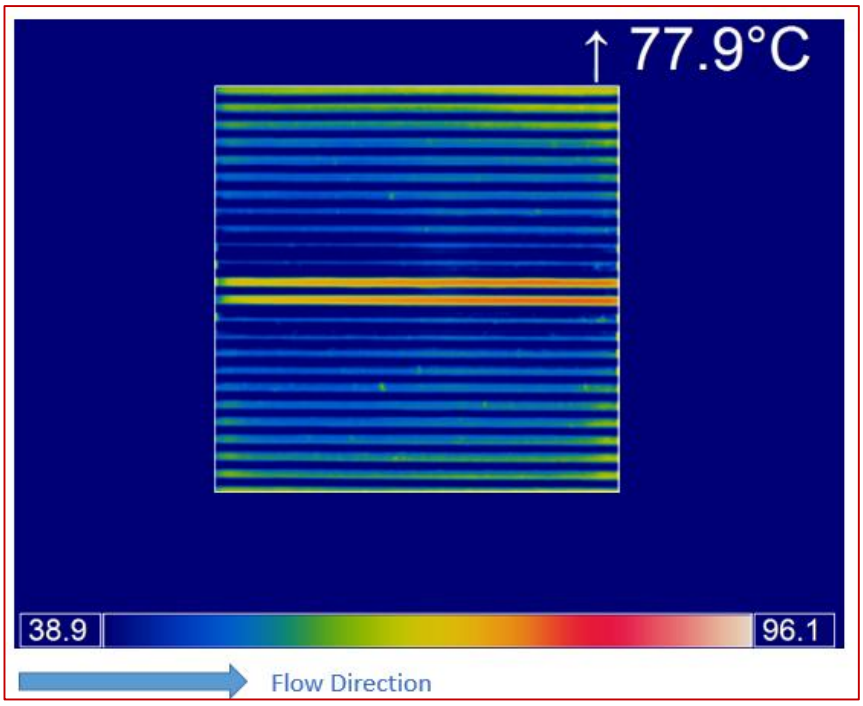

Figure 6.31 T_{max} for the plate fin ($S_T/W = 0.0208$) with U = 7 m/s

T_{base_ave} can be expressed as:

$$T_{base\_ave} = \frac{T_1 + T_2 + T_3 + T_4}{4} \text{ (square and cylindrical fins) (see Figure 5.11)} \quad (6.1)$$

$$T_{base\_ave} = \frac{T_1 + T_2}{2} \text{ (plate fins) (see Figure 5.11)} \quad (6.2)$$

Temperatures at the bottom of the heater and insulation material are monitored with thermocouples T_5 and T_6, respectively. Free-stream velocities (U), air inlet (T_{air_i}) and outlet temperatures (T_{air_o}) are monitored with the hot wire anemometers placed front and back side of the fins. The error between numerical and experimental results are calculated as:

$$\varepsilon = \% \left| \frac{T_{max}(\exp) - T_{max}(num)}{T_{max}(num)} \right| x100 \quad (6.3)$$

Experimental results for the square, cylindrical and plate fins are tabulated in Table 6.1, Table 6.2 and Table 6.3, respectively.

Table 6.1 Experimental results for square fins

S_L/L	S_T/W	U (m/s)	T_{air_i} (℃)	T_{air_o} (℃)	T_{max} (exp) (℃)	T_{max} (num) (℃)	ε %	T_{base_ave} (℃)	T_5 (℃)	T_6 (℃)
0.0500	**0.0500**	**3.1**	24.8	57.1	142.1	157.8	10.0	137.6	181.3	24.2
0.0500	**0.0316**	**2.9**	24.6	50.0	129.9	139.2	6.7	123.5	165.5	23.5
0.0500	**0.0208**	**2.9**	24.7	46.1	127.0	135.6	6.3	120.1	162.0	23.5
0.0500	**0.0500**	**4.9**	25.1	47.1	109.6	119.0	7.9	104.8	139.8	25.5
0.0500	**0.0316**	**4.8**	24.8	41.2	98.8	108.3	8.7	94.2	127.8	24.6
0.0500	**0.0208**	**4.9**	25.2	38.0	96.0	102.6	6.5	90.3	126.3	24.9
0.0500	**0.0500**	**7.1**	25.4	44.1	94.0	100.4	6.4	90.9	122.9	25.7
0.0500	**0.0316**	**6.9**	25.4	38.0	86.1	92.3	6.7	81.1	112.8	24.8
0.0500	**0.0208**	**6.8**	25.5	35.4	84.3	87.8	4.0	78.9	109.3	24.9
0.0316	**0.0500**	**2.9**	25.4	58.5	135.8	149.4	9.1	128.6	172.1	25.3
0.0316	**0.0316**	**3.0**	24.2	51.3	116.4	131.5	11.5	108.3	148.5	23.6
0.0316	**0.0208**	**3.2**	24.3	44.7	114.5	128.9	11.1	105.4	145.6	23.1
0.0316	**0.0500**	**4.9**	25.5	46.0	100.6	112.3	10.4	94.8	128.5	26.1
0.0316	**0.0316**	**5.0**	24.9	42.0	92.5	102.0	9.3	84.1	120.7	25.3
0.0316	**0.0208**	**4.9**	24.7	38.8	89.8	98.5	8.9	80.1	116.5	24,4
0.0316	**0.0500**	**6.8**	25.8	37.9	87.3	93.7	6.8	81.7	115.3	24.5
0.0316	**0.0316**	**6.9**	25.2	38.9	79.7	86.9	8.3	73.2	105.5	25.0
0.0316	**0.0208**	**7.2**	25.1	36.8	78.8	83.4	5.5	70.0	103.1	24.8
0.0208	**0.0500**	**3.0**	25.6	53.3	132.2	147.5	10.4	124.1	168.9	26.3
0.0208	**0.0316**	**2.9**	23.1	53.2	118.7	130.5	9.1	111.7	149.4	23.3
0.0208	**0.0208**	**2.9**	24.2	44.0	115.7	125.1	7.5	107.3	148.6	23.2
0.0208	**0.0500**	**5.1**	25.3	42.3	99.1	110.0	9.9	89.5	128.7	26.5
0.0208	**0.0316**	**4.9**	24.7	43.3	89.6	99.3	9.7	82.8	116.7	24.4
0.0208	**0.0208**	**4.8**	24.7	37.5	85.3	94.2	9.4	78.3	111.2	23.5
0.0208	**0.0500**	**6.8**	25.8	37.2	86.2	91.4	5.7	79.8	113.7	26.7
0.0208	**0.0316**	**7.2**	25.0	41.0	78.4	83.6	6.2	72.2	102.1	24.9
0.0208	**0.0208**	**7.1**	24.9	35.3	74.3	79.9	7.0	67.4	98.6	24.4

Table 6.2 Experimental results for cylindrical fins

S_L/L	S_T/W	U (m/s)	T_{air_i} (℃)	T_{air_o} (℃)	T_{max} (exp) (℃)	T_{max} (num) (℃)	ε %	T_{base_ave} (℃)	T_5 (℃)	T_6 (℃)
0.0500	**0.0500**	**2.9**	24.2	51.2	127.8	149.5	14.5	121.6	164.6	23.2
0.0500	**0.0316**	**2.9**	24.3	50.9	121.3	130.8	7.3	112.3	156.4	22.2
0.0500	**0.0208**	**3.0**	24.9	48.5	124.5	133.5	6.7	118.3	159.9	23.6
0.0500	**0.0500**	**4.9**	24.7	45.1	100.2	110.8	9.5	94.9	133.8	23.7
0.0500	**0.0316**	**4.8**	24.8	40.8	93.9	98.8	5.0	85.2	121.1	23.5
0.0500	**0.0208**	**5.0**	25.3	39.1	94.2	98.8	4.7	87.0	123.2	24.9
0.0500	**0.0500**	**6.9**	25.1	39.0	87.8	94.7	7.2	82.3	114.2	24.9
0.0500	**0.0316**	**7.1**	25.3	37.0	82.4	85.3	3.4	76.3	108.6	24.7
0.0500	**0.0208**	**6.9**	25.6	36.9	80.7	82.6	2.3	74.9	107.7	23.6
0.0316	**0.0500**	**2.9**	25.4	59.1	125.1	146.9	14.9	117.8	161.4	25.4
0.0316	**0.0316**	**3.2**	24.5	46.8	113.2	125.4	9.7	108.0	146.4	23.2
0.0316	**0.0208**	**3.1**	24.8	46.6	116.9	123.9	5.6	109.5	148.0	22.9
0.0316	**0.0500**	**4.9**	25.4	41.9	89.6	99.7	10.1	82.2	116.6	26.4
0.0316	**0.0316**	**5.1**	24.7	39.9	87.6	93.2	6.0	81.0	114.9	24.5
0.0316	**0.0208**	**5.0**	25.3	40.1	87.5	93.8	6.8	80.7	114.6	24.4
0.0316	**0.0500**	**7.0**	25.7	37.9	77.8	86.0	9.5	72.6	102.4	26.5
0.0316	**0.0316**	**6.9**	25.2	36.6	76.4	80.1	4.6	70.5	101.3	24.9
0.0316	**0.0208**	**6.8**	25.5	36.1	75.6	78.9	4.2	69.0	100.4	24.9
0.0208	**0.0500**	**2.9**	25.6	57.3	123.9	136.1	9.0	113.3	168.2	26.4
0.0208	**0.0316**	**2.8**	25.3	50.4	110.9	119.3	7.0	104.5	142.8	23.2
0.0208	**0.0208**	**2.9**	25.1	45.7	115.2	122.8	6.2	107.3	147.4	22.4
0.0208	**0.0500**	**4.9**	25.7	46.1	88.9	95.4	6.8	82.8	115.9	26.6
0.0208	**0.0316**	**4.8**	25.5	42.6	84.8	91.4	7.2	79.5	110.2	24.5
0.0208	**0.0208**	**5.1**	25.5	38.6	85.2	90.9	6.2	78.1	112.4	23.9
0.0208	**0.0500**	**7.0**	26.0	39.3	75.9	80.8	6.1	70.2	100.7	27.3
0.0208	**0.0316**	**7.0**	25.5	37.6	72.1	76.7	6.0	66.8	96.4	24.9
0.0208	**0.0208**	**6.9**	25.5	35.7	73.3	76.1	3.7	66.6	98.2	24.8

Table 6.3 Experimental results for plate fins

S_L/L	S_T/W	U (m/s)	T_{air_i} (℃)	T_{air_o} (℃)	T_{max} (exp) (℃)	T_{max} (num) (℃)	ε %	T_{base_ave} (℃)	T_5 (℃)	T_6 (℃)
-	**0.0500**	**3.0**	24.9	50.0	135.2	148.2	8.7	128.4	173.7	23.5
-	**0.0316**	**2.9**	25.7	51.0	116.7	126.8	7.9	111.4	152.6	26.4
-	**0.0208**	**3.1**	25.6	49.9	118.7	128.4	7.5	109.7	154.1	26.4
-	**0.0500**	**5.2**	24.7	37.5	113.0	122.0	7.4	106.6	146.6	24.9
-	**0.0316**	**4.8**	25.9	45.4	95.4	103.5	7.8	90.8	123.8	26.5
-	**0.0208**	**4.9**	25.9	41.2	89.8	94.1	4.5	84.7	115.9	26.5
-	**0.0500**	**7.1**	24.7	37.5	88.5	96.5	8.2	83.6	115.4	26.5
-	**0.0316**	**6.9**	26.0	39.9	85.4	90.6	5.8	81.2	112.6	26.6
-	**0.0208**	**6.7**	25.6	38.7	77.9	84.5	7.8	72.4	103.7	26.5

Experimental results are compared with the numerical ones to validate the numerical model. Error between the numerical and experimental results for the T_{max} varies between %2.3 for the cylindrical fin (S_L/L = 0.05, S_T/W = 0.0208 at 7 m/s free-stream velocity) and %14.9 for the cylindrical fin (S_L/L = 0.0316, S_T/W = 0.05 at 3 m/s free-stream velocity).

T_{max} of square and cylindrical fins with non-dimensional streamwise spacing value of 0.0208 and plate fins occurring at numerical and experimental studies are compared and plotted in Figure 6.32, Figure 6.33, Figure 6.34 at 3 m/s free-stream velocity, respectively to illustrate aggreement of numerical and experimental results.

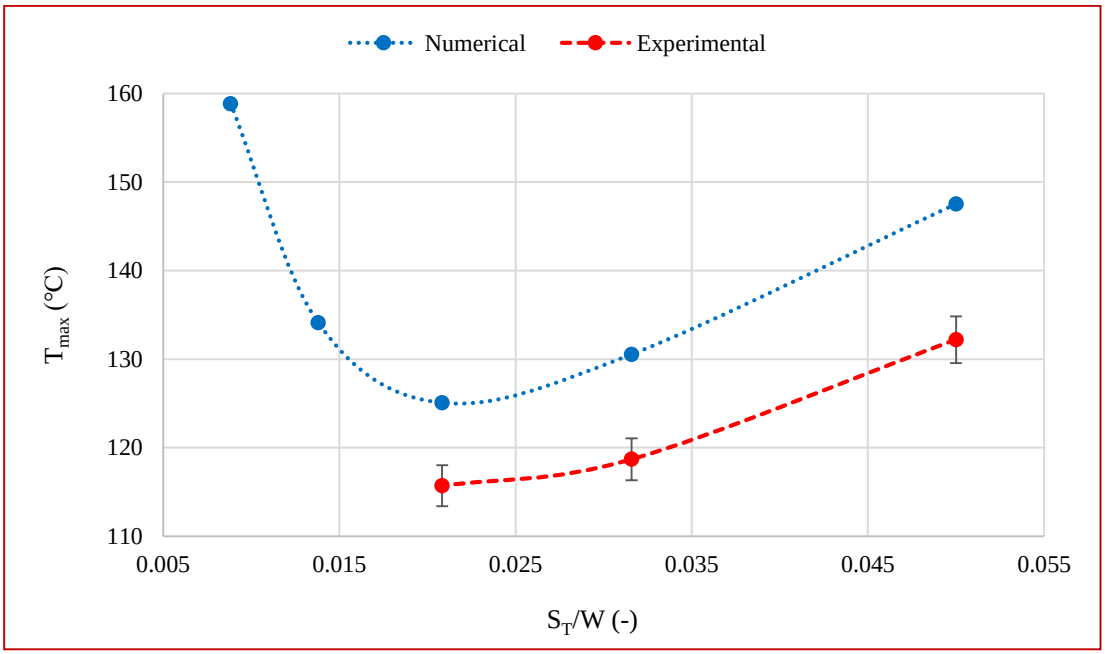

Figure 6.32 Square fins (S_L/L = 0.0208) with U = 3 m/s and Q = 150 W

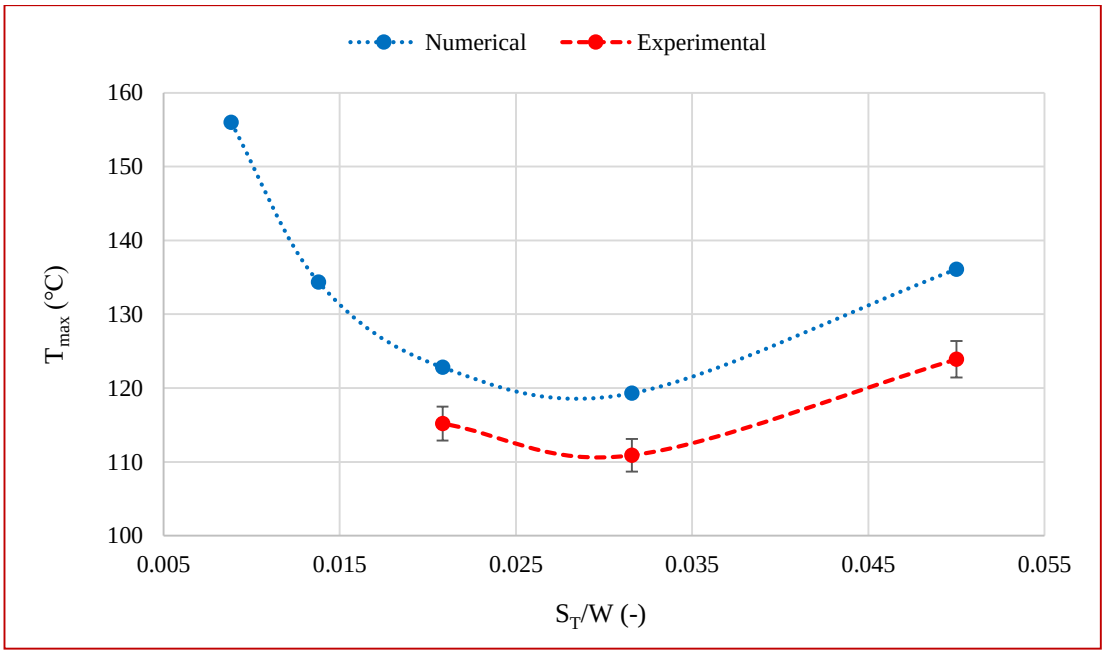

Figure 6.33 Cylindrical fins (S_L/L = 0.0208) with U = 3 m/s and Q = 150 W

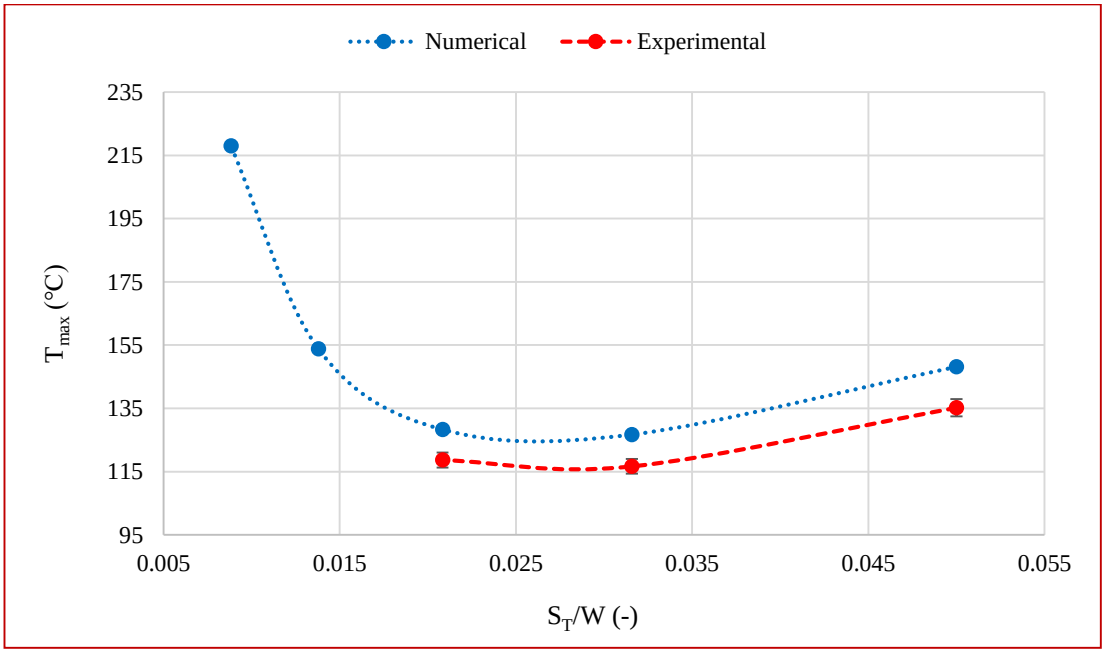

Figure 6.34 Plate fins with U = 3 m/s and Q = 150 W

6.3 Determination of Average Heat Transfer Coefficient

Heat input supplied to the finned surface can be calculated by Eqn. (6.4).

$$Q_{input} = VI \tag{6.4}$$

where;

V : voltage,

I : current.

Measurements are done for the power supplied to the heater with respect to the equation (6.4). Average voltage and current are measured as 82.68 V and 1.81 A, respectively. So, Q_{input} is found as 149.66 W.

Convection heat transfer rate (Q_{conv}) can be calculated baed on equation (3.11).

Heat transfer rate from the insulation layer (Q_{ins}) can be determined from following equation as Ayli et al. [30] did in their study:

$$Q_{ins} = k_{ins} A_{ins} \frac{\Delta T}{L_{ins}} \tag{6.5}$$

where;

k_{ins} : thermal conductivity of insulation material [37],

A_{ins} : insulation area (base plate bottom area) (0.01 m^2),

L_{ins} : insulation thickness (0.15 m).

Temperature difference between top and bottom layer of the insulation material (ΔT) can be expressed as:

$$\Delta T = T_5 - T_6 \tag{6.6}$$

Thermal conductivity of insulation material (k_{ins}) is expressed in terms of average insulation temperature (T_{ins_ave}) with third order polynomial fit [37]:

$$k_{ins} = -4.2x10^{-22}(T_{ins\_ave})^3 + 4x10^{-7}(T_{ins\_ave})^2 - 1.2x10^{-4}T_{ins\_ave} + 0.032 \quad (6.7)$$

$$T_{ins\_ave} = \frac{T_5 + T_6}{2} \quad (6.8)$$

Radiation heat transfer rate can be determined from equation (3.10). Variables in equation (3.10) can be described as:

ε_{fin} : emissivity of unoxidized aluminum (0.2) [46],

ε_{surr} : emissivity of plexiglass (0.86) [48],

A_{rad} : fin is assumed to be a solid quadrangular (0.022 m^2),

A_{surr} : fin is assumed to be almost surrounded by plexiglass walls as presented in Figure 6.35 (1.32 m^2),

$F_{(fin)\rightarrow(surr)}$: fin is almost surrounded by plexiglass walls (1),

T_{surr} : inlet air temperature (T_{air_i}).

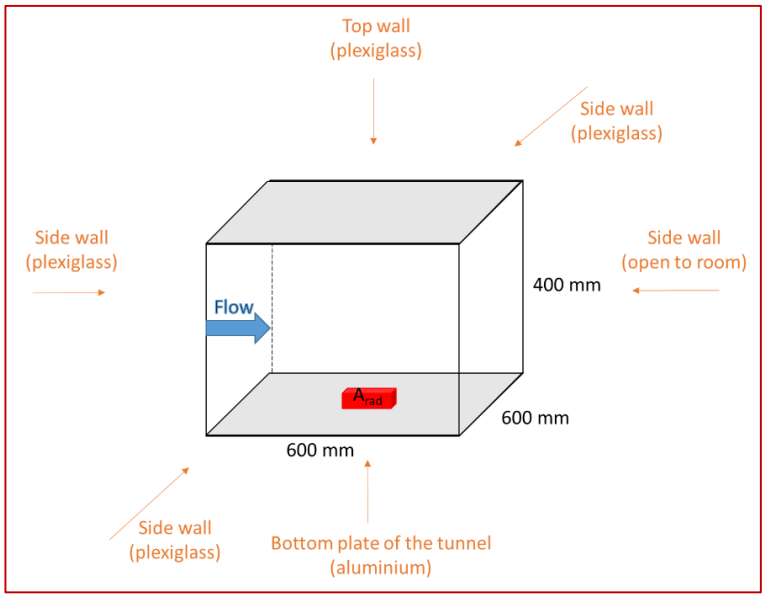

Figure 6.35 Schematic representation of enclosure for radiation calculation

In literature, researchers [13], [21], [49], [50] used classical fin equation in order to find average heat transfer coefficient (h_{avg}). Diani et al. [13] and Mon et al. [49] described the temperature difference in logarithmic mean temperature form and made iterative solutions to find h_{avg}. Mon et al. [49] and Wirtz et al. [50] assumed that average heat transfer coefficient is equal to heat transfer coefficient of a single fin and uniform for the fin array, while Jonsson and Moshfegh [21] assumed fin efficiency (η_f) is % 100.

In the present study, average heat transfer coefficient is assumed to be equal to the heat transfer coefficient of a single fin, and the temperature difference between the fin and ambient is expressed in terms of logarithmic mean.

In order to find average heat transfer coefficient (h_{avg}), equation (3.9) can be considered and logarithmic mean temperature difference (ΔT_{lm}) can be evaluated as [13], [49]:

$$\Delta T_{lm} = \frac{\left(T_2 - T_{air\_o}\right) - \left(T_1 - T_{air\_i}\right)}{\ln\left(\frac{T_2 - T_{air\_o}}{T_1 - T_{air\_i}}\right)} \tag{6.9}$$

where;

T_2 : temperature at the back of base plate,

T_1 : temperature at the front of base plate,

T_{air_o} : average air temperature at the outlet,

T_{air_i} : average air temperature at the inlet.

Overall efficiency of fin array (η_o), fin efficiency (η_f) and geometrical parameters related to fins with convection tip condition are calculated based on equations presented in [2], [29].

Equation (3.9) results in a non linear equation which can be solved by numerical

methods. False position method mentioned in Appendix A is used to obtain h_{avg}.

Convection heat transfer rates and average heat transfer coefficient values for square, cylindrical and plate fins are presented in Table 6.4, Table 6.5 and Table 6.6, respectively.

Table 6.4 Convection heat transfer rates and average heat transfer coefficient values for square fins

S_L/L	S_T/W	U (m/s)	Q_{conv} (W)	h_{avg} (W/m^{2}K)
0.0500	**0.0500**	**3.1**	144.0	31.2
0.0500	**0.0316**	**2.9**	145.0	28.3
0.0500	**0.0208**	**2.9**	145.2	24.5
0.0500	**0.0500**	**4.9**	146.2	45.0
0.0500	**0.0316**	**4.8**	146.8	41.6
0.0500	**0.0208**	**4.9**	147.0	36.8
0.0500	**0.0500**	**7.1**	147.0	56.3
0.0500	**0.0316**	**6.9**	147.5	52.4
0.0500	**0.0208**	**6.8**	147.6	45.0
0.0316	**0.0500**	**2.9**	144.7	28.4
0.0316	**0.0316**	**3.0**	146.0	28.5
0.0316	**0.0208**	**3.2**	146.1	22.8
0.0316	**0.0500**	**4.9**	146.8	42.9
0.0316	**0.0316**	**5.0**	147.3	40.0
0.0316	**0.0208**	**4.9**	147.5	34.8
0.0316	**0.0500**	**6.8**	147.4	51.7
0.0316	**0.0316**	**6.9**	147.8	49.8
0.0316	**0.0208**	**7.2**	148.0	45.1
0.0208	**0.0500**	**3.0**	145.0	23.4
0.0208	**0.0316**	**2.9**	145.7	22.0
0.0208	**0.0208**	**2.9**	146.0	18.7
0.0208	**0.0500**	**5.1**	147.0	37.0
0.0208	**0.0316**	**4.9**	147.4	33.9
0.0208	**0.0208**	**4.8**	147.6	29.5
0.0208	**0.0500**	**6.8**	147.5	41.8
0.0208	**0.0316**	**7.2**	147.9	43.0
0.0208	**0.0208**	**7.1**	148.1	38.1

Table 6.5 Convection heat transfer rates and average heat transfer coefficient values for cylindrical fins

S_L/L	S_T/W	U (m/s)	Q_{conv} (W)	h_{avg} (W/m^2K)
0.0500	**0.0500**	**2.9**	145.1	42.7
0.0500	**0.0316**	**2.9**	145.7	38.9
0.0500	**0.0208**	**3.0**	145.4	30.8
0.0500	**0.0500**	**4.9**	146.7	61.3
0.0500	**0.0316**	**4.8**	147.2	58.5
0.0500	**0.0208**	**5.0**	147.2	47.3
0.0500	**0.0500**	**6.9**	147.4	74.9
0.0500	**0.0316**	**7.1**	147.7	67.6
0.0500	**0.0208**	**6.9**	147.8	61.6
0.0316	**0.0500**	**2.9**	145.4	38.6
0.0316	**0.0316**	**3.2**	146.0	33.7
0.0316	**0.0208**	**3.1**	145.9	27.0
0.0316	**0.0500**	**4.9**	147.4	61.9
0.0316	**0.0316**	**5.1**	147.4	50.8
0.0316	**0.0208**	**5.0**	147.5	42.8
0.0316	**0.0500**	**7.0**	147.9	76.4
0.0316	**0.0316**	**6.9**	148.0	63.3
0.0316	**0.0208**	**6.8**	148.0	54.0
0.0208	**0.0500**	**2.9**	145.6	34.1
0.0208	**0.0316**	**2.8**	146.2	30.6
0.0208	**0.0208**	**2.9**	146.0	23.4
0.0208	**0.0500**	**4.9**	147.4	55.0
0.0208	**0.0316**	**4.8**	147.5	45.6
0.0208	**0.0208**	**5.1**	147.6	37.4
0.0208	**0.0500**	**7.0**	148.0	69.6
0.0208	**0.0316**	**7.0**	148.1	59.6
0.0208	**0.0208**	**6.9**	148.1	48.8

Table 6.6 Convection heat transfer rates and average heat transfer coefficient values for plate fins

S_L/L	S_T/W	U (m/s)	Q_{conv} (W)	h_{avg} (W/m^2K)
-	**0.0500**	**3.0**	144.7	21.5
-	**0.0316**	**2.9**	145.8	21.3
-	**0.0208**	**3.1**	145.9	17.7
-	**0.0500**	**5.2**	146.1	26.2
-	**0.0316**	**4.8**	147.0	28.5
-	**0.0208**	**4.9**	147.3	25.3
-	**0.0500**	**7.1**	147.3	38.3
-	**0.0316**	**6.9**	147.5	32.7
-	**0.0208**	**6.7**	147.9	32.4

6.4 Heat Transfer Correlation

There are different Nusselt number definitions in literature in terms of characteristic length [15], [21], [22], [50], [51]. Tahat et al. [15] and Jubran et al. [22] studied with cylindrical fins and described diameter of cylinder as characteristic length (D_h). Kadle et al. [51] worked with plate fins and described inter-fin spacing as characteristic length. Jonsson et al. [21] and Wirtz et al. [50] studied with fins with different profiles and assumed base plate length and width as characteristic length, respectively.

In present study, characteristic length, which is explained in Section 3.2, is constant for all fins and taken as 2 mm. Therefore, Nusselt number is only function of the average heat transfer coefficient [21]. So, Nusselt number can be defined as:

$$Nu = \frac{h_{avg} D_h}{k_{air}} \tag{6.10}$$

Thermal conductivity of air (k_{air}) is interpolated as [29]:

$$k_{air} = 0.0257 + \left(\frac{0.0057}{80} \right) \left(T_{air\_ave} - 20 \right) \tag{6.11}$$

$$T_{air\_ave} = \frac{T_{air\_i} + T_{air\_o}}{2} \tag{6.12}$$

Kinematic viscosity of air (ν) is expressed in terms of average air temperature (T_{air_ave}) with third order polynomial fit [29]:

$$\nu = -10^{-13} T_{air\_ave}^3 + 1.34x10^{-10} T_{air\_ave}^2 + 8.45x10^{-8} T_{air\_ave} + 13.36x10^{-6} \tag{6.13}$$

Experimental Reynolds and Nusselt number are calculated by using equations (3.12), (3.13) and (6.10) and presented in Table 6.7, Table 6.8 and Table 6.9 for square, cylindrical and plate fins, respectively.

Table 6.7 Experimental Reynolds and Nusselt numbers for square fins

S_L/L	S_T/W	U (m/s)	Re	Nu
0.0500	**0.0500**	**3.1**	509.2	2.3
0.0500	**0.0316**	**2.9**	567.2	2.1
0.0500	**0.0208**	**2.9**	688.1	1.8
0.0500	**0.0500**	**4.9**	827.1	3.4
0.0500	**0.0316**	**4.8**	962.1	3.1
0.0500	**0.0208**	**4.9**	1187.8	2.8
0.0500	**0.0500**	**7.1**	1207.7	4.2
0.0500	**0.0316**	**6.9**	1393.5	3.9
0.0500	**0.0208**	**6.8**	1659.5	3.4
0.0316	**0.0500**	**2.9**	473.8	2.1
0.0316	**0.0316**	**3.0**	585.3	2.1
0.0316	**0.0208**	**3.2**	763.1	1.7
0.0316	**0.0500**	**4.9**	828.6	3.2
0.0316	**0.0316**	**5.0**	999.3	3.0
0.0316	**0.0208**	**4.9**	1187.0	2.6
0.0316	**0.0500**	**6.8**	1176.0	3.9
0.0316	**0.0316**	**6.9**	1390.5	3.8
0.0316	**0.0208**	**7.2**	1752.2	3.4
0.0208	**0.0500**	**3.0**	496.9	1.7
0.0208	**0.0316**	**2.9**	564.5	1.6
0.0208	**0.0208**	**2.9**	693.1	1.4
0.0208	**0.0500**	**5.1**	872.1	2.8
0.0208	**0.0316**	**4.9**	976.5	2.5
0.0208	**0.0208**	**4.8**	1166.9	2.2
0.0208	**0.0500**	**6.8**	1178.5	3.2
0.0208	**0.0316**	**7.2**	1443.1	3.2
0.0208	**0.0208**	**7.1**	1736.5	2.9

Table 6.8 Experimental Reynolds and Nusselt numbers for cylindrical fins

S_L/L	S_T/W	U (m/s)	Re	Nu
0.0500	**0.0500**	**2.9**	485.1	3.2
0.0500	**0.0316**	**2.9**	566.3	2.9
0.0500	**0.0208**	**3.0**	706.7	2.3
0.0500	**0.0500**	**4.9**	832.7	4.6
0.0500	**0.0316**	**4.8**	963.1	4.4
0.0500	**0.0208**	**5.0**	1208.2	3.6
0.0500	**0.0500**	**6.9**	1191.8	5.6
0.0500	**0.0316**	**7.1**	1438.2	5.1
0.0500	**0.0208**	**6.9**	1676.4	4.6
0.0316	**0.0500**	**2.9**	473.0	2.8
0.0316	**0.0316**	**3.2**	631.7	2.5
0.0316	**0.0208**	**3.1**	734.1	2.0
0.0316	**0.0500**	**4.9**	838.7	4.6
0.0316	**0.0316**	**5.1**	1026.2	3.8
0.0316	**0.0208**	**5.0**	1204.7	3.2
0.0316	**0.0500**	**7.0**	1211.0	5.8
0.0316	**0.0316**	**6.9**	1399.6	4.8
0.0316	**0.0208**	**6.8**	1656.0	4.1
0.0208	**0.0500**	**2.9**	475.1	2.5
0.0208	**0.0316**	**2.8**	545.9	2.3
0.0208	**0.0208**	**2.9**	688.0	1.7
0.0208	**0.0500**	**4.9**	827.9	4.1
0.0208	**0.0316**	**4.8**	956.5	3.4
0.0208	**0.0208**	**5.1**	1233.2	2.8
0.0208	**0.0500**	**7.0**	1205.1	5.2
0.0208	**0.0316**	**7.0**	1414.5	4.5
0.0208	**0.0208**	**6.9**	1682.7	3.7

Table 6.9 Experimental Reynolds and Nusselt numbers for plate fins

S_L/L	S_T/W	U (m/s)	Re	Nu
-	**0.0500**	**3.0**	502.6	1.6
-	**0.0316**	**2.9**	563.9	1.6
-	**0.0208**	**3.1**	725.8	1.3
-	**0.0500**	**5.2**	902.9	2.0
-	**0.0316**	**4.8**	947.8	2.1
-	**0.0208**	**4.9**	1174.7	1.9
-	**0.0500**	**7.1**	1232.9	2.9
-	**0.0316**	**6.9**	1383.4	2.5
-	**0.0208**	**6.7**	1619.3	2.4

Least square linear regression can be used for determination of heat transfer correlation [30], [52]. General form of correlation equation can be written as [52] :

$$Nu_{corr} = aRe^{b}\left(\frac{S_T}{W}\right)^{c}\left(\frac{S_L}{L}\right)^{z} \tag{6.14}$$

Equation (6.14) can be linearized by taking logarithm of both side [30]:

$$\log\left(Nu_{corr}\right) = \log\left(a\right) + b\log\left(Re\right) + c\log\left(\frac{S_T}{W}\right) + z\log\left(\frac{S_L}{L}\right) \tag{6.15}$$

Error definition is done between experimental Nusselt number and correlated Nusselt number [52] :

$$\sum_{i=1}^{n} e_i = \left(\log\left(Nu_{exp}\right) - \log\left(Nu_{corr}\right)\right) \tag{6.16}$$

where;

n : 27 for square and cylindrical fins, 9 for plate fins.

Squares of both side are taken to avoid error minimization effect of different datas which have positive and negative values. So, sum of the squares of residuals can be written as [52]:

$$S_r = \sum_{i=1}^{n} e_i^2 = \left(\log\left(Nu_{exp}\right) - \log\left(Nu_{corr}\right)\right)^2 \tag{6.17}$$

If correlated Nusselt number in equation (6.15) is placed into equation (6.17), modified S_r can be expressed as:

$$S_r = \sum_{i=1}^{n} e_i^2 = \left(\log\left(Nu_{exp}\right) - \log\left(a\right) - b\log\left(Re\right) - c\log\left(\frac{S_T}{W}\right) - z\log\left(\frac{S_L}{L}\right)\right)^2 \tag{6.18}$$

Equation (6.18) is differentiated with respect to all unknown coefficients (a, b, c and z). Their derivatives are set to zero in order to minimize error and solved by Gauss Elimination Method [52].

Error calculations related with the heat transfer correlations are done based on equations presented in [52]:

Mean value of Nu_{exp}:

$$\overline{Nu_{exp}} = \frac{\sum Nu_{exp}}{n} \tag{6.19}$$

Summation of squares of residuals between data points and arithmetic mean:

$$S_t = \sum \left(Nu_{exp} - \overline{Nu_{exp}} \right)^2 \tag{6.20}$$

Standart deviaton:

$$S_y = \sqrt{\frac{S_t}{n-1}} \tag{6.21}$$

Coefficient of variation:

$$C.V. = \frac{S_y}{\overline{Nu_{exp}}} 100\% \tag{6.22}$$

Summation of squares of residuals between data points and correlation points:

$$S_r = \sum \left(Nu_{exp} - Nu_{corr} \right)^2 \tag{6.23}$$

Standart error of estimate:

$$S_{y/x} = \sqrt{\frac{S_r}{n-y-1}} \tag{6.24}$$

where;

Predictor variable (y) is 3 for square and cylindrical fins and 2 for plate fins.

If, $S_{y/x} < S_y$, linear regression model has merit. So, coefficient of determination (r^2) and correlation coefficient (r) can be determined as:

$$r^2 = \frac{S_t - S_r}{S_t} 100\% \tag{6.25}$$

$$r = \sqrt{\frac{S_t - S_r}{S_t}} \tag{6.26}$$

Heat transfer correlation for the square fins is plotted with in Figure 6.36.

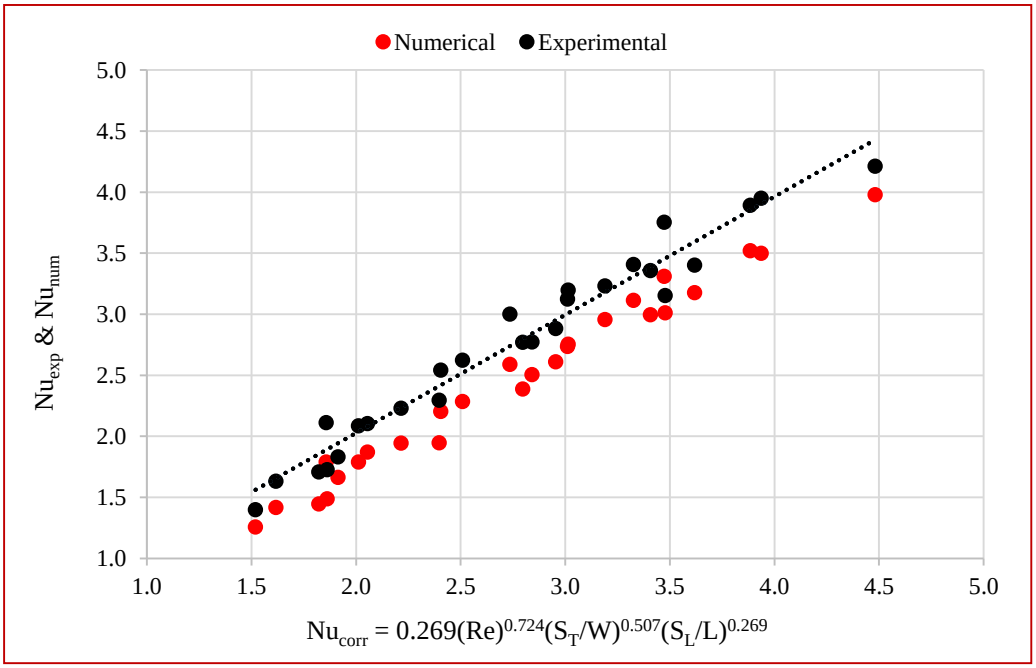

Figure 6.36 Heat transfer correlation for square fins

Range for the correlation can be defined as:

$$509.2 \le Re \le 1752.2$$
$$0.0208 \le \frac{S_T}{W} \le 0.0500$$
$$0.0208 \le \frac{S_L}{L} \le 0.0500 \qquad (6.27)$$

Table 6.10 Error analysis of heat transfer correlation for square fins

$\overline{\mathbf{Nu_{exp}}}$	$\mathbf{\Sigma S_t}$	$\mathbf{\Sigma S_r}$	$\mathbf{S_y}$	$\mathbf{S_{y/x}}$	$\mathbf{S_{y/x} < S_y}$	**C.V. %**	$\mathbf{r^2}$ **%**	**r**
2.75	15.79	0.61	0.78	0.16	√	28.29	96.13	0.98

Heat transfer correlation for the cylindrical fins is plotted in Figure 6.37.

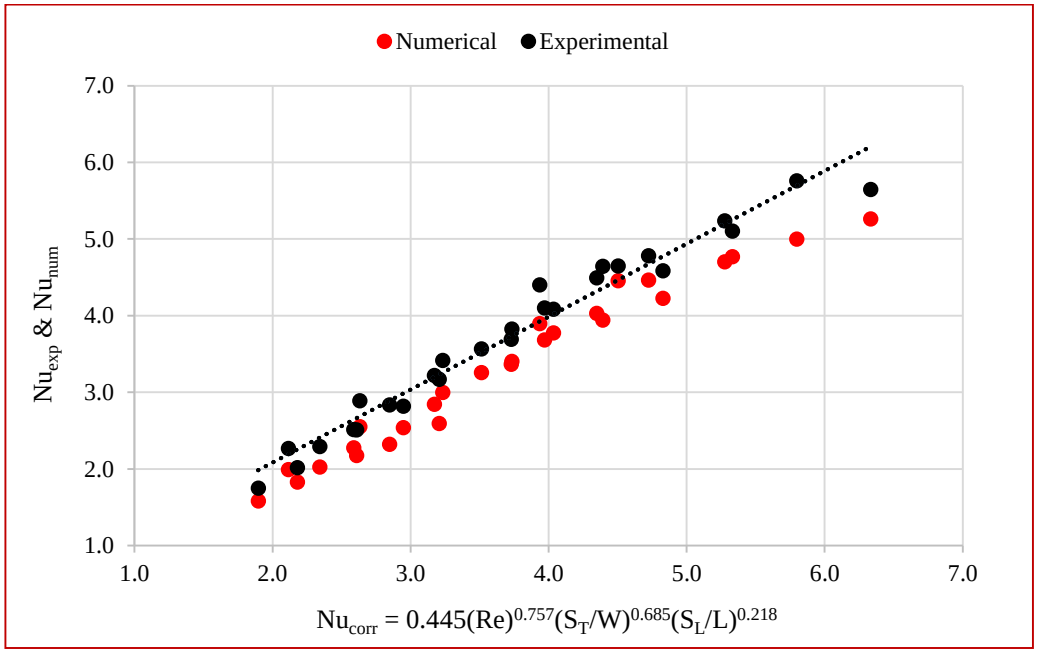

Figure 6.37 Heat transfer correlation for cylindrical fins

Range for the correlation can be defined as:

$$485.1 \le Re \le 1682.7$$
$$0.0208 \le \frac{S_T}{W} \le 0.0500$$
$$0.0208 \le \frac{S_L}{L} \le 0.0500 \qquad (6.28)$$

Result of the error analysis for the correlation of cylindrical fins is presented in Table 6.11.

Table 6.11 Error analysis of heat transfer correlation for cylindrical fins

$\overline{Nu_{exp}}$	ΣS_t	ΣS_r	S_y	$S_{y/x}$	$S_{y/x} < S_y$	C.V. %	r^2 %	r
3.71	33.81	1.15	1.14	0.22	√	30.73	96.59	0.98

Heat transfer correlation for the plate fins is plotted with in Figure 6.38.

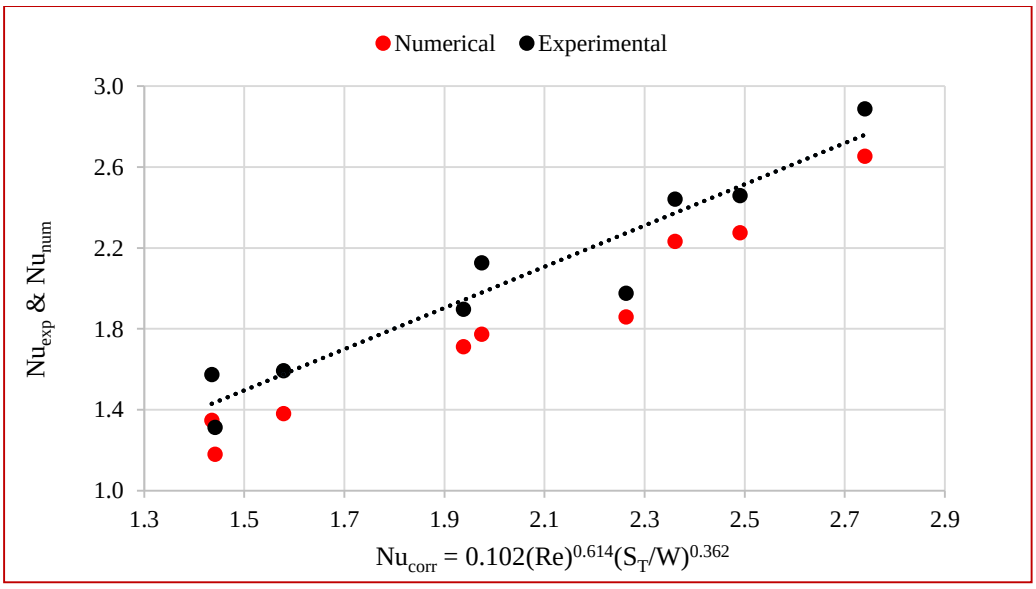

Figure 6.38 Heat transfer correlation for plate fins

Range for the correlation can be defined as:

$$502.6 \le Re \le 1619.3$$
$$0.0208 \le \frac{S_T}{W} \le 0.0500 \tag{6.29}$$

Result of the error analysis for the correlation of plate fins is tabulated in Table 6.12.

Table 6.12 Error analysis of heat transfer correlation for plate fins

$\overline{\mathbf{Nu_{exp}}}$	$\mathbf{\Sigma S_t}$	$\mathbf{\Sigma S_r}$	$\mathbf{S_y}$	$\mathbf{S_{y/x}}$	$\mathbf{S_{y/x} < S_y}$	**C. V.** %	$\mathbf{r^2}$ %	**r**
2.03	2.03	0.17	0.50	0.17	√	24.83	91.53	0.96

6.5 Uncertainty Analysis

Uncertainty analysis is done according to the study of Moffat [53]. First order analysis is conducted which is interested in only variable (measurement) errors, and fixed errors related to the sensitivity of the measuring devices are neglected.

Uncertainty of Q_{conv} can be calculated based on equation (3.11):

$$\delta Q_{conv} = \sqrt{\left(\delta Q_{input}\right)^2 + \left(-\delta Q_{rad}\right)^2 + \left(-\delta Q_{ins}\right)^2} \tag{6.30}$$

Uncertainty of Q_{input} can be calculated based on equation (6.4):

$$\delta Q_{input} = \sqrt{\left(I\delta V\right)^2 + \left(V\delta I\right)^2} \tag{6.31}$$

General measurement is done for the uncertainty of the heat input at the beginning of the experiments. δQ_{input} is found as 1.43 W.

ΔT_{lm} term can be sent to the left-hand side of equation (3.9) and uncertainty at the left-hand side of the equation (3.9) can be found as:

$$\delta\left(\frac{Q_{conv}}{\Delta T_{lm}}\right)=\sqrt{\left(\frac{\delta Q_{conv}}{\Delta T_{lm}}\right)^2+\left(\frac{-Q_{conv}}{\left(\Delta T_{lm}\right)^2}\delta\Delta T_{lm}\right)^2} \tag{6.32}$$

After adding deviations obtained from the equation (6.32), right-hand side of the equation (6.32) is solved again to find uncertainty at average heat transfer coefficient (h_{avg}) with the numerical method explained in Appendix A. Four numerical calculations are done with the combinations of positive and negative values of δQ_{conv} and $\delta\Delta T_{lm}$, then absolute maximum deviation value among four results is accepted as δh_{avg}.

Uncertainty at Nusselt number can be calculated like that:

$$\delta Nu=\sqrt{D_h{}^2\left(\left(\frac{\delta h_{avg}}{k_{air}}\right)^2+\left(\frac{-h_{avg}}{k_{air}{}^2}\delta k_{air}\right)^2\right)} \tag{6.33}$$

Uncertainty values of average heat transfer coefficient and Nusselt number for square, cylindrical and plate fins are presented in Table 6.13, Table 6.14 and Table 6.15, respectively.

Table 6.13 Uncertainty values of h_{avg} and Nu for the square fins

S_L/L	S_T/W	U (m/s)	δQ_{conv} (W)	$\delta \Delta T_{lm}$ (°C)	δh_{avg} (W/m^2K)	$\%h_{avg}$	δNu	%Nu
0.0500	**0.0500**	**3.1**	1.523	0.571	0.536	1.719	0.040	1.724
0.0500	**0.0316**	**2.9**	2.752	0.573	0.756	2.668	0.056	2.672
0.0500	**0.0208**	**2.9**	2.958	0.705	0.736	3.002	0.055	3.007
0.0500	**0.0500**	**4.9**	1.780	0.664	1.044	2.318	0.078	2.323
0.0500	**0.0316**	**4.8**	2.382	0.602	1.157	2.782	0.087	2.786
0.0500	**0.0208**	**4.9**	2.186	0.681	1.046	2.845	0.079	2.850
0.0500	**0.0500**	**7.1**	2.134	0.734	1.677	2.978	0.126	2.983
0.0500	**0.0316**	**6.9**	2.021	0.770	1.674	3.196	0.126	3.202
0.0500	**0.0208**	**6.8**	1.738	0.614	1.195	2.658	0.091	2.663
0.0316	**0.0500**	**2.9**	2.609	0.587	0.737	2.593	0.054	2.597
0.0316	**0.0316**	**3.0**	2.328	0.818	0.834	2.929	0.062	2.936
0.0316	**0.0208**	**3.2**	2.037	0.587	0.527	2.313	0.040	2.318
0.0316	**0.0500**	**4.9**	1.871	0.588	1.039	2.423	0.078	2.427
0.0316	**0.0316**	**5.0**	1.994	0.715	1.189	2.975	0.089	2.981
0.0316	**0.0208**	**4.9**	1.792	0.787	1.065	3.063	0.080	3.070
0.0316	**0.0500**	**6.8**	1.946	0.771	1.610	3.117	0.122	3.123
0.0316	**0.0316**	**6.9**	1.711	0.628	1.456	2.921	0.110	2.926
0.0316	**0.0208**	**7.2**	1.824	0.596	1.379	3.058	0.104	3.062
0.0208	**0.0500**	**3.0**	2.766	0.631	0.638	2.733	0.047	2.736
0.0208	**0.0316**	**2.9**	2.267	0.846	0.624	2.833	0.046	2.840
0.0208	**0.0208**	**2.9**	1.845	0.729	0.444	2.381	0.033	2.389
0.0208	**0.0500**	**5.1**	2.068	0.677	1.019	2.758	0.077	2.764
0.0208	**0.0316**	**4.9**	1.961	0.608	0.928	2.737	0.070	2.741
0.0208	**0.0208**	**4.8**	1.871	0.533	0.757	2.562	0.057	2.565
0.0208	**0.0500**	**6.8**	1.756	0.681	1.133	2.711	0.086	2.716
0.0208	**0.0316**	**7.2**	1.815	0.644	1.335	3.104	0.100	3.108
0.0208	**0.0208**	**7.1**	1.672	0.668	1.218	3.202	0.092	3.207

Table 6.14 Uncertainty values of h_{avg} and Nu for the cylindrical fins

S_L/L	S_T/W	U (m/s)	δQ_{conv} (W)	$\delta \Delta T_{lm}$ (°C)	δh_{avg} (W/m^{2}K)	$\%h_{avg}$	δNu	%Nu
0.0500	**0.0500**	**2.9**	2.212	0.823	1.125	2.634	0.084	2.642
0.0500	**0.0316**	**2.9**	2.634	0.748	1.145	2.942	0.085	2.948
0.0500	**0.0208**	**3.0**	2.470	0.779	0.860	2.792	0.064	2.799
0.0500	**0.0500**	**4.9**	1.756	0.728	1.582	2.579	0.118	2.585
0.0500	**0.0316**	**4.8**	2.137	0.552	1.579	2.698	0.119	2.702
0.0500	**0.0208**	**5.0**	1.838	0.676	1.266	2.675	0.096	2.680
0.0500	**0.0500**	**6.9**	1.887	0.655	2.103	2.806	0.159	2.811
0.0500	**0.0316**	**7.1**	1.974	0.801	2.283	3.380	0.173	3.386
0.0500	**0.0208**	**6.9**	2.102	0.751	2.149	3.492	0.162	3.497
0.0316	**0.0500**	**2.9**	2.385	0.710	1.045	2.706	0.077	2.711
0.0316	**0.0316**	**3.2**	2.478	0.626	0.913	2.713	0.068	2.717
0.0316	**0.0208**	**3.1**	2.256	0.715	0.713	2.638	0.053	2.644
0.0316	**0.0500**	**4.9**	1.896	0.785	1.930	3.119	0.145	3.125
0.0316	**0.0316**	**5.1**	1.780	0.696	1.450	2.855	0.109	2.860
0.0316	**0.0208**	**5.0**	1.778	0.655	1.182	2.763	0.089	2.768
0.0316	**0.0500**	**7.0**	1.886	0.552	2.202	2.883	0.166	2.886
0.0316	**0.0316**	**6.9**	1.592	0.647	1.883	2.977	0.142	2.981
0.0316	**0.0208**	**6.8**	1.988	0.713	1.886	3.491	0.143	3.496
0.0208	**0.0500**	**2.9**	2.544	0.668	0.953	2.795	0.070	2.799
0.0208	**0.0316**	**2.8**	1.810	0.575	0.680	2.225	0.051	2.229
0.0208	**0.0208**	**2.9**	2.726	0.664	0.687	2.935	0.051	2.939
0.0208	**0.0500**	**4.9**	1.931	0.727	1.702	3.094	0.127	3.099
0.0208	**0.0316**	**4.8**	1.994	0.611	1.328	2.914	0.100	2.917
0.0208	**0.0208**	**5.1**	2.164	0.739	1.243	3.323	0.094	3.329
0.0208	**0.0500**	**7.0**	1.667	0.772	2.437	3.500	0.183	3.505
0.0208	**0.0316**	**7.0**	1.936	0.784	2.328	3.909	0.176	3.914
0.0208	**0.0208**	**6.9**	1.961	0.703	1.766	3.620	0.134	3.625

Table 6.15 Uncertainty values of h_{avg} and Nu for the plate fins

S_L/L	S_T/W	U (m/s)	δQ_{conv} (W)	$\delta \Delta T_{lm}$ (°C)	δh_{avg} (W/m^{2}K)	$\%h_{avg}$	δNu	%Nu
-	**0.0500**	**3.0**	2.298	0.711	0.520	2.424	0.039	2.430
-	**0.0316**	**2.9**	2.073	0.834	0.560	2.636	0.042	2.643
-	**0.0208**	**3.1**	2.086	0.625	0.416	2.349	0.031	2.353
-	**0.0500**	**5.2**	2.031	0.610	0.591	2.255	0.045	2.260
-	**0.0316**	**4.8**	2.136	0.576	0.735	2.576	0.055	2.580
-	**0.0208**	**4.9**	2.180	0.818	0.806	3.187	0.061	3.194
-	**0.0500**	**7.1**	1.928	0.662	1.021	2.668	0.077	2.673
-	**0.0316**	**6.9**	2.131	0.626	0.930	2.842	0.070	2.846
-	**0.0208**	**6.7**	1.596	0.653	0.911	2.810	0.069	2.815

CHAPTER 7

DISCUSSION AND CONCLUSION

Numerical geometric optimization of square, cylindrical and plate fins for heat transfer augmentation is done. Flow is external in transition regime. Effect of different frontal velocities and heat inputs on the heat transfer performance of the fins are investigated. Heat transfer performance of the geometrically optimized fins with different profiles are compared with each other when Reynolds number values are same. Experimental studies are also conducted with the manufacturable fins to verify numerical model. Heat transfer correlations are derived for fins with different profiles between at a certain range of Reynolds number, non-dimensional streamwise and spacing values. First order uncertainty analyses are performed to determine range of error in experimental studies.

Decreasing inter-fin spacing increases heat transfer area while other geometrical parameters are constant. So, heat transfer performance of fins enhance. If the spanwise spacing continues to be reduced, the pressure drop begins to dominate over the positive effect of increasing heat transfer area on thermal performance. Thus, undesired decrease of the heat transfer performance occurs. This phenomenon is the driving force of present study.

Numerical analyses revealed that, T_{max} of the square fins having a non-dimensional spanwise spacing value of 0.0208 reach their minimum values with free-stream velocity of 3 m/s as plotted in Figure 6.1. In other words, thermal performances of the square fins having narrower or wider non-dimensional spanwise spacing than 0.0208 worsen. The heat transfer performances of square fins are mostly at the highest level

at this value with higher free-stream velocities (5 m/s and 7 m/s), too. Heat transfer augmentation is done in streamwise spacing, too. T_{max} reaches its minimum value when non-dimensional streamwise spacing value is 0.0138 for all three free-stream velocities, but geometrical optimization in streamwise spacing is not as sharp as in spanwise one. Because, flow bypass occurs from the top side of the fin due to hydraulic resistance and flow field can not efficiently penetrate in spanwise direction as illustrated in Figure 6.4.

Square fins having the non-dimensional streamwise spacing value of 0.0138, which satisfies minimum T_{max} among other square fins, are chosen for further studies. Numerical analyses are carried out to see the effect of higher frontal velocities and heat inputs on the non-dimensional spanwise spacing value as plotted in Figure 6.5, Figure 6.6 and Figure 6.7. Amount of heat input does not have any effect on the relation between non-dimensional spacing and thermal characteristic. Higher free-stream velocities improve heat transfer performance as expected and do not change optimum spanwise spacing value, but increasing velocity brings the thermal performance to the hydrodynamic limits and acceleration of the thermal characteristic improvement starts to decrease.

Heat removal capacity of cylindrical fins maximizes mostly at the non-dimensional spanwise spacing value of 0.0316 with 3 m/s free-stream velocity as presented in Figure 6.8. Decreasing non-dimensional streamwise spacing up to 0.0088 improves thermal performance as illustrated in Figure 6.8, Figure 6.9 and Figure 6.10 for free-stream velocities of 3 m/s, 5 m/s and 7 m/s. Thermal characteristic of cylindrical fins is less sensitive to change in streamwise spacing than spanwise spacing as commented for square fins.

T_{max} of optimum cylindrical fin configuration ($S_L/L = 0.0088$) in terms of streamwise spacing are examined for higher free-stream velocities and heat inputs. Optimum spanwise spacing is independent of heat input as presented in Figure 6.12, Figure 6.13 and Figure 6.14. Increasing free-stream velocity enhances heat transfer performance and do not change optimum spanwise spacing, but dependency of heat transfer

augmentation to spanwise spacing decreases as hydrodynamic limits becomes dominant with higher free-stream velocities.

Non-dimensional spanwise spacing value of 0.0316 results in minimum T_{max} at the base plate of plate fins with 3 m/s free-stream veloctiy as illustrated in Figure 6.16. Optimization in streamwise spacing can not be mentioned for plate fins due to the continuity of the fin strip. Higher velocities result in shift of optimum spanwise spacing to lower values, because fin configurations, whose heat transfer areas are higher, benefit better from flow field penetrating through back side of fin. This comment can be merged with the hydrodynamic limit phenomenon mentioned for square and cylindrical fins. Heat transfer characteristic of plate fins is independent of heat input as plotted in Figure 6.17, Figure 6.18 and Figure 6.19.

In order to investigate the superiority of geometries; square (S_L/L = 0.0138), cylindrical (S_L/L = 0.0088) fins, whose heat transfer performances are better in terms of streamwise spacing, and plate fins are compared with each other from the point of thermal characteristic. Beahivours of fins with different profiles are investigated with changing free-stream velocity from 3 m/s to 7 m/s and heat input from 150 W to 250 W as illustrated in Figure 6.20 - Figure 6.28. Fins, whose spanwise spacings are same, have same Reynolds number. Increasing heat input does not have any effect on the optimum spanwise spacing value for all fins with different profiles. Cylindrical fins perform better in terms of heat transfer characteristic than square and plate ones under the influence of 3 m/s free-stream velocity as presented in Figure 6.20, Figure 6.23 and Figure 6.26, while square and plate ones have close T_{max} values. Coefficients of heat transfer correlations can be used to comment about heat transfer performance of fins. Superiority of circular fins can be observed from heat transfer correlation equations presented in Figure 6.36, Figure 6.37 and Figure 6.38 for all fins with different profiles. Correlation coefficient “a” of cylindrical fins is found as 0.445, while it has a value of 0.269 and 0.102 for square fins and plate fins, respectively. Heat tranfer augmentation of cylindrical fins become more dominant than square and plate ones with increasing free-stream velocity as illustrated in Figure 6.20, Figure 6.21 and Figure 6.22. It can be observed from power coefficient of Reynolds number “b” in

correlation equations presented in Figure 6.36, Figure 6.37 and Figure 6.38, too. It has values of 0.724, 0.757 and 0.614 for square, cylindrical and plate fins, respectively. Superiority of cylindrical fins to others can be explained with a phenomenon called as Coanda effect [17]. Flow field seperation from the curved bodies occurs late. So, cylindrical fins benefit maximum from flow field, although, total heat transfer area of cylindrical fins are lower than square and plate ones.

Error between the numerical and experimental results are calculated. Maximum error is % 14.9 occurring for the cylindrical fin ($S_L/L = 0.0316$, $S_T/W = 0.05$) with 3 m/s free-stream velocity, while minimum error is %2.3 occurring for the cylindrical fin ($S_L/L = 0.05$, $S_T/W = 0.0208$) with 7 m/s free-stream velocity. Remaining error values change between these minimum and maximum points. There are possible causes of errors between results. Heat transfer rate through insulation layer can be considered as one of the reasons for disparity between results, although insulation measures are reflected in the numerical model. Because, the insulation material is placed in layers in the experimental setup as shown in Figure 5.2, but it is modeled as bulk in numerical studies. So, contact problems may occur between layers of insulation material and heat can be transferred outside in the lateral direction to the insulation. Moreover, edges of the fins are placed 10 mm on each sides away from the bottom aluminum plate of the tunnel to avoid conduction between fin and tunnel bottom plate as presented in Figure 5.11. The gap between tunnel and fin is filled with insulation material. It is very difficult to cut and place it in exact dimensions as it is very soft material, so insulation material is placed in particles to fill this gap and unaccounted losses may occur from this region, unlike the numerical model. Furthermore, there are rigid cables, which are not considered in the numerical model, below the heater as shown in Figure 5.11. Difficulties to insulate these cables could result in the gap around them and undesired losses may happen. Heater, gap pad and fin are perfectly mounted to each other in the numerical model, but contact problems may occur between these components in experimental setup and conduction heat transfer rates to the fin may reduce. The uncertainty of the heat input is presented in section 6.5 as 1.43 W, so this uncertainty can be one of the reasons for the difference between results.

Radiation is neglected in numerical analyses to reduce computational time and storage needs as Jubran et al. [22] reported that radiation heat transfer rates for heat sink experiments are around % 2.5 of total heat input.

So, radiation included numerical analyses are conducted to increase accuracy of numerical results. Analyses are performed for the fins whose spanwise and streamwise spacings satisfying minimum T_{max} among others with 150 W heat input. Optimum fin configurations do not change with changing free-stream velocity for square and cylindrical fins, but change for plate fins. Moreover, error between numerical (radiation not included) and experimental results decrease with increasing velocity as expected and tabulated in Table 6.1 and Table 6.2 for square and cylindrical fins, respectively. So, radiation included numerical analyses are done for square and cylindrical fins with lowest free-stream velocity (3 m/s) and for plate fins with all three free-stream velocities. T_{max} observed at numerical analyses (radiation not included and included) and experiments (with manufacturable fins) are presented in Table 7.1.

Table 7.1 T_{max} comparison of numerical and experimental studies

Geometry	**S_L/L**	**S_T/W**	**U (m/s)**	**T_{max} (num) (℃)**	**T_{max} (num_rad) (℃)**	**T_{max} (exp) (℃)**
Square	0.0138	0.0208	3	122.7	120.8	-
Cylindrical	0.0088	0.0316	3	115.1	113.2	-
Plate	-	0.0316	3	126.8	124.6	116.7
Plate	-	0.0208	5	94.1	92.8	89.8
Plate	-	0.0138	7	79.6	78.7	-

Some recommedations can be made for future work. Flow visualization techniques can be used in experiments to understand flow field around fin. Moreover, streamwise and spanwise spacing values around optimum point can be discretized more intense to define more accurate design points in both directions. Furthermore, staggered allignment of fins can be studied and comparison of heat transfer performance can be done. Numerical analyses including radiation heat transfer can be performed for all cases.

7.1 Updated Numerical Analyses

Numerical analyses are updated with free-stream velocity and ambient temperature boundary condition values obtained from experiments for the cases whose results are presented in Figure 6.32, Figure 6.33, Figure 6.34 and experiments are conducted. Moreover, uncertainty value of the heater is represented by substracting deviation of power from the mean value. Furthermore, radiation heat transfer is enabled. Maximum base plate temperatures of square, cylindrical and plate fins with updated numerical analyses are illustrated in Figure 7.1, Figure 7.2 and Figure 7.3, respectively.

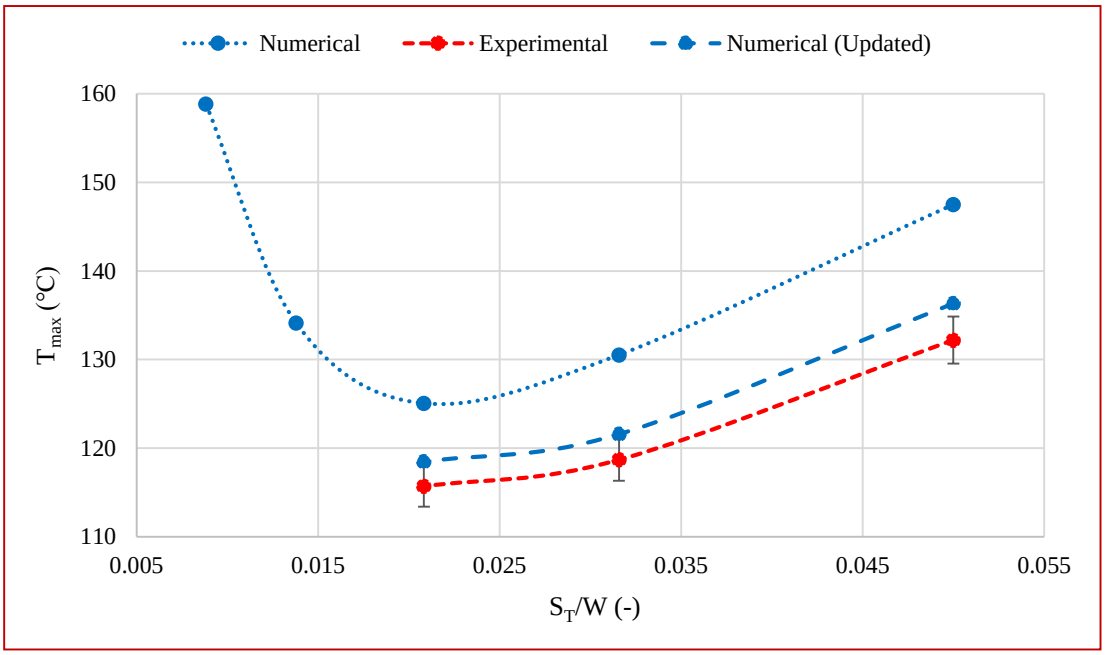

Figure 7.1 Square fins (S_L/L = 0.0208)

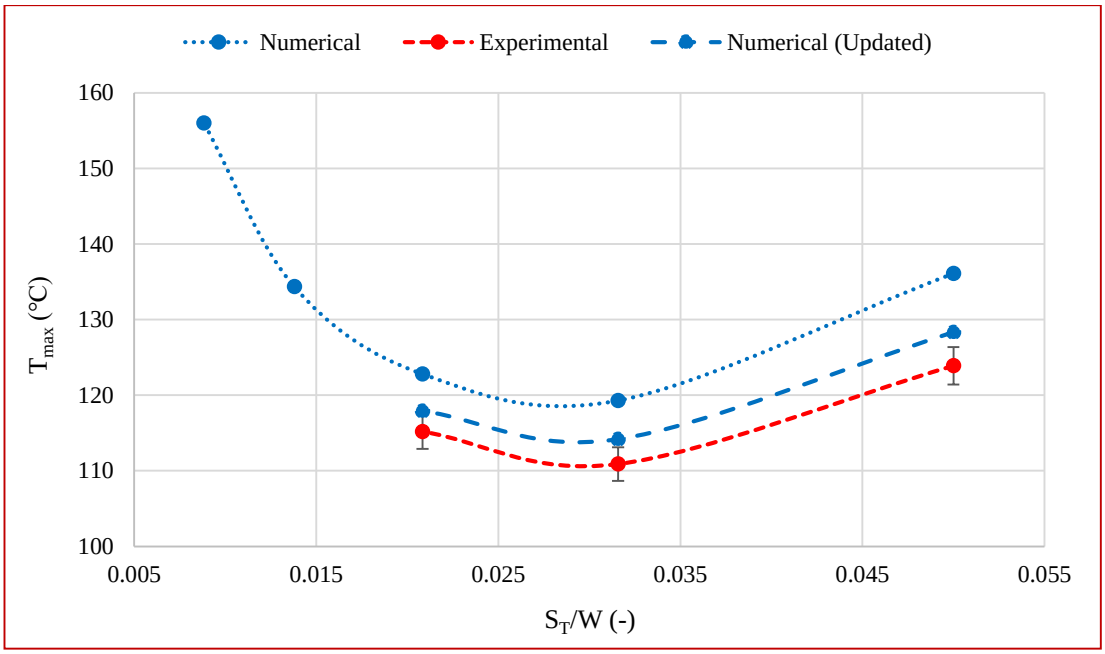

Figure 7.2 Cylindrical fins (S_L/L = 0.0208)

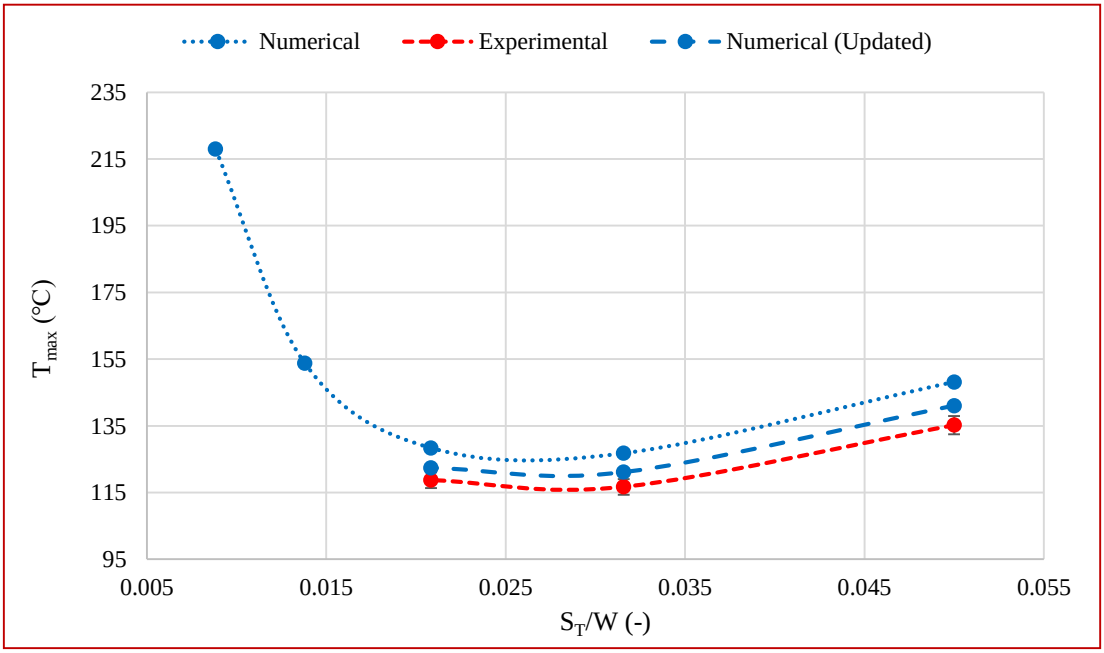

Figure 7.3 Plate fins

REFERENCES

[1] Intel Corporation, “Moore’s law and Intel Innovation.” [Online]. Available: https://www.intel.com/content/www/us/en/history/museum-gordon-moore-law.html. [Accessed: 12-Feb-2018].

[2] Y. A. Cengel, “Heat Transfer: A Practical Approach,” *Mc Graw-Hill*, pp. 785–841, 2003.

[3] TELEREX, “Heat Sinks.” [Online]. Available: https://www.telerex-europe.com/en-gb/heat-sinks. [Accessed: 12-Feb-2018].

[4] S. Lee, “Optimum Design and Selection of Heat Sinks,” *IEEE Trans. Components Packag. Manuf. Technol. Part A*, vol. 18, no. 4, pp. 812–817, 1995.

[5] M. Reynell, “Advanced thermal analysis of packaged electronic systems using computational fluid dynamics techniques,” no. August, pp. 104–106, 1990.

[6] N. Sahiti, A. Lemouedda, D. Stojkovic, F. Durst, and E. Franz, “Performance comparison of pin fin in-duct flow arrays with various pin cross-sections,” *Appl. Therm. Eng.*, vol. 26, no. 11–12, pp. 1176–1192, 2006.

[7] A. Zukauskas, *Heat Transfer from Tubes in Crossflow*. Vilnius, 1975.

[8] M. Behnia, D. Soodphakdee, and S. P. Products, “A Comparison of Heat Sink Geometries for Laminar Forced Convection: Numerical Simulation of Periodically Developed Flow,” pp. 310–315, 1998.

[9] Y. T. Yang, H. S. Peng, and H. T. Hsu, “Numerical Optimization of Pin-Fin Heat Sink with Forced Cooling,” vol. 7, no. 7, pp. 884–891, 2013.

[10] W. A. Khan, “Modeling of Fluid Flow and Heat Transfer for Optimization of Pin-Fin Heat Sinks,” *Univ. Waterloo*, 2004.

[11] J. R. Culham and Y. S. Muzychka, “Optimization of plate fin heat sinks using entropy generation minimization,” *IEEE Trans. Components Packag. Technol.*, vol. 24, no. 2, pp. 159–165, 2001.

[12] P. A. Deshmukh, “Comparison of Thermal Performance of Circular and Elliptical Pin Fin Heat Sinks in Assisting Mixed Convection,” vol. 50, pp. 178–184, 2013.

[13] A. Diani, S. Mancin, C. Zilio, and L. Rossetto, “An assessment on air forced convection on extended surfaces: Experimental results and numerical modeling,” *Int. J. Therm. Sci.*, vol. 67, pp. 120–134, 2013.

[14] R. F. Babus’Haq, K. Akintunde, and S. D. Probert, “Thermal performance of a pin-fin assembly,” *Int. J. Heat Fluid Flow*, vol. 16, no. 1, pp. 50–55, 1995.

[15] M. Tahat, Z. H. Kodah, B. A. Jarrah, and S. D. Probert, “Heat transfers from pin-fin arrays experiencing forced convection,” *Appl. Energy*, vol. 67, no. 4, pp. 419–442, 2000.

[16] R. S. Matos, T. A. Laursen, J. V. C. Vargas, and A. Bejan, “Three-dimensional optimization of staggered finned circular and elliptic tubes in forced convection,” *Int. J. Therm. Sci.*, vol. 43, no. 5, pp. 477–487, 2004.

[17] K. S. Yang, W. H. Chu, I. Y. Chen, and C. C. Wang, “A comparative study of the airside performance of heat sinks having pin fin configurations,” *Int. J. Heat Mass Transf.*, vol. 50, no. 23–24, pp. 4661–4667, 2007.

[18] E. N. S. Ishigai, “Experimental study of structure of gas flow in tube banks with tube axes normal to flow Part II; on the structure of gas flow in single-column, single-row, and double-rows tube banks,” *Bull. JSME*, vol. 18, pp. 528–535, 1975.

[19] A. J. Fowler, G. A. Ledezma, and A. Bejan, “Optimal geometric arrangement of staggered plates in forced convection,” *Int. J. Heat Mass Transf.*, vol. 40, no. 8, pp. 1795–1805, 1997.

[20] K. Azar and C. D. Mandrone, “Effect of Pin Fin Density of the Thermal Performance of Unshrouded Pin Fin Heat Sinks,” vol. 116, no. December 1994, 2016.

[21] H. Jonsson and B. Moshfegh, “Modeling of the thermal and hydraulic performance of plate fin, strip fin, and pin fin heat sinks-influence of flow bypass,” *IEEE Trans. Components Packag. Technol.*, vol. 24, no. 2, pp. 142–149, 2001.

[22] B. A. Jubran, M. A. Hamdan, and R. M. Abdualh, “Enhanced Heat Transfer, Missing Pin, and Optimization for Cylindrical Pin Fin Arrays,” *ASME J. Heat Transf.*, vol. 576–583, no. August 1993, p. 115, 1993.

[23] C. L. Chapman, S. Lee, and B. L. Schmidt, “Thermal Performance of an Elliptical Pin Fin Heat Sink,” *Tenth IEEE SEMI-THERM*, vol. 94, pp. 24–31, 1994.

[24] A. B. Samarth and K. S. Sawankar, “Thermal Performance of Perforated Pin-Fin Arrays in Staggered Arrangement,” vol. 5, no. 7, pp. 777–783, 2014.

[25] C. J. Kobus and T. Oshio, “Predicting the thermal performance characteristics of staggered vertical pin fin array heat sinks under combined mode radiation and mixed convection with impinging flow,” *Int. J. Heat Mass Transf.*, vol. 48, no. 13, pp. 2684–2696, 2005.

[26] Q. Li, Z. Chen, U. Flechtner, and H. J. Warnecke, “Heat transfer and pressure drop characteristics in rectangular channels with elliptic pin fins,” *Int. J. Heat Fluid Flow*, vol. 19, no. 3, pp. 245–250, 1998.

[27] Mentor Graphics, “FloEFD, Technical Reference.” Mentor Graphics Corporation, Oregon/USA, p. 238, 2015.

[28] MIT, “Turbulence Modeling.” [Online]. Available: http://www.mit.edu/~cuongng/Site/Publication_files/TurbulenceModeling_04NOV05.pdf. [Accessed: 12-Feb-2018].

[29] T. L. Bergman, A. S. Lavine, F. P. Incropera, and D. P. Dewitt, *Introduction to Heat Transfer*, 6th ed. United States of America: John Wiley & Sons, Inc., 2011.

[30] E. Ayli, O. Bayer, and S. Aradag, “Experimental investigation and CFD analysis of rectangular profile FINS in a square channel for forced convection regimes,” *Int. J. Therm. Sci.*, vol. 109, pp. 279–290, 2016.

[31] I. Corporation, “Intel ® Xeon ® Processor,” 2013. [Online]. Available: https://ark.intel.com/products/120503/Intel-Xeon-Platinum-8164-Processor-35_75M-Cache-2_00-GHz. [Accessed: 12-Feb-2018].

[32] Intel Corporation, “Intel Xeon Phi Processor 7290,” 2016. [Online]. Available: http://ark.intel.com/products/95830/Intel-Xeon-Phi-Processor-7290-16GB-1_50-GHz-72-core. [Accessed: 12-Feb-2018].

[33] Intel Corporation, “Processors advanced search.” [Online]. Available: https://ark.intel.com/Search/FeatureFilter?productType=processors. [Accessed: 12-Feb-2018].

[34] F. Moukalled, L. Mangani, and M. Darwish, *The Finite Volume Method in Computational Fluid Dynamics*, vol. 113. 2016.

[35] The Bergquist Company, “Gap Pad 5000S35.” [Online]. Available: http://www.bergquistcompany.com/pdfs/dataSheets/PDS_GP_5000S35_0711 v2.pdf. [Accessed: 12-Feb-2018].

[36] Matweb, “6063-T6 Aluminum.” [Online]. Available: http://asm.matweb.com/search/SpecificMaterial.asp?bassnum=MA6063T6. [Accessed: 12-Feb-2018].

[37] İZOCAM, “Taş yünü klima levhası.” [Online]. Available: http://www.izocam.com.tr/userfiles/files/urunler/yalitim-uygulamalari/tesisat-yalitimi/tasyunu-klima-levhasi/tasyunu-klima-levhasi.pdf. [Accessed: 12-Feb-2018].

[38] J. Dong, J. Chen, W. Zhang, and J. Hu, “Experimental and numerical investigation of thermal -hydraulic performance in wavy fin-and-flat tube heat exchangers,” *Appl. Therm. Eng.*, vol. 30, no. 11–12, pp. 1377–1386, 2010.

[39] W. Yuan, J. Zhao, C. P. Tso, T. Wu, W. Liu, and T. Ming, “Numerical simulation of the thermal hydraulic performance of a plate pin fin heat sink,” *Appl. Therm. Eng.*, vol. 48, pp. 81–88, 2012.

[40] M. G. Corporation, “Solving Engineering Problems.” Mentor Graphics Corporation, Oregon/USA, p. 98, 2015.

[41] EBMPAPST, “6314/2 Tdhhp.” [Online]. Available: http://www.ebmpapst.com/en/products/compact-fans/axial-compact-fans/axial_compact_fans_detail.php?pID=120080. [Accessed: 12-Feb-2018].

[42] FLUKE, “115 True Rms Multimeter.” [Online]. Available: http://www.fluke.com/fluke/trtr/dijital-multimetreler/fluke-115.htm?pid=55993.

[43] FLUKE, “322 Clamp Meter.” [Online]. Available: http://www.myflukestore.com/pdfs/cache/www.myflukestore.com/fluke/multimeter/322/manual/fluke_322_multimeter_manual.pdf. [Accessed: 12-Feb-2018].

[44] ATS, “İQ-200.” [Online]. Available: https://www.qats.com/Products/Instruments/Temperature-and-Velocity-Measurement/iQ-200. [Accessed: 12-Feb-2018].

[45] A. S. Technologies, “Thermocouples.” [Online]. Available: http://www.appliedsensortech.com/pdf/sensor_overview.pdf. [Accessed: 12-Feb-2018].

[46] OPTRIS, “Pi 640.” [Online]. Available: http://www.optris.com.tr/infrared-cameras. [Accessed: 12-Feb-2018].

[47] H. Packard, “Z 820.” [Online]. Available: http://www8.hp.com/us/en/campaigns/workstations/z820.html. [Accessed: 12-Feb-2018].

[48] Electronic Temperature Instruments, “Emissivity Table.” [Online]. Available: https://thermometer.co.uk/img/documents/emissivity_table.pdf. [Accessed: 12-Feb-2018].

[49] M. S. Mon and U. Gross, “Numerical study of fin-spacing effects in annular-finned tube heat exchangers,” *Int. J. Heat Mass Transf.*, vol. 47, no. 8–9, pp. 1953–1964, 2004.

[50] R. A. Wirtz, W. Chen, and R. Zhou, “Effect of flow bypass on the performance of longitudinal fin heatsinks,” *J. Electron. Packag.*, vol. 116, no. September 1994, pp. 206–211, 1994.

[51] D. S. Kadle, “Effect of Tip-to-Shroud Clearance on Turbulent Heat Transfer From a Shrouded , Longitudinal Fin Array,” vol. 1, no. August 1986, 2017.

[52] S. C. Chapra and R. P. Canale, *Numerical methods for engineers*, vol. 33, no. 3. McGraw-Hill Science/Engineering/Math, 2015.

[53] R. J. Moffat, “Describing the uncertainties in experimental results,” *Exp. Therm. Fluid Sci.*, vol. 1, no. 1, pp. 3–17, 1988.

APPENDIX A

FALSE POSITION METHOD

If, Q_{conv} term is sent to the right-hand side, equation (3.9) turns into:

$$f\left(h_{avg}\right)=0=h_{avg}A_T\eta_o\Delta T_{lm}-Q_{conv} \tag{A.1}$$

In order to find h_{avg}, false position method can be used [52]:

$$h_{avg(r)}=h_{avg(u)}-\frac{f\left(h_{avg(u)}\right)\left(h_{avg(l)}-h_{avg(u)}\right)}{f\left(h_{avg(l)}\right)-f\left(h_{avg(u)}\right)} \tag{A.2}$$

Arbitrary h_{avg} values are chosen for upper ($h_{avg(u)}$) and lower ($h_{avg(l)}$) limits. $f(h_{avg(r)})$ value is checked after finding $h_{avg(r)}$ value in equation (A.2). If $f(h_{avg(r)})$ value is lower than 0, new $h_{avg(l)}$ becomes $h_{avg(r)}$. Otherwise, $h_{avg(r)}$ is assigned as new $h_{avg(u)}$. This operation is repeated when relative error is smaller than the preset stopping criteria (ε_s) . Relative error can be defined as [52]:

$$\varepsilon_a=\left|\frac{h_{avg(r)}^{new}-h_{avg(r)}^{old}}{h_{avg(r)}^{new}}\right|100\% \tag{A.3}$$

$$\varepsilon_S=10^{-7} \tag{A.4}$$